1986

Experimental fracture mechanics through digital image analysis

Alireza Mehdi-Soozani
Iowa State University

Mehdi-Soozani, Alireza

EXPERIMENTAL FRACTURE MECHANICS THROUGH DIGITAL IMAGE ANALYSIS

Iowa State University PH.D. 1986

PLEASE NOTE:

In all cases this material has been filmed in the best possible way from the available copy. Problems encountered with this document have been identified here with a check mark __√__.

1. Glossy photographs or pages _____
2. Colored illustrations, paper or print _____
3. Photographs with dark background __√__
4. Illustrations are poor copy _____
5. Pages with black marks, not original copy _____
6. Print shows through as there is text on both sides of page _____
7. Indistinct, broken or small print on several pages __√__
8. Print exceeds margin requirements _____
9. Tightly bound copy with print lost in spine _____
10. Computer printout pages with indistinct print _____
11. Page(s) _____ lacking when material received, and not available from school or author.
12. Page(s) _____ seem to be missing in numbering only as text follows.
13. Two pages numbered _____. Text follows.
14. Curling and wrinkled pages _____
15. Dissertation contains pages with print at a slant, filmed as received _____
16. Other _____

_____

_____

Experimental fracture mechanics through digital image analysis

by

Alireza Mehdi-Soozani

A Dissertation Submitted to the
Graduate Faculty in Partial Fulfillment of the
Requirements for the Degree of
DOCTOR OF PHILOSOPHY

Department: Engineering Science and Mechanics
Major: Engineering Mechanics

Approved:

Signature was redacted for privacy.

In Charge of Major Work

Signature was redacted for privacy.

For the Major Department

Signature was redacted for privacy.

For the Graduate College

Iowa State University
Ames, Iowa
1986

TABLE OF CONTENTS

Page

CHAPTER 1. GENERAL INTRODUCTION

Introduction

The Industrial Revolution in the nineteenth century resulted in an enormous increase in the use of metals (mainly irons and steels) for structural applications. Unfortunately, there also occurred many accidents, with loss of life, due to failure of these structures. In particular, there were numerous accidents involving steam boiler explosions and railway equipment.

Some of these accidents were due to poor design, but it was also gradually discovered that material deficiencies in the form of pre-existing flaws could initiate cracking and fracture. The presence of cracks has long been recognized as the main cause of failure of structures operating well below their design limit. The study of the effect of presence of cracks on the load-bearing capability of structures is therefore of great practical importance.

Fracture Mechanics

Strength failures of load bearing structures can be either of the yielding-dominant or fracture-dominant types. Fracture mechanics is concerned almost entirely with fracture-dominant failure and, depending on the state of stress and strain near a crack tip, it can be divided into two general categories:

1. Linear elastic fracture mechanics (LEFM): Here the state of

stress at the crack tip is below the yield strength of the material. The deformation near the crack tip is linear elastic and fracture occurs in a brittle manner, i.e., sudden rapid extension of the crack.

2. Elastic-plastic fracture mechanics: Here the state of stress at regions close to the crack tip exceeds the yield strength of the material but the yield region is small in comparison to the length of the crack. Substantial crack growth may occur prior to fracture.

The theory of linear elastic fracture mechanics is well developed and forms the basis of both categories. There are two approaches for characterizing the severity of cracks in a linear elastic medium; the Griffith energy balance approach [1] and the stress intensity approach [2]. However, the stress intensity approach is generally accepted as the more practical and convenient of the two approaches.

Methods of Determination of Stress Intensity Factors (SIFs)

Analytical Methods: Analytical solutions for SIFs exist for a wide class of two dimensional single and multiple crack problems [3]. However, for only a few three-dimensional crack problems analytical solutions have been developed [4,5]. Up to today, no analytical solutions exist for SIFs for complex 3-D crack problems such as the interaction of a crack with a free surface or with another crack. Approximate formulations such as the the boundary integral method [6]

and the body force method [7] and Schwartz' alternating method [8] exist for estimation of 3-D SIFs.

Numerical Methods: At present, three numerical methods exist for determination of SIFs: finite element, finite difference and boundary element. Among these, finite element method is the most extensively explored and it may be employed in three different approaches:

1. The direct approach estimates the SIFs by comparing the values of the stresses obtained by a conventional finite element analysis to those produced by the governing equations for the stress field near the crack tip. Naturally, very small elements are needed at the crack tip in order to cope with the steep stress gradient.

2. The second approach is based upon the principle of strain energy release rate. The total strain energy of a cracked body before and after crack extension are calculated by finite element analysis and the stress intensity factor is deduced from the change in the total strain energy of the body due to small crack extension. This approach is not suitable for analyzing 3-D crack problems with varying stress intensity along the crack front.

3. The third approach utilizes a special element at the crack

tip with built-in stress singularity. The major disadvantage of this approach is that assumption of the type of the crack tip singularity is required.

In general, finite element analysis of 3-D crack problems is extremely expensive and the accuracy of the results require verification.

Experimental Methods: The stress distribution in the immediate vicinity of a crack tip can be determined experimentally using the optical methods of caustics, holography, moire or photoelasticity [9]. Apart from photoelasticity, all these methods determine the relative displacement at the surface and are therefore only suitable for the study of two-dimensional crack problems. Conventional two-dimensional photoelasticity has been extensively used to estimate the SIF for a single crack in a plate. At present, the photoelastic frozen stress technique is the only viable technique for three-dimensional stress analysis. Stresses at the interior points of a three-dimensional body can be determined by analyzing thin slices cut from the frozen stress model. Frozen stress photoelasticity has been applied successfully to solve simple three-dimensional crack problems [9,10,11].

CHAPTER 2. LINEAR ELASTIC FRACTURE MECHANICS

Introduction

In this chapter, the concept of linear elastic fracture mechanics (LEFM) is presented. The global energy balance fracture criterion (The Griffith Theory) and the stress intensity factor approach which characterize fracture by its local character are discussed. The advantages and limitations are examined.

Linear Elastic Fracture Mechanics

The Griffith Energy Balance Approach [1]: The basis of Griffith's criterion is that if, owing to the action of a stress, a new crack is formed or a pre-existing crack is caused to extend, the increase in the potential energy of the elastic body due to the creation of the new crack surfaces must be balanced by the applied stress and the decrease in the strain energy of the body. The total potential energy of the body is always a constant.

Consider an infinite plate of unit thickness that contains a through-thickness crack of length 2a and that is subjected to uniform tensile stress, σ, applied at infinity as shown in Figure 2.1.

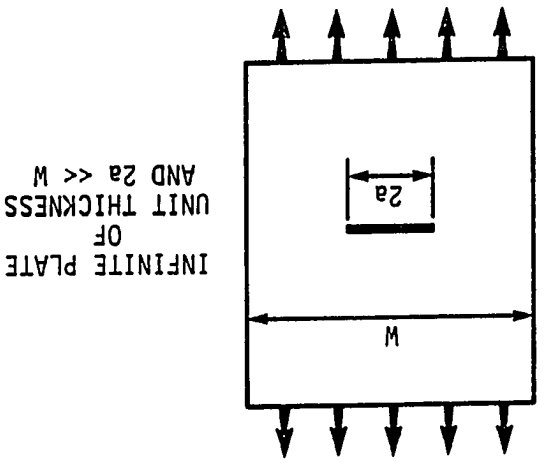

Figure 2.1. A through-cracked plate

The total energy per unit thickness U of the cracked plate may be written as

$$U = U_o + U_a + U_\gamma - F \tag{2.1}$$

where

U_o = elastic energy per unit thickness of the loaded uncracked plate,

U_a = change in the elastic energy per unit thickness caused by introducing the crack in the plate (this is a negative term),

U_γ = change in the elastic surface energy per unit thickness caused by the formation of the crack surfaces (this is a positive term),

F = work performed by external forces per unit thickness: this must be subtracted in Equation (2.1), since it is not part of the internal (potential) energy of the plate.

Griffith used a stress analysis developed by Inglis [12] to show that for unit thickness (see Figure 2.1)

$$U_a = \pi\sigma^2 a^2/E \tag{2.2}$$

where E is the Young's Modulus of the material.

Moreover, the elastic surface energy per unit thickness, U_γ, is equal to the product of the elastic surface energy of the material, γ_e, and the new surface area of the crack:

$$U_\gamma = 2(2a\gamma_e) \tag{2.3}$$

For the case where no work is done by external forces, the so-called fixed grip condition, F = 0. Since the change in elastic energy U_a, caused by introducing the crack in the plate, is negative; there is a decrease in elastic strain energy of the plate because it loses stiffness and the load applied by the fixed grips will therefore drop. Consequently, the total energy U of the cracked plate is

$$\begin{aligned} U &= U_o + U_a + U_\gamma \\ &= U_o - \pi\sigma^2 a^2/E + 4a\gamma_e \end{aligned} \tag{2.4}$$

Since Uo is constant, dU_o/da is zero, and the equilibrium condition for crack extension is obtained by setting du/da equal to zero

$$\frac{d}{da}(-\pi\sigma^2a^2/E + 4a\gamma_e) = 0 \qquad (2.5)$$

This is illustrated in Figure 2.2. Figure 2.2a schematically represents the two energy terms in Equation (2.5) and their sum as functions of the introduced crack length, 2a. Figure 2.2b represents the derivative, dU/da. When the elastic energy release due to a potential increment of crack growth, da, outweighs the demand for surface energy for the same crack growth, the introduction of a crack will lead to its unstable propagation.

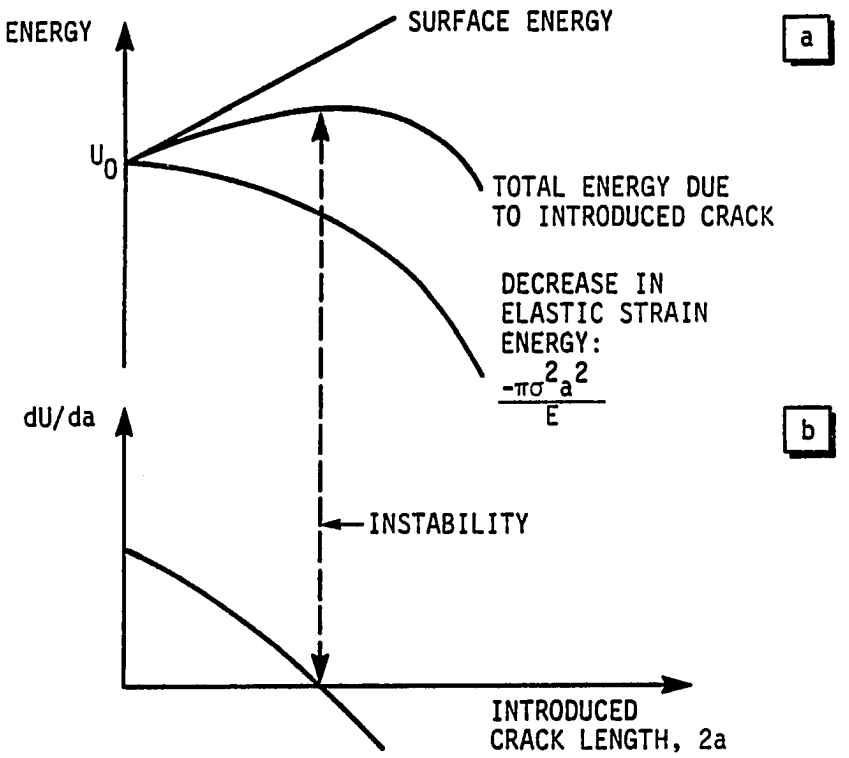

Figure 2.2. Energy balance of a crack in an infinite plate when no work is done by external forces

From the equilibrium condition (Equation. 2.5) one obtains

$$2\pi\sigma^2 a/E = 4\gamma_e \qquad (2.6)$$

Thus, crack extension occurs when $|2\pi\sigma^2 a/E| \rangle |4\gamma_e|$.
Equation 2.6 can be rearranged to

$$\sigma\sqrt{a} = (2E\gamma_e/\pi)^{1/2} \tag{2.7}$$

Equation (2.7) indicates that crack extension in ideally brittle materials is governed by the product of the remotely applied stress and the square root of the crack length and by material properties. Because E and γ_e are material properties the right-hand side of Equation (2.7) is equal to a constant value characteristic of a given ideally brittle material. Consequently, Equation (2.7) indicates that crack extension in such materials occurs when the product $\sigma\sqrt{a}$ attains a critical value.

Irwin's Modification to The Griffith Theory: Equation (2.6) may be rearranged in the form

$$\pi\sigma^2 a/E = 2\gamma_e \tag{2.8}$$

The left-hand side of Equation (2.8) has been designated the energy release rate, G, and represents the elastic energy per unit crack surface area that is available for infinitesimal crack extension. The right-hand side of Equation (2.8) represents the surface energy increase that would occur owing to infinitesimal crack extension and is designated the crack resistance, R. It follows that G must be at

least equal to R before unstable crack growth occurs. If R is a constant, this means that G must exceed a critical value G_c. Thus fracture occurs when

$$\pi\sigma^2 a/E \geq \pi\sigma^2_c a/E = G_c = R \qquad (2.9)$$

The critical value G_c can be determined by measuring the stress σ_c required to fracture a plate with a crack of size 2a.

In 1948, Irwin [2] suggested that the Griffith theory for ideally brittle materials could be modified and applied to both brittle materials and metals that exhibit plastic deformation. A similar modification was proposed by Orowan in 1955 [13]. The modification recognized that a material's resistance to crack extension is equal to the sum of the elastic surface energy, $2\gamma_e$, and the plastic strain work, γ_p, accompanying crack extension. Consequently, Equation (2.8) was modified to

$$\pi\sigma^2 a/E = 2(\gamma_e + \gamma_p) \qquad (2.10)$$

For relatively ductile materials $\gamma_p >> \gamma_e$, i.e., R is mainly plastic energy and the surface energy can be neglected.

Although Irwin's modification includes a plastic energy term, the energy balance approach to crack extension is still limited to defining the conditions required for instability of an ideally sharp crack.

The Stress Intensity Approach: Griffith's criterion is a global one and cannot be conveniently used to characterize different modes of fracture, i.e., crack opening versus shear or tear modes at the crack tip. Owing to the practical difficulties of this criterion a major advance was made by Irwin [14] in the 1957 when he developed the stress intensity approach. Irwin examined the analyses of Westergaard [15] and Sneddon [4] and noted that the strain energy release rate of an elastic body containing cracks could be related to the crack tip stresses by a single parameter.

First, from linear elastic theory Irwin [14] showed that for pure crack opening loads the stresses in the vicinity of a crack tip take the following form

$$\sigma_{xx} = [K/\sqrt{(2\pi r)}]\cos(\Theta/2)[1 - \sin(\Theta/2)\sin(3\Theta/2)] + ...$$

$$\sigma_{yy} = [K/\sqrt{(2\pi r)}]\cos(\Theta/2)[1 + \sin(\Theta/2)\sin(3\Theta/2)] + ...$$

$$\tau_{xy} = [K/\sqrt{(2\pi r)}]\cos(\Theta/2)\sin(\Theta/2)\cos(3\Theta/2) + ... \qquad (2.11)$$

where x, y are the cartesian coordinates and r, Θ are the cylindrical polar coordinates of a point with respect to the crack tip as shown in Figure 2.3.

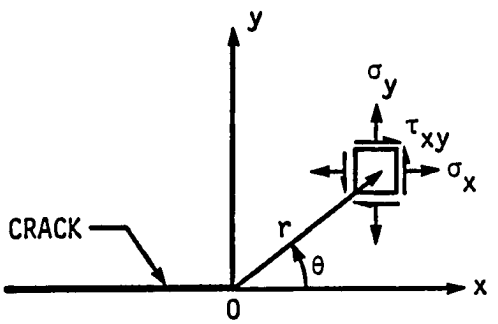

Figure 2.3. Stresses at a point ahead of a crack tip

In Equations 2.11, K is a constant which gives the magnitude of the elastic stress field. It is called the stress intensity factor. Dimensional analysis shows that K must be linearly related to stress and to the square root of a characteristic length. Equation (2.7) from Griffith's analysis indicates that this characteristic length is the crack length, and it turns out that the general form of the stress intensity factor is given by

$$K = \sigma\sqrt{(\pi a)} \cdot f(a/W) \qquad (2.12)$$

where f(a/W) is a dimensionless parameter that depends on the geometries of the specimen and crack.

Irwin then demonstrated that if a crack is extended by an amount da, the work done by the stress field ahead of the crack when moving through the displacements corresponding to a crack of length (a + da) is formally equivalent to the change in strain energy Gda. Thus the achievement of a critical stress intensity factor, K_c, is exactly equivalent to the Griffith-Irwin energy balance approach, which requires the achievement of a stored elastic strain energy equal to G_c.

The parameter governing fracture may therefore be stated as a critical stress intensity, K_c, instead of a critical energy value G_c. For tensile loading the relationships between K_c and G_c are

$$\begin{aligned} G_c &= K_c^2/E && \text{for plane stress and} \\ G_c &= K_c^2(1-\nu^2)/E && \text{for plane strain.} \end{aligned} \qquad (2.13)$$

Here ν is Poisson's ratio for the material. For plane strain it is customary to write G_{Ic} and K_{Ic}, where the subscript I indicates crack opening loads.

The Griffith-Irwin solution for a through-cracked plate can now be written as

$$\sigma\sqrt{(\pi a)} = [2E(\gamma_e + \gamma_p)]^{1/2} = (EG)^{1/2} = K \qquad (2.14)$$

and so the failure criterion is

$$\sigma\sqrt{(\pi a)} \geq \sigma_c\sqrt{(\pi a)} = K_c \tag{2.15}$$

More generally, however, it is to be noted that, as in the Griffith approach, the use of a critical stress intensity indicates that crack extension occurs when the product $\sigma\sqrt{a}$ attains a critical value. The value K_c can be determined experimentally by measuring the fracture stress for a large plate that contains a through-thickness crack of known length. This value can also be measured by using other specimen geometries, or else can be used to predict critical combinations of stress and crack length in these other geometries. What makes the stress intensity approach to fracture so powerful is that values of K for different specimen geometries can be computed with conventional elastic stress analyses. There are now several handbooks which give the stress intensity factor for many types of cracked bodies with different crack sizes, orientations, shapes, and loading conditions. Furthermore, the stress intensity factor, K, is applicable to stable crack extension and does to some extent characterize processes of subcritical cracking like fatigue and stress corrosion.

Another advantage of the stress intensity approach is that it is a local criterion, thus allowing different modes of crack tip deformations to be characterized separately. There are generally three basic modes of crack tip deformations as shown in Figure 2.4. K_I corresponds to opening mode, K_{II} to shearing mode, and K_{III} to tearing mode.

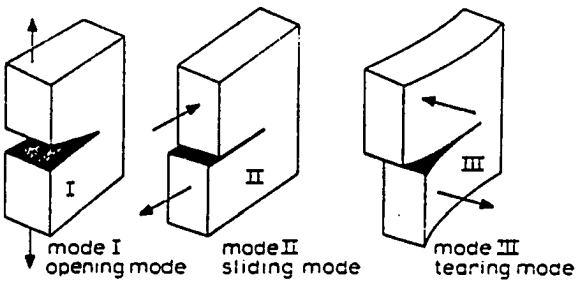

Figure 2.4. The three modes of loading at crack tips

The limitations of the stress intensity factor approach are inherent from the Westergaard equations [15]. Therefore, it is instructive to examine these equations.

Westergaard [15] used the properties of complex variable functions and showed that the stresses in an important group of elasticity problems are

$$\sigma_{xx} = \mathrm{Re}Z(z) - y\,\mathrm{Im}Z'(z)$$

$$\sigma_{yy} = \mathrm{Re}Z(z) + y\,\mathrm{Im}Z'(z)$$

$$\tau_{xy} = -y\,\mathrm{Re}Z'(z) \qquad (2.16)$$

where Z is an analytic function of the complex variable $z = x + iy = re^{i\Theta}$ and $Z' = \partial Z/\partial z$ and coordinates x, y, r and Θ are

as defined in Figure 2.3.

Westergaard [15] proposed the following stress function for a crack opened by symmetric loadings at infinity:

$$Z(z) = \sigma_\infty / [1-(a/z)^2]^{1/2} \qquad (2.17)$$

where, as before, a is equal to half the crack length.

Expanding Equation (2.17) and its derivative in a Taylor's series, retaining only the singular term, i.e., the term containing the $r^{1/2}$, and substituting into Equation (2.16) gives Equations (2.11) which are Westergaard approximate solutions for Equations (2.16).

The limitations of Westergaard solutions, apart from the obvious one of linear elastic behavior, are

a. As $r \to \infty$; $r^{-1/2} \to \infty$ and all stresses tend to infinity at the crack tip

b. $\sigma_{xx} = \sigma_{yy}$ and $\tau_{xy} = 0$ when $\Theta = 0$ along the line $y = 0$

Limitation (a) may be regarded as the result of a discrete discontinuity, a notch, present in an elastically loaded body. Its effect should be very localized and, according to St. Venant's

principle, the disturbance due to the discontinuity should vanish at a small distance away from the crack tip. Limitation (b) is required in order to satisfy the conditions of equilibrium and compatibility and its effect only becomes important at a distance remote from the crack tip.

Today, in spite of the above limitations, the stress intensity approach forms the basis of modern fracture technology.

CHAPTER 3. PHOTOELASTIC METHODS FOR DETERMINATION OF STRESS INTENSITY FACTORS

Introduction

In recent years, photoelasticity has emerged as a viable technique for determining stress intensity factors for a crack in a structural component. Several methods [16]-[47] have been proposed for the evaluation of the isochromatic fringes in a photoelastic experiment for stress intensity factor determination and it has been found that good agreement with available analytical results is possible. All these methods have their advantages and limitations. In this chapter, a critical review of these photoelastic methods is presented.

Relationship of Stress Intensity Factors to Isochromatic Fringe Order

The two-dimensional stress field in the vicinity of the tip of a crack loaded in both the opening and shearing modes is given [16] as:

$$\sigma_{xx} = \frac{K_I}{\sqrt{(2\pi r)}}\cos\frac{\Theta}{2}\left(1 - \sin\frac{\Theta}{2}\sin\frac{3\Theta}{2}\right) - \frac{K_{II}}{\sqrt{(2\pi r)}}\sin\frac{\Theta}{2}\left(2 + \cos\frac{\Theta}{2}\cos\frac{3\Theta}{2}\right) - \sigma_{ox}$$

$$\sigma_{yy} = \frac{K_I}{\sqrt{(2\pi r)}}\cos\frac{\Theta}{2}\left(1 + \sin\frac{\Theta}{2}\sin\frac{\Theta}{2}\right) + \frac{K_{II}}{\sqrt{(2\pi r)}}\sin\frac{\Theta}{2}\cos\frac{\Theta}{2}\cos\frac{3\Theta}{2}$$

$$\tau_{xy} = \frac{K_I}{\sqrt{(2\pi r)}}\cos\frac{\Theta}{2}\sin\frac{\Theta}{2}\cos\frac{3\Theta}{2} + \frac{K_{II}}{\sqrt{(2\pi r)}}\cos\frac{\Theta}{2}\left(1 - \sin\frac{\Theta}{2}\sin\frac{3\Theta}{2}\right) \qquad (3.11)$$

In the above equations, x and y are cartesian coordinates and r and Θ are polar coordinates with the origin defined at the crack tip as shown in Figure (3.1). K_I and K_{II} are the Mode one and Mode two stress intensity factors respectively and σ_{ox} is a far field non-singular stress term.

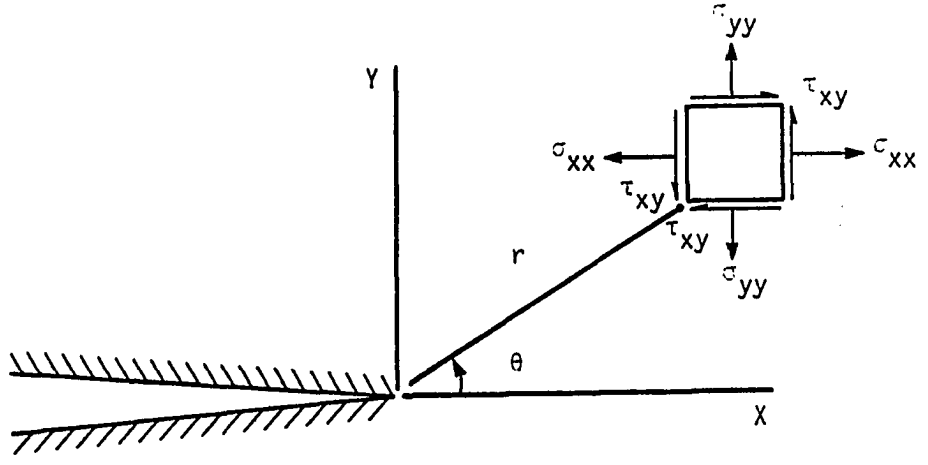

Figure 3.1. The cooordinate system for Equation 3.1

The stress optic law relates the maximum in-plane shear stress τ_{max} to the isochromatic fringe order N as

$$2\tau_{max} = (\sigma_1 - \sigma_2) = (Nf_\sigma)/h \qquad (3.2)$$

where N is the fringe order, f_σ is the material fringe value and h is the specimen thickness.

The maximum in-plane shear stress τ_{max} is related to the cartesian

components of stress by

$$2\tau_{max} = [(\sigma_{xx} - \sigma_{yy})^2 + 4\tau_{xy}]^{1/2} \tag{3.3}$$

Thus Equations (3.1) and Equation (3.2) may be substituted into Equation (3.3) to obtain the relationship between the isochromatic fringe order and the stress intensity factors as follows:

$$\left(\frac{Nf_\sigma}{h}\right)^2 = \frac{1}{2\pi r}[(K_I\sin\Theta + 2K_{II}\cos\Theta)^2 + (K_{II}\sin\Theta)^2]$$

$$+ \frac{2\sigma_{ox}}{\sqrt{(2\pi r)}}\sin(\Theta/2)[K_I\sin\Theta(1 + 2\cos\Theta)$$

$$+ K_{II}(1 + 2\cos^2\Theta + \cos\Theta)] + (\sigma_{ox})^2 \tag{3.4}$$

Photoelastic Methods for Determination of Mode One Stress Intensity Factor K_I

For cases where there is no shear or mode two loading on the crack, i.e, for pure mode one loading, several methods for estimation of K_I have been proposed in recent years. Five of these methods are reviewed here.

1. Irwin's Two-parameter Method: Irwin [17], in a discussion of a paper by Post and Wells [18], was the first to suggest the use of photoelastic data for determination of stress intensity factors. He

proposed a two-parameter method for determining K_I the opening mode stress intensity factor from the isochromatic fringe pattern. The two parameters are K_I and σ_{ox}. K_I is the stress intensity factor and σ_{ox} is the non-singular stress term, added to the Westergaard equations to satisfy the uniaxial loading condition and explaining the tilting of fringe loops away from the normal of the crack plane.

For opening mode crack tip deformation, i.e., $K_{II} = 0$, Equation (3.4) reduces to

$$(2\tau_{max})^2 = \frac{K_I^2 \sin^2\Theta}{2\pi r} + \frac{2K_I\sigma_{ox}}{\sqrt{(2\pi r)}} \sin\Theta \sin\frac{3\Theta}{2} + (\sigma_{ox})^2 \qquad (3.5)$$

Irwin observed the geometry of the fringe loops (Figure 3.2) and noted that at the extreme positions on the fringe loops where $r=r_m$ and $\Theta=\Theta_m$:

$$\frac{\partial \tau_{max}}{\partial \Theta} = 0$$

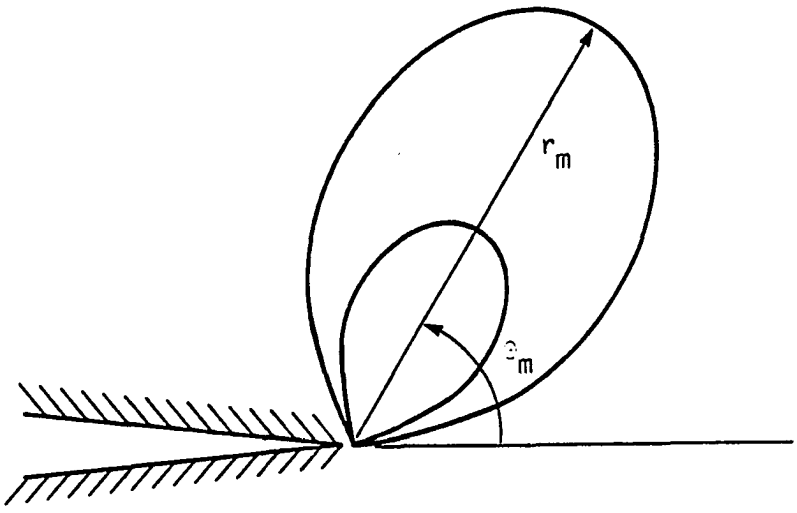

Figure 3.2. Irwin's two-parameter method

Differentiating Equation (3.5) with respect to Θ and using Equation (3.6) yields

$$\frac{K_I}{2\pi r_m}\sin 2\Theta_m + \frac{2K_I\sigma_{ox}}{\sqrt{(2\pi r_m)}}\left[\sin 2\Theta_m + \frac{1}{2}\sin\Theta_m \sin(3\Theta_m/2)\right] = 0 \qquad (3.7)$$

The two unknown parameters K_I and σ_{ox} are determined from the complete solution of Equations (3.5) and (3.7) as:

$$K_I = \frac{2\tau_{max}\sqrt{(2\pi r_m)}}{\sin\Theta_m}\left[1 + \frac{2\tan(3\Theta_m/2)}{3\tan\Theta_m}\right]\left\{1 + \left[\frac{2}{3\tan\Theta_m}\right]^2\right\}^{-1/2} \qquad (3.8)$$

and

$$\sigma_{ox} = \frac{-2\tau_{max}\cos\Theta_m}{\cos(3\Theta_m/2)[\cos^2\Theta_m + (9/4)\sin^2\Theta_m]^{1/2}} \qquad (3.9)$$

Equation (3.8) shows that the accuracy of K_I that can be obtained with Irwin's two-parameter method depends upon the precision in measuring r_m and Θ_m. In photoelastic analysis, due to the uncertainity as to the exact position of the crack tip and the difficulties in locating the extreme point on a given fringe loop, errors of ≥ 2 in measuring Θ_m are common and can result in large errors in the determination of K_I [18]-[20].

Etheridge and Dally [19] showed that Irwin's method is also sensitive to angular variation of Θ_m. They studied the problem of a centrally cracked infinite plate subjected to various combinations of biaxial loadings at the boundaries. Figure (3.3) shows that the error in K_I determined by Irwin's method varies from 3% at $\Theta_m = 90$ to infinity near $\Theta_m = 73$ or 139 .

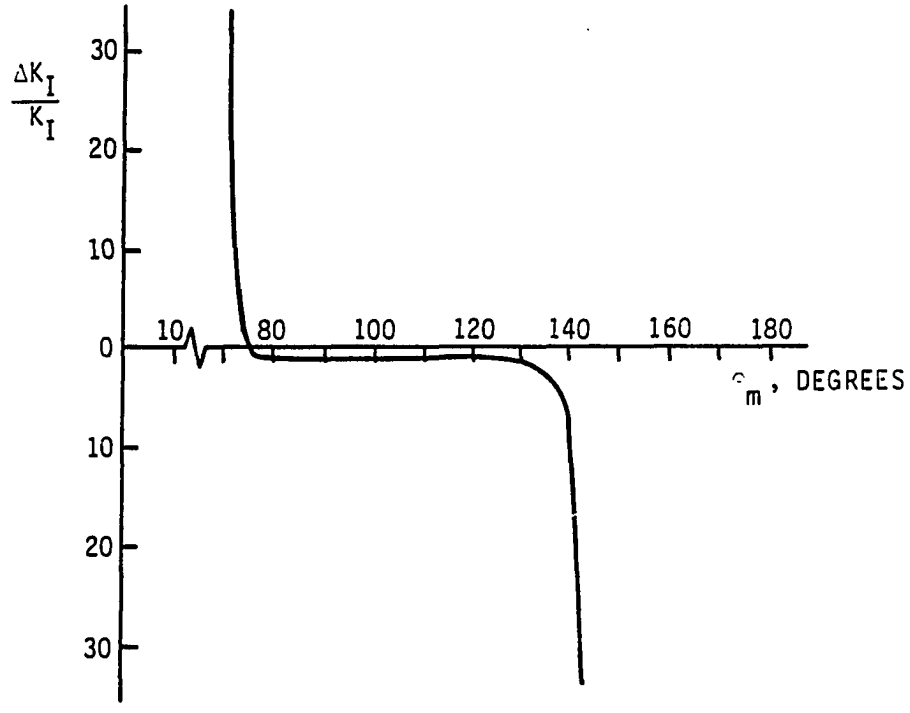

Figure 3.3 Relative error $[\Delta K_I/K_I]$ as function of tilt angle Θ_m [18]

2. Bradley-Kobayashi's Two-parameter Method: Bradley and Kobayashi [21,22] proposed a modification to the Irwin's method to reduce its sensitivity to error when Θ_m is close to either 73 or 139 . They made the following assumption:

$$\sigma_{ox} = \frac{K_I}{\sqrt{(2\pi r)}} \tag{3.10}$$

This reduces the Irwin's method to a single parameter characterization of the isochromatic fringe pattern. Equation (3.10) may be substituted into Equation (3.5) to obtain

$$2\tau_{max} = \frac{K_I}{\sqrt{(2\pi r)}} g(r,a,\Theta) \tag{3.11}$$

where

$$g(r,a,\Theta) = \left[\sin^2\Theta + 2\sqrt{(a/2r)}\, \sin\Theta \sin(3\Theta/2) + 2r/a \right]^{1/2}$$

Bradley and Kobayashi used data from two isochromatic fringe loops (r_1,Θ_1) and (r_2,Θ_2) in order to reduce the error associated with measuring r very close to the crack tip. They subtracted the corresponding maximum shear stresses τ_1 and τ_2 for the two fringe loops to obtain

$$2(\tau_2 - \tau_1)_{max} = K_I(g_2\sqrt{r_1} - g_1\sqrt{r_2})(2\pi r_1 r_2)^{-1/2} \tag{3.12}$$

which may be solved for K_I in terms of fringe orders as

$$K_I = 2(N_1 - N_2)(f_\sigma/h)(g_2\sqrt{r_1} - g_1\sqrt{r_2})(2\pi r_1 r_2)^{-1/2} \tag{3.13}$$

The advantages of Bradley-Kobayashi's method are that the need for obtaining data at the extreme position of the fringe loop is avoided and r may be measured along any angular direction.

3. Schroedl and Smith's Two-parameter Method: Schroedl and Smith [23,24] proposed a statistical iteration procedure for estimation of mode one stress intensity factor. This method uses several data points along any single, arbitrarily chosen angular direction and therefore takes advantage of the whole field nature of photoelastic data. Setting $\Theta = \pi/2$ in Equation (3.5) yields

$$(2\tau_{max})^2 = \frac{K_I^2}{2\pi r} + \frac{K_I \sigma_{ox}}{\sqrt{(\pi r)}} + \sigma_{ox}^2 \tag{3.14}$$

which may be solved for K_I:

$$K_I = \sqrt{(2\pi r)}\left\{ \left[2(Nf_\sigma/h)^2 - \sigma_{ox}^2 \right]^{1/2} - \sigma_{ox} \right\} \tag{3.15}$$

To simplify Equation (3.15), Schroedl and Smith neglected the σ^2_{0x} term and made use of the maximum shear stress differencing method for the i^{th} and j^{th} fringe loops to obtain the equation for estimating K_I:

$$(K_I)_{ij} = \frac{\sqrt{(2\pi r_i r_j)}}{\sqrt{r_j} - \sqrt{r_i}} (N_i - N_j)\frac{f_\sigma}{h} \tag{3.16}$$

The statistical iteration procedure they used consists of first obtaining a set of $(K_I)_{ij}$ values by applying Equation (3.16) to all

permutations of pairs of r and N. The average value, $(K_I)_{ave}$, and the absolute average deviation in the average value, $(\Delta K_I)_{ave}$, are calculated from this initial set of $(KI)_{ij}$ values. All those values of $(KI)_{aj}$ exceeding the value of $[(K_I)_{ave} \supset (\Delta K_I)_{ave}]$ are then eliminated. The remaining values of $(K_I)_{ij}$ are used to recalculate a new $(K_I)_{ave}$ value. The estimated value of K_I is equal to the new $(K_I)_{ave}$ value.

The accuracy of Schroedl-Smith's method depends on the initial photoelastic data. Generally, in stress analysis of crack problems, three distinct regions are defined near the crack tip. These are:

1. A nonlinear region (I) dominated by the effects of crack tip blunting, material and optical nonlinearities, triaxial stress field, etc.,
2. A linear region (II) dominated by the stress singularity associated with linear elastic fracture mechanics,
3. A far field region (III) dominated by the influence of boundaries and applied loads.

Figure (3.4) illustrates these regions.

I = NONLINEAR REGION
II = LINEAR REGION
III = FAR-FIELD REGION

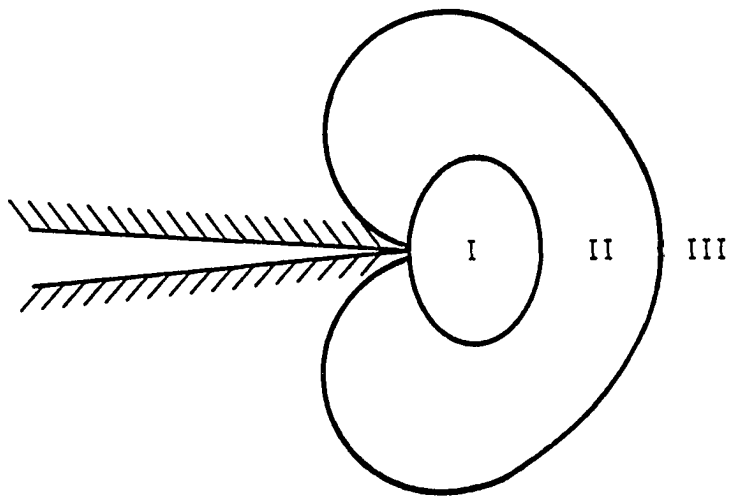

Figure 3.4. Three regions near the crack tip

It should be noted that in this method the value of K_I estimated from photoelastic data obtained from regions other than the linear region is inaccurate. Therfore, special care should be taken when applying the statistical iteration procedure to all the values of $(K_I)_{ij}$.

4. The Linear Slope Method: Ruiz [25,26] proposed this method for determining K_I from the whole field isochromatic fringe pattern. In this method, the maximum shear stress along a given angular direction is plotted against the inverse square root distance from the crack tip, $1/\sqrt{r}$. Substituting $k_I = K_I/[\sigma_\infty\sqrt{(\pi a)}]$ and $2\tau_{max} = \sigma_1 - \sigma_2$ in Equation (3.14) and dividing both sides by $(\sigma_\infty)^2$ yields (σ_∞ is the far-field uniform tensile stress):

$$\left[\frac{\sigma_1 - \sigma_2}{\sigma_\infty}\right]^2 = k_I^2\left[\frac{a}{2r}\right] + k_I\left[\frac{\sigma_{ox}}{\sigma_\infty}\right]\left[\frac{a}{r}\right]^{1/2} + \left[\frac{\sigma_{ox}}{\sigma_\infty}\right]^2 \qquad (3.17)$$

Equation (3.17) can be rearranged in the following form:

$$\left[\frac{\sigma_1 - \sigma_2}{\sigma_\infty}\right] = k_I\left[\frac{a}{2r}\right]^{1/2}\left\{1 + 2\sum_{m=1}^{2}\left[\frac{1}{k}\frac{\sigma_{ox}}{\sigma_\infty}\left[\frac{r}{a}\right]^{1/2}\right]^m\right\} \qquad (3.18)$$

If $(\sigma_1 - \sigma_2)/\sigma_\infty$ is plotted against $(a/2r)^{1/2}$ a straight line of slope k_I in the singular stress region is obtained as shown in Figure 3.5.

Nonlinearity effects very close to the crack tip and the far field nonsingular stress terms cause the departure from linearity in regions (I) and (II) respectively.

The nondimensional stress intensity factor k_I can be directly evaluated from the slope of the plot over the linear singular stress region.

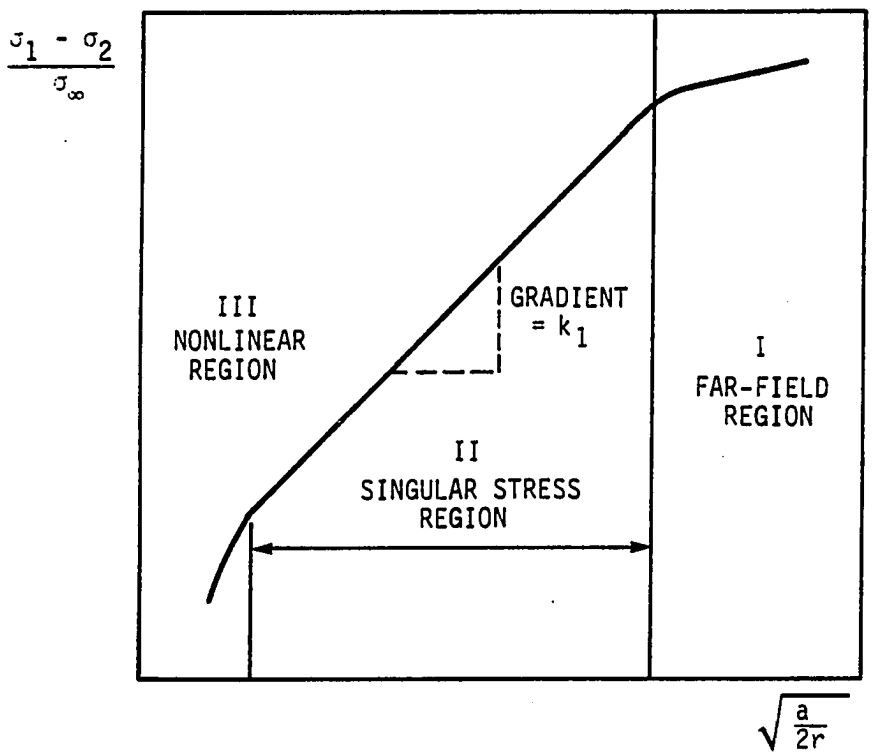

Figure 3.5 Linear slope plot

Ruiz and Pearson [27,28] applied the linear slope method to a compact tension specimen and reported good agreement between experimental and analytical results. The linear slope method has also been applied to various cracked pressure vessel configurations [26-31].

5. Taylor Series Correction Method: Smith [32] suggested that the maximum in-plane shearing stress may be expressed in terms of a standard singular stress term with additional terms expressed by a Taylor series expansion to account for the far field effect. He proposed the following expression for the Taylor series:

$$\tau_{max} = \frac{A}{\sqrt{r}} + \sum_{n=1}^{\infty} \left[B_n (r)^{n/2} \right] \qquad (3.19)$$

where $A = K_I/\sqrt{(8\pi)}$. Equation 3.19 is then combined with the stress-optic law (Equation 3.2), and experimental values of r and N are used in a least square curve fitting procedure to determine the unknown coefficients (A and B_n) and hence the stress intensity factor.

Smith [33]; Smith et al. [34] stated that proper truncation criteria for the Taylor series correction method has not yet been established and the use of the Taylor series correction method for estimation of K_I should be avoided. He modified the method by defining an "apparent" stress intensity factor as:

$$K_{AP} = \tau_{max}\sqrt{(8\pi r)} \qquad (3.20)$$

Equation (3.20) is then substituted for τ_{max} in Equation (3.19) and both sides of the resulting equation are divided by $\sigma_\infty\sqrt{(\pi a)}$ to obtain:

$$\frac{K_{AP}}{\sigma_\infty\sqrt{(\pi a)}} = \frac{K_I}{\sigma_\infty\sqrt{(\pi a)}} + \sum_{n=1}^{\infty} C_n \left[\frac{r}{a}\right]^{n/2} \tag{3.21}$$

If only the first term of the summation series is considered and $K_{AP}/\sigma_\infty\sqrt{(\pi a)}$ is plotted against $(r/a)^{1/2}$ a linear region is obtained as shown in Figure (3.6).

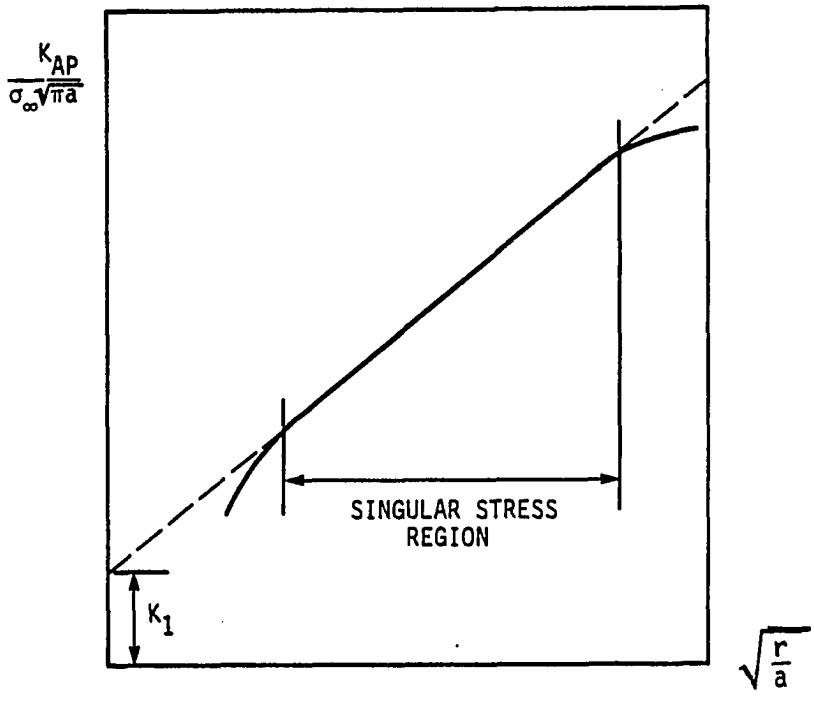

Figure 3.6. Smith's apparent stress intensity factor plot

The nondimensional stress intensity factor K_I is obtained by fitting a straight line through the linear region and extrapolating the straight line to the crack tip, r = 0.

Photoelastic Methods for Determination of Mixed Mode Stress Intensity Factors K_I and K_{II}

Mixed mode stress intensity factors K_I and K_{II} control the severity of the stress singularity at the tip of a crack subjected to both tensile and shearing stresses.

Recently, photoelasticity has been applied to study mixed mode crack problems [20,35-37]. The isochromatic fringe pattern for the mixed mode case is similar to the opening mode case except that the pattern is now rotated at an angle Θ, which depends upon the ratio of K_{II}/K_I. This is shown in Figure (3.7).

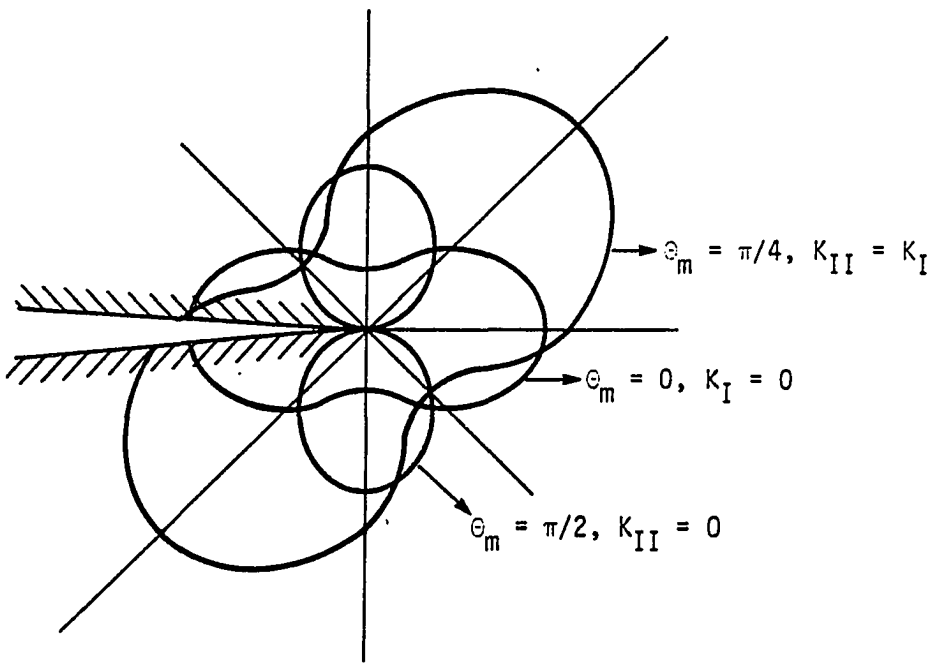

Figure 3.7. Mixed mode isochromatic fringe pattern

Six different photoelastic methods for determination of SIFs which can be applied to the mixed mode case are discussed below.

1. Smith-Smith Method [35]: This method in principle is similar to the two-parameter method for determination of mode one stress intensity factor proposed by Irwin. Letting $\sigma_{ox} = 0$ in Equation (3.4) yields

$$2\tau_{max} = \sigma_1 - \sigma_2 = \frac{1}{\sqrt{(2\pi r)}} \left\{ (K_I \sin\Theta + 2K_{II}\cos\Theta)^2 + (K_{II}\sin\Theta)^2 \right\}^{1/2} \quad (3.22)$$

This equation can be differentiated with respect to Θ and then the condition $(\partial\tau_{max}/\partial\Theta) = 0$ at the extreme position of the fringe loop, $r = r_m$ and $\Theta = \Theta_m$, may be applied to obtain

$$(K_{II}/K_I)^2 - (4/3)(K_{II}/K_I)\cot\Theta_m - 1/3 = 0 \quad (3.23)$$

It can be seen from Equation (3.23) that Θ_m alone controls the ratio of K_{II}/K_I. Therefore, the values of K_I and K_{II} can be determined using Equation (3.23) together with Equation (3.22) from any point (r,Θ) on the fringes.

The derivation of Equation (3.23) assumed that $\sigma_{ox} = 0$. Smith and Smith [35] suggested that the influence of σ_{ox} can be eliminated by obtaining a set of K_I and K_{II} values from fringes near to the crack tip.

These values are then extrapolated to the crack tip to give the estimated values of K_I and K_{II}.

2. The Linear Slope Method: Phang and Ruiz [38] suggested that the idea of the linear slope method proposed by Ruiz can also be extended to the determination of mixed mode stress intensity factors. To determine the two unknown stress intensity factors measurements along two angular directions are made. The two angular directions chosen are usually along the line parallel to the crack plane ($\Theta = 0$) and along the line normal to the crack plane ($\Theta = 90$). Substituting $\Theta = 0$ and $\Theta = 90$ into Equation (3.22) gives:

$$\Theta = 0: \qquad \left[\frac{\sigma_1 - \sigma_2}{\sigma_\infty}\right] = 2k_{II}\left[\frac{a}{2r}\right]^{1/2} \tag{3.24}$$

and

$$\Theta = 90: \qquad \left[\frac{\sigma_1 - \sigma_2}{\sigma_\infty}\right] = \left[k_I^2 + k_{II}^2\right]^{1/2}\left[\frac{a}{2r}\right]^{1/2} \tag{3.25}$$

A plot of $(\sigma_1 - \sigma_2)/\sigma_\infty$ against $(a/2r)^{1/2}$ would yield a straight line of slope $2K_{II}$ for Equation (3.24) and $(k_I^2 + k_{II}^2)^{1/2}$ for Equation (3.25) over the singular stress region. From the slope of these plots, the values of k_I and k_{II} may be deduced.

Sanford and Dally [20] proposed four different methods for determination of mixed mode stress intensity factors.

3. The Selected Line Method: This method is based on the Bradley-Kobayashi shear differencing method. Letting $\Theta = 0$ or 180 in Equation (3.4) yields

$$\frac{Nf_\sigma}{h} = \frac{2K_{II}}{\sqrt{(2\pi r)}} + \sigma_{ox} \tag{3.26}$$

Substituting two fringes (N_i, r_i) and (N_j, r_j) and eliminating σ_{ox} gives

$$K_{II} = \left[\frac{\pi}{2}\right]^{1/2} \left[\frac{(N_i - N_j)f_\sigma}{h}\right] \left[\frac{\sqrt{(r_i r_j)}}{\sqrt{r_i} - \sqrt{r_j}}\right] \tag{3.27}$$

Equations (3.26) and (3.27) are now solved simultaneously to determine σ_{ox} as:

$$\sigma_{ox} = - \left\{ \frac{2K_{II}}{\sqrt{(2\pi r)}} + \left[\frac{Nf_\sigma}{h}\right] \right\} \tag{3.28}$$

Values of K_{II} and σ_{ox} obtained from Equations (3.27) and (3.28) are then substituted into Equation (3.4) which can be solved quadratically to determine K_I.

4. The Classical Method: In this method the classical Irwin two-parameter method is coupled with the Newton-Raphson finite difference method. From Equation (3.4) the following function may be defined:

$$F(K_I, K_{II}, \sigma_{ox}) = (Nf_\sigma/h)^2 - f(K_I, K_{II}, \sigma_{ox}, r, \Theta) = 0 \qquad (3.29)$$

Equation (3.4) may be differentiated with respect to Θ to obtain

$$G(K_I, K_{II}, \sigma_{ox}) = \frac{\partial \tau_{max}}{\partial \Theta}$$

$$= \frac{1}{2\pi r}(K_I^2 \sin 2\Theta + 4K_I K_{II} \cos 2\Theta - 3K_{II}^2 \sin 2\Theta)$$

$$+ \frac{2\sigma_{ox}}{\sqrt{2\pi r}}\left\{\sin\frac{\Theta}{2}[K_I(\cos\Theta + 2\cos 2\Theta) - K_{II}(\sin\Theta + 2\sin 2\Theta)]\right\}$$

$$+ \frac{1}{2}\cos\frac{\Theta}{2}[K_I(\sin\Theta + \sin 2\Theta) + K_{II}(2 + \cos\Theta + \cos 2\Theta)] \qquad (3.30)$$

Values of r_m and Θ_m obtained from the extreme positions of any two fringe loops near to the crack tip are now substituted into Equation (3.30) to yield two independent equations as follow

$$G_i(K_I, K_{II}, \sigma_{ox}) = 0$$
$$G_j(K_I, K_{II}, \sigma_{ox}) = 0 \qquad (3.31)$$

The subscripts i,j refer to the i^{th} and j^{th} loops respectively.

Equations (3.31) together with Equation (3.29) form three independent equations which are solved numerically by the Newton-Raphson finite difference method to determine the three unknowns K_I, K_{II}, and σ_{ox}.

5. The Three-point Deterministic Method: In this method three arbitrary data points (r_1,Θ_1), (r_2,Θ_2) and (r_3,Θ_3) are selected from the isochromatic fringes. These data are used together with Equation (3.4) to generate three simultaneous equations

$$F_k(K_I, K_{II}, \sigma_{ox}) = 0, \qquad k = 1,2,3 \qquad (3.32)$$

The Newton-Raphson finite difference method is used to solve these equations to determine K_I, K_{II} and σ_{ox}.

6. The Multiple-Points Over Deterministic Method: In this method Equation (3.4) is fitted to a large number of data points over the isochromatic field to determine K_I, K_{II} and σ_{ox}. The fitting process involves both the Newton-Raphson method and the minimization

process associated with a least squares method.

Initial estimations of $(K_I)_i$, $(K_{II})_i$ and $(\sigma_{ox})_i$ are made in Equation (3.32). Because the initial estimations are always in error, it will follow that

$$F_k[(K_I)_i,(K_{II})_i,(\sigma_{ox})_i] = 0 \tag{3.33}$$

Equation (3.32) is now expanded as a Taylor series in order to make corrections for the initial estimations in the following form:

$$(F_k)_{i+1} = (F_k)_i + (\partial F/\partial K_I)_i \Delta K_I + (\partial F/\partial K_{II})_i \Delta K_{II} + (\partial F/\partial \sigma_{ox})_i \Delta \sigma_{ox} \tag{3.34}$$

ΔK_I, ΔK_{II} and $\Delta \sigma_{ox}$ are the corrections for the initial estimations. For a set of m data points, Equation (3.34) can be expressed in matrix form as follow:

$$\begin{bmatrix} F_1 \\ \vdots \\ F_m \end{bmatrix}_{i+1} = \begin{bmatrix} F_1 \\ \vdots \\ F_m \end{bmatrix}_i + \begin{bmatrix} \frac{\partial F_1}{\partial K_I} & \frac{\partial F_1}{\partial K_{II}} & \frac{\partial F_1}{\partial \sigma_{ox}} \\ \vdots & \vdots & \vdots \\ \frac{\partial F_m}{\partial K_I} & \frac{\partial F_m}{\partial K_{II}} & \frac{\partial F_m}{\partial \sigma_{ox}} \end{bmatrix} \begin{bmatrix} \Delta K_I \\ \Delta K_{II} \\ \Delta \sigma_{ox} \end{bmatrix} \tag{3.35}$$

In Equation (3.35), the subscript i refers to the i^{th} iteration step. The corrections are determined by the Newton-Raphson finite difference method such that

$$[F_k]_{i+1} = 0 \tag{3.36}$$

or

$$[F] = [C]\ [\Delta K] \tag{3.37}$$

In Equation (3.37), the matrixes are defined as follow

$$\left[F \right] = \begin{bmatrix} F_1 \\ \cdot \\ \cdot \\ \cdot \\ \cdot \\ \cdot \\ F_m \end{bmatrix}, \qquad \left[C \right] = - \begin{bmatrix} \frac{\partial F_1}{\partial K_I} & \frac{\partial F_1}{\partial K_{II}} & \frac{\partial F_1}{\partial \sigma_{ox}} \\ \cdot & \cdot & \cdot \\ \cdot & \cdot & \cdot \\ \cdot & \cdot & \cdot \\ \cdot & \cdot & \cdot \\ \cdot & \cdot & \cdot \\ \cdot & \cdot & \cdot \\ \frac{\partial F_m}{\partial K_I} & \frac{\partial F_m}{\partial K_{II}} & \frac{\partial F_m}{\partial \sigma_{ox}} \end{bmatrix}$$

and

$$\left[\Delta K \right] = \begin{bmatrix} \Delta K_I \\ \Delta K_{II} \\ \Delta \sigma_{ox} \end{bmatrix}$$

For $m > 3$, [c] is not a square matrix, the determination of the elements of the corrections matrix $[\Delta K]$ is accomplished by multiplying both sides of Equation (3.37) by the transpose of matrix [C]:

$$\begin{aligned}[a]^T[F] &= [C]^T[C][\Delta K] \\ &= [D][\Delta K] \end{aligned} \tag{3.38}$$

The values of ΔK_I, ΔK_{II} and $\Delta\sigma_{ox}$ are obtained with matrix manipulation and used to correct the previous estimations of K_I, K_{II} and σ_{ox} in order to obtain a better fit to the function $F_k(K_I, K_{II}, \sigma_{ox})$ of m data points, as follow

$$\begin{aligned}[K_I]_{i+1} &= (K_I)_i + (\Delta K_I)_i \\ [K_{II}]_{i+1} &= (K_{II})_i + (\Delta K_{II})_i \\ [\sigma_{ox}]_{i+1} &= (\sigma_{ox})_i + (\Delta\sigma_{ox})_i \end{aligned} \tag{3.39}$$

The above procedures are repeated until $[\Delta K]$ becomes acceptably small.

Effect of Some Factors on Photoelastic Determination of Stress Intensity Factors

Effect of Nonlinearity Near the Crack-Tip: The basic causes for the existence of nonlinearity near the crack-tip in a photoelastic model are: a) the physical effect and b) the artificial sharp-notch effect.

The physical effect arises from the presence of very high stresses, the existence of triaxial stress field and the rapid variations of stress gradient and refractive index at the crack tip. The consequences of the physical effect are the accruing of blunting, finite rotation and deformation at the crack tip. McGowan and Smith [39] and Smith et al. [41] investigated the influence of the near crack tip nonlinearities, resulting from the physical effects, on the photoelastic determination of stress intensity factor. They employed plane strain small deformation plasticity theory and predicted that the onset of nonlinearity would occur at approximately $(r/a)^{1/2} = 0.173$, i.e., the enclave of the nonlinear region is less than 0.03 of the crack length from the crack tip. Taking their analysis to be exact, it is clear that the crack tip nonlinearities due to the physical effect are extremely local and would not normally be measurable in photoelastic experiments.

In photoelastic analysis, it is necessary to simulate the crack tip behavior by artificial notches of finite root radius. One of the most commonly used artificial notches is that of a rectangular slot with rounded ends as shown in Figure (3.8).

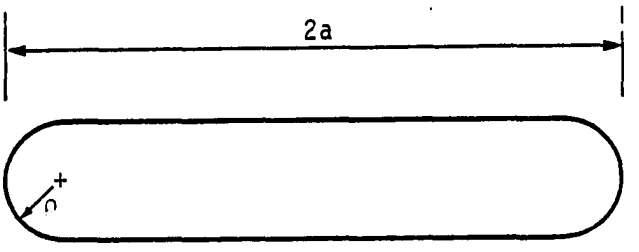

Figure 3.8. Rectangular slot with rounded ends

Schroedl et al. [24] studied the influence of the finite root radius on the stress distribution by comparing the well known Kolosoff-Inglis solution for an oblong elliptic hole, approximately equivalent to a rectangular slot with rounded ends, to the solution of a line crack and found that the stress distribution very near to the notch tip depends on its root radius. However away from the notch tip, the influence diminishes rapidly and the stress distribution approaches that of a line crack.

Schroedl and Smith [42], using the conformal mapping technique, showed that the influence of notch root radii on the stress distribution are in general small and a notch of any geometry can be use to simulate crack tip behavior provided the root radius and width are small and photoelastic data are taken sufficiently far away from the affected region.

Effect of Far Field Nonsingular Stress Term: In early

application of photoelasticity to fracture mechanics analysis, various techniques [35,43,44] were introduced which emphasized the omission of the nonsingular stress term. However, except for the case of the problem of a central crack in a specimen subjected to uniform equibiaxial load factor of 1.0, all other problems [45] show the isochromatic fringes begin their shift under biaxial loading right from the crack tip. This suggests that nonsingular stress term should be incorporated in the maximum shear difference for correct evaluation of isochromatic fringes. Sih [46] also Eftis and Liebowitz [47] showed that the non-singular stress term always influences the behavior of the crack tip in an infinite sheet under biaxial loading. Lee and Liebowitz [48] and Oladimeji [49,50] demonstrated numerically that the same influence exists in finite sheet specimens.

Irwin [17], in a discussion of the paper by Post and Wells [18], was first to suggest the inclusion of an adjustable nonsingular stress term in the maximum shear expression to take into account the effect of the far field stresses. Specific expressions have since been developed [46,48] which show the relationship of the nonsingular stress to the boundary loading and the specimen geometry.

Effect of Poisson's Ratio: Shah and Kobayashi [51] investigated the influence of Poisson's ratio on the value of the stress intensity factor. They found that the effect of a high Poisson ratio is to increase the value of the stress intensity factor by an amount that depends upon the local stress intensity. For example, the influence of Poisson's ratio on the value of the stress intensity factor is higher

for two interacting cracks with high local stress intensity than for a single crack.

References

1. A. A. Griffith. "The Theory of Rupture." Proc. 1st Int. Cong. Appl. Mech., Delft (1924), 55-63.

2. G. R. Irwin. "Fracture Dynamics." Fracturing of Metals, ASM publ., (1948), 147-166.

3. G. C. Sih. Mechanics of Fracture (I): Methods of Analysis and Solutions of Crack Problems. Leyden: Noordhoff Int. Publ., 1973.

4. I. N. Sneddon. "The Distribution of Stress in the Neighbourhood of a Crack in an Elastic Solid." Proc. R. Soc., A187 (1946), 229-260.

5. A. E. Green and I. N. Sneddon. "The Distribution of Stress in the Neighbourhood of a Flat Elliptical Crack in an Elastic Solid." Proc. of Camb. Phil. Soc., No. 46 (1950), 159-163.

6. T. A. Cruse and F. J. Rizzo (ed.). "Boundary-Integral Equation Method: Computational Applications in Applied Mechanics." ASME, AMD, (1975).

7. H. Nisitani and Y. Murakami. "Stress Intensity Factors of an Elliptical Crack or a Semi-Elliptical Crack Subject to Tension." Int. J. Fract., No. 10 (1974), 353-368.

8. G. C. Sih. Mechanics of Fracture (II): Three-dimensional Crack Problems. Leyden: Noordhoof Int. Publ., 1975.

9. G. C. Sih (ed.). Mechanics of Fracture (VII): Experimental Evaluation of Stress Concentration and Intensity Factors. New York: Martinus-Nijhoff Publ., 1981.

10. C. W. Smith. "Use of Three-dimensional Photoelasticity in Fracture Mechanics." Expt. Mech., 13, No. 12 (1973), 539-544.

11. J. Morton and C. Ruiz. "Photoelasticity in the Assessment of Structural Integrity." Expt. Mech., 22, No. 6 (1982), 7.

12. C. E. Inglis. "Stresses in a Plate due to the Presence of Cracks and Sharp Corners." Trans. Inst. Naval Architects, 55 (1913), 219-241.

13. E. Orowan. "Energy Criteria of Fracture." Welding Journal, No. 34 (1955), 1575-1605.

14. G. R. Irwin. "Analysis of Stresses and Strains Near the End of a Crack Transversing a Plate." J. Appl. Mech., No. 24 (1957), 361-364.

15. H. M. Westergaard. "Bearing Pressures and Cracks." J. Appl. Mech., No. 6 (1939), 49-53.

16. P. C. Paris and G. C. Sih. "Stress Analysis of Cracks." ASTM, STP, No. 381 (1964), 30-81.

17. G. R. Irwin. "Discussion of Ref. (3)." Proc. Soc. Expt. Stress Analysis, No. 16 (1958), 93-968.

18. D. Post and A. A. Wells. "The Dynamic Stres Distribution Surrounding a Running Crack - a Photoelastic Analysis." Proc. Soc. Expt. Stress Analysis, No. 16 (1958), 69-92.

19. J. M. Etheridge and J. W. Dally. "A Critical Review of Methods for Determining Stress Intensity Factors from Isochromatic Fringes." Expt. Mech., 17, No. 7 (1977), 248-254.

20. R. J. Sanford and J. W. Dally. "A General Method for Determining Mixed Mode Stress Intensity Factors from Isochromatic Fringe Patterns." Eng. Fract. Mech., No. 11 (1979), 621-633.

21. W. B. Bradley and A. S. Kobayashi. "An Investigation of Propagation Cracks by Dynamic Photoelasticity." Expt. Mech., 10, No. 3 (1970), 106-113.

22. A. S. Kobayashi and W. B. Bradley. "Fracture Dynamics - An Photoelastic Investigation." Eng. Fract. Mech., 3, No. 3 (1971), 317-332.

23. M. A. Schroedl and C. W. Smith. "Local Stresses Near Deep Surface Flaws Under Cylindrical Fields." ASTM, STP, No. 538 (1973), 45-57.

24. M. A. Schroedl, J. J. McGowan and C. W. Smith. "An Assessment of Factors Influencing Data Obtained by the Photoelastic Stress Freezing Technique for Stress Field Near Crack Tips." Eng. Fract. Mech., No. 7 (1975), 341-355.

25. C. Ruiz. "Experimental Determination of Stress Distribution Near Notches and Slits in Cylindrical Pressure Vessels." Proc. Conf. Expt. Stress Analysis Inst. Mech. Eng., London, 1970.

26. C. Ruiz. "Stress and Strain Distribution Around Cracks in Complex Pressure Vessel Configurations." Conf. Struct. Mech. & Reactor Tech. BAM, Berlin, 1971.

27. C. Ruiz and G. Pearson. "Stress Intensity Factors for Cracks in Pressure Vessel Nozzles." Int. J. Fract., No. 13 (1977), 319-339.

28. G. Pearson and C. Ruiz. "Photoelastic Determination of Stres Intensity Factors in Vessels." Proc. Conf. on tolerance of flaws in pressurized Components, I. Mech. Eng., London, 1978.

29. J. Morton and C. Ruiz. "Through Cracks in Pipes and Pipe Bends." Proc. 4th Int. Conf. in Press. Vessal tech. I. Mech. Eng., London, 1980.

30. A. Astiz, M. Elices, J. Morton and A. Valiente. "A Photoelastic Determination of K_I for an Edge-Cracked Rod in Tension." Proc. SESA, Dearborn, 1981.

31. J. Morton and C. Ruiz. "Photoelasticity in the Assessment of Structural Integrity." Expt. Mech., 22, No. 6 (1982).

32. C. W. Smith. "Use of Three-dimensional Photoelasticity in Fracture Mechanics." Expt. Mech., 13, No. 12 (1973), 539-544.

33. C. W. Smith. "Use of Photoelasticity in Fracture Mechanics." Mechanics of fracture (7): Experimental Evaluation of Stress Concentration and Intensity Factor. (Ed. G. C. Sih). New York: Martinus-Nijhoff Publ., 1982.

34. C. W. Smith, W. H. Peters, W. T. Hardrath and T. S. Fleischmn. "Stress Intensity Distributions in Nozzle Corner Cracks of Complex Geometry." Virg. Poly. Inst., VPI-E-79-2 1979.

35. D. G. Smith and C. W. Smith. "Photoelastic Determination of Mixed Mode Stress Intensity Factors" Eng. Fract. Mech., No. 4 (1972), 357-366.

36. E. E. Gdoutos and P. S. Theocaris. "A Photoelastic Determination of Mixed Mode Stress Intensity Factors." Expt. Mech., 18, No. 3 (1978), 87-96.

37. C. W. Smith and J. S. Epstein. "An Assessment of Far Field Effects on the Photoelastic Determination of Mixed Modes Stress Intensity Factors." Eng. Fract. Mech., 16, No. 5 (1982), 605-612.

38. Y. Phang and C. Ruiz. "Photoelastic Determination of Stress Intensity Factors for Single and Interacting Cracks and Comparison with Calculated Results." J. Strain Analysis, 19, No. 1 (1984), 23-41.

39. J. J. McGowan and C. W. Smith. "A Finite Deformation Analysis of Near Field Surrounding the Tip of Crack Like Elliptical Perforations." Int. J. Fract., 11, No. 6 (1975), 977-987.

40. J. J. McGowan and C. W. Smith. "A Plane Strain Analysis of Blunted Crack Tip Using Small Deformation Plasticity Theory." Advances in Eng. Sci., 2 (1976), 585.

41. C. W. Smith, J. J. McGowan and W. H. Peters. "A Study of Crack Tip Nonlinearities in Frozen Stress Field." Expt. Mech., 18, No. 8 (1978), 309-314.

42. M. A. Schroedl and C. W. Smith. "A Study of Near and Far Field Effects in Photoelastic Stress Intensity Determination." Eng. Fract. Mech., 4, No. 4 (1972), 801-809.

43. R. H. Marloff, M. M. Leven, T. V. Ringer and R. I. Johnson. "Photoelastic Determination of Stress Intensity Factors." Expt. Mech., 11. No. 12 (1971), 529-539.

44. D. B. Chisholm and D. L. Jones. "An Analytical and Experimental Stress Analysis of a Practical Mode II Fracture Test Specimen." Expt. Mech., 17, No. 1 (1977), 7-13.

45. J. W. Dally and R. J. Sanford. "Classification of Stress Intensity Factors From Isochromatic Fringe Patterns." Expt. Mech., 18, No. 2 (1978), 441-448.

46. G. C. Sih. "On The Westergaard Method of Crack Analysis." Int. J. Fract. Mech., 2 (1966), 628-630.

47. J. Eftis and H. Liebowitz. "On The Modified Westergaard Equations for Certain Plane Crack Problems." Int. J. Fract. Mech., 8, No. 4 (1972), 383-392.

48. J. D. Lee and H. Liebowitz. "A Finite Element Analysis of the Effects of Biaxial Loading on Fracture." U. S. Department of Navy, NAVY-14-77-c-946.

49. M. K. Oladimeji. "An Analytical and Experimental Investigation of Biaxial Loading Effects on Cracks Emanating From a Circular Hole." D. Sci. Dissertation, The George Washington University, Washington, D.C., 1980.

50. M. K. Oladimeji. "Cracks Emanating From a Circular Hole Under Biaxial Load." Engng. Fract. Mech., 15, No. (3-4) (1981), 391-405.

51. R. C. Shah and A. S. Kobayashi. "Stress Intensity Factors for an Embedded Crack Approaching the Surfaceof a Semi Infinite Solid." J. of Fract., 9, No. 2 (1973), 133-146.

PAPER I. STRESS INTENSITY FACTORS FOR NEAR EDGE CRACKS BY DIGITAL IMAGE ANALYSIS

Abstract

Experimental stress intensity factors (SIFs) are evaluated for single, straight near edge cracks in a plate of finite width. The cracks are positioned at various angles and distances with respect to the edge of the plate. The far field stress is uniform tension parallel to the edge. On-line digital image analysis procedures are used to extract photoelastic data from the whole field isochromatic fringe patterns.

Two different techniques are used to obtain information on the near crack tip stress field: (1) Half fringe photoelasticity (HFP), which requires adjusting the load to keep the maximum fringe order less than 0.5 in the data extraction zone, and (2) Trace, a digital fringe sharpening procedure, which accurately produces traces of all half- and full-order fringes. The load is adjusted to yield multiple fringes in the field of data extraction.

Experimental SIFs from HFP and Trace are compared to each other and to the numerical results that are determined by the boundary integral equation method.

Notation

α = orientation of crack line with respect to the long axis

a = one-half crack length

A = crack tip further from the centroidal axis

B = crack tip closer to the centroidal axis

c = distance from the center of crack to the closer free edge

d = ligament size (i.e., distance between the free edge and the closer crack tip)

K_I = mode one stress intensity factor

K_{II} = mode two stress intensity factor

N = fringe order

r, θ = polar coordinates (as defined in Fig. 2)

σ = stress

SIF = stress intensity factor

HFP = half fringe photoelasticity

E = Young's Modulus

ν = Poisson's Ratio

f_σ = Material Fringe Value

Introduction

Half fringe photoelasticity (HFP) [1] combines digital image analysis with interactive computer technology into an on-line photoelastic system through a video scanner. Since this technique offers high resolution in fields of low birefringence, it overcomes the two disadvantages of contemporary photoelasticity--the need for model materials with high birefringence and/or the need to apply large loads--for studies of stress fields at crack tips. Both limitations tend to produce nonlinear material responses that may violate linear elastic fracture mechanics concepts and large deformations that may change the geometry sufficiently to violate the assumption of "small deformations."

The HFP method has been applied with sufficient accuracy to the evaluation of stress intensity factors (SIF) for some well-known cases, e.g., a double-edged cracked tension strip, where only mode one exists [2]. For a mixed-mode problem, such as slanted edge cracks in a tension strip, the method yielded accurate results when compared with numerical solutions [2,3,4]. In these studies Williams' stress function [5] was used to describe the stress field ahead of the crack.

The Trace method utilizes a computer program called TRACE [6] to sharpen the finite width bands of fringe loops into fine lines that define fringe orders of the order n/2, where n represents all integers from zero to infinity. Data (N, r, θ) are collected from the stored

digitized image of the sharpened fringe loops using the EyeCom II[1] digital image analysis system.

In this study the HFP method and the Trace method are applied to near edge cracks in tension strips. The mixed-mode SIFs are evaluated for cracks oriented at an angle α as shown in Fig. 1.

Data used for the evaluation of SIF were only collected from a region that was predetermined as a valid zone for the asymptotic stress field equations. This zone was demarcated through specific programs [9] that sampled data from a large zone and determined the area within the zone where SIF values were independent of position r. The SIF values were extracted from the collected data using an overdeterministic-least-squares method proposed by Sanford and Dally [7]. This method was chosen over the other photoelastic methods of determining SIF because it does not have a preferred way of data acquisition. Hence, the whole field in the vicinity of the crack tip can be utilized to improve the overall accuracy of the results. A review of this method and other photoelastic methods of determining SIF can be found in Ref. [8].

Experimental Procedure

This study used seven tension strips 254-mm long by 50.80-mm wide (10" × 2") and 3.20-mm (0.125") thick made from PSM1,[2] a polycarbonate,

[1]Product of Spatial Data Systems.

[2]Product of Measurement Group, Inc.

which is completely free of the time-edge effect and exhibits very little creep at room temperature. PSM1 is very sensitive to thermal stresses and therefore all machining was done with the specimens submerged in a coolant. A slit 0.15-mm (0.006") wide and 20.30-mm (0.8") long was machined close to one of the long edges of the strip as shown in Fig. 1. The specimen geometries and material properties are summarized in Table 1.

The experimental setup, described in Refs. [1,2], consists of a traditional polariscope setup and a digital image analysis system, EyeCom II. The EyeCom II unit consists of a video scanner, a real-time digitizer, a display system, and a LSI-11 minicomputer (Fig. 2).

Half-Fringe Photoelasticity The light intensity, as output by the EyeCom II unit, has values ranging from Z = 0 for the darkest area in the field of view to Z = 255 for the brightest area. This Z value is related to the light intensity, I, through the log-linear sensitivity curve of the video scanner,

$$Z = I^{\gamma} \tag{1}$$

where γ is the slope of the video scanner sensitivity curve.

For a dark field polariscope setup, the light intensity is

$$I = I_o \sin^2 (N\pi) \tag{2}$$

where N is the fringe order and I_o is the maximum value of the light intensity that corresponds to N = 0.5. It follows from Eq. (1) that Z

and I reach their respective maximum values simultaneously. Hence, the ratio of Z/Z_{max} can be written as

$$\frac{Z}{Z_{max}} = \left(\frac{I}{I_o}\right)^{\gamma} = [\sin^2(N\pi)]^{\gamma} \tag{3}$$

and

$$N = \frac{1}{\pi} \sin^{-1} \left[\left(\frac{Z}{Z_{max}}\right)^{1/2\gamma}\right] \tag{4}$$

Hence, if γ and Z_{max} are known, then the partial fringe orders can be computed everywhere in the field with Eq. (4) provided that $0 \leq N \leq 0.5$.

As mentioned earlier, Z_{max}, which corresponds to I_{max}, is the value of the digitized light intensity at $N = 0.5$, and γ can be obtained by using a calibration procedure which implements Tardy compensation [2]. The data from the calibration procedure (Z, N) are then used in Eq. (3) to determine γ by a logarithmic curve fit.

After calibration, the specimens were loaded in tension via friction grips at the two ends. Care was taken that the fringe order in the vicinity of the crack was always less than 0.5. With the help of the friction grips, a uniform stress, σ_o, was obtained across the width of the strip away from the crack.

The viewing area was selected to show the crack tip and its vicinity. The image from this area was digitized, and the x,y coordinates of each pixel and the light intensities at the pixel were stored in the refresh memory of the EyeCom II system. Data were collected with respect

to the polar coordinate system at the crack tip as shown in Fig. 3. The data collected (r, θ, N) were then stored in a file on a floppy disk for future analysis.

The coordinate system at the crack tip was set up with the help of a joystick cursor. After the coordinate system was established, data were collected along eight radial lines; at 5 equally spaced points along each line for a total of 40 points per data set. The direction of the radial lines were specified with the help of the joystick cursor. The data points along a radial line were taken between lower and upper limits $r_L \leq r \leq r_u$. When collecting data at tip A (Fig. 1) of the crack, if the ligament size, d, was less than r_u then the upper limit was taken as $r_u = d$. For this study $r_L/a = 0.15$ and $r_u/a = 0.5$. To avoid errors that might be introduced through the various sources of "noise" in the system, the eight radial lines were selected in a region around the crack tip where the fringe loops were most distinct and the fringe orders were relatively high ($N > 0.1$).

Since the calibration procedure to determine γ and the data collection schemes are very fast because of the interactive computer ability, numerous data sets can be obtained with ease from one image. Thus a good statistical average value can be calculated for the SIFs. All the software necessary to perform the operations mentioned above are listed in Ref. [9].

Trace The accuracy of data collection can be increased using TRACE, a computer program that is an image enhancement routine specifically designed for locating photoelastic fringes on the order of n/2 (n representing all positive integers from zero to infinity). Trace therefore requires at least one-half fringe order from which to take data. The load is typically adjusted to produce up to 1-1/2 fringes, that is three sharp trace lines at N = 0.5, 1.0, and 1.5. The sharpened fringe pattern is then displayed on the image monitor. Figures 4a and 4b show an example of an original and a sharpened image. Data are collected by manually positioning a cursor on different points along the sharpened fringe. The polar coordinates (r, θ) of each data point are recorded by EyeCom II with the origin at the crack tip as shown in Fig. 3. The corresponding fringe orders are entered at the same time. Forty such data points were used for each crack tip [10].

Interpretation of Experimental Data

For a crack subjected to both tensile and shearing stresses, as is the case in this paper, the two-dimensional stress field in the neighborhood of the crack tip may be approximated by the following stress function in polar coordinates given by Hellan [11] who uses Williams' approach [5]:

$$\chi = \sum_{n=1} r^{n+1/2} \left\{ a_{2n-1} \left[\cos(n - 3/2)\theta - \frac{2n - 3}{2n + 1} \cos (n - 1/2)\theta \right] \right.$$
$$\left. + b_{2n-1} [\sin (n - 3/2)\theta - \sin (n + 1/2)\theta] \right\}$$
$$+ \sum_{n=1} r^{n+1} \left\{ a_{2n} [\cos (n - 1)\theta - \cos (n + 1)\theta] \right.$$
$$\left. + b_{2n} \left[\sin (n - 1)\theta - \frac{n - 1}{n + 1} \sin (n + 1)\theta \right] \right\} \qquad (5)$$

where the terms multiplied by a_{2n-1} and a_{2n} are symmetric (mode one), and the terms multiplied by b_{2n-1} and b_{2n} are antisymmetric (mode two) with respect to $\theta = 0$. Note that the polar coordinates are measured from the crack tip in the above equation. The stress intensity factors K_I and K_{II} are related to a_1 and b_1 through

$$a_1 = K_I (2\pi)^{-1/2}$$
$$b_1 = K_{II} (2\pi)^{-1/2} \qquad (6)$$

The polar components of stress are [12]

$$\sigma_r = \frac{1}{r} \frac{\partial \chi}{\partial r} + \frac{1}{r^2} \frac{\partial^2 \chi}{\partial \theta^2} \qquad (7a)$$

$$\sigma_\theta = \frac{\partial^2 \chi}{\partial r^2} \qquad (7b)$$

$$\tau_{r\theta} = \frac{1}{r^2} \frac{\partial \chi}{\partial \theta} - \frac{1}{r} \frac{\partial^2 \chi}{\partial r \partial \theta} = - \frac{\partial}{\partial r} \left(\frac{1}{r} \frac{\partial \chi}{\partial \theta} \right) \qquad (7c)$$

The cartesian components of stress can be expressed in terms of the polar components in the following form:

$$\sigma_x = \sigma_r \cos^2\theta + \sigma_\theta \sin^2\theta - 2\tau_{r\theta} \sin\theta \cos\theta \tag{8a}$$

$$\sigma_y = \sigma_r \sin^2\theta + \sigma_\theta \cos^2\theta + 2\tau_{r\theta} \sin\theta \cos\theta \tag{8b}$$

$$\tau_{xy} = (\sigma_r - \sigma_\theta) \sin\theta \cos\theta + \tau_{r\theta}(\cos^2\theta - \sin^2\theta) \tag{8c}$$

Thus, cartesian components of the stress may be obtained from Eq. (5) as

$$\begin{aligned}
\sigma_{xx} = \sum_{n=1}^{\infty} r^{n-3/2} \Bigg\{ & \left[A''_{2n-1} + \left(n + \tfrac{1}{2}\right) A_{2n-1} \right] \cos^2\theta + \\
& + \left(n + \tfrac{1}{2}\right)\left(n - \tfrac{1}{2}\right) A_{2n-1} \sin^2\theta \\
& + 2\left(n - \tfrac{1}{2}\right) A'_{2n-1} \sin\theta \cos\theta \Bigg\} a_{2n-1} \\
& + \sum_{n=1}^{\infty} r^{n-3/2} \Bigg\{ \left[B''_{2n-1} + \left(n + \tfrac{1}{2}\right) B_{2n-1} \right] \cos^2\theta \\
& + \left(n + \tfrac{1}{2}\right)\left(n - \tfrac{1}{2}\right) B_{2n-1} \sin^2\theta \\
& + 2\left(n - \tfrac{1}{2}\right) B'_{2n-1} \sin\theta \cos\theta \Bigg\} b_{2n-1} \\
& + \sum_{n=1}^{\infty} r^{n-1} \Bigg\{ \left[A''_{2n} + (n+1) A_{2n} \right] \cos^2\theta \\
& + n(n+1) A_{2n} \sin^2\theta + 2n A'_{2n} \sin\theta \cos\theta \Bigg\} a_{2n}
\end{aligned}$$

$$+ \sum_{n=1}^{\infty} r^{n-1} \left\{ \left[B''_{2n} + (n+1) B_{2n} \right] \cos^2\theta \right.$$

$$\left. + n(n+1) B_{2n} \sin^2\theta + 2n B'_{2n} \sin\theta \cos\theta \right\} b_{2n} \qquad (9a)$$

$$\sigma_{yy} = \sum_{n=1}^{\infty} r^{n-3/2} \left\{ \left[A''_{2n-1} + \left(n + \tfrac{1}{2}\right) A_{2n-1} \right] \sin^2\theta \right.$$

$$+ \left(n + \tfrac{1}{2}\right)\left(n - \tfrac{1}{2}\right) A_{2n-1} \cos^2\theta$$

$$\left. - 2\left(n - \tfrac{1}{2}\right) A'_{2n-1} \sin\theta \cos\theta \right\} a_{2n-1}$$

$$+ \sum_{n=1}^{\infty} r^{n-3/2} \left\{ \left[B''_{2n-1} + \left(n + \tfrac{1}{2}\right) B_{2n-1} \right] \sin^2\theta \right.$$

$$+ \left(n + \tfrac{1}{2}\right)\left(n - \tfrac{1}{2}\right) B_{2n-1} \cos^2\theta$$

$$\left. - 2\left(n - \tfrac{1}{2}\right) B'_{2n-1} \sin\theta \cos\theta \right\} b_{2n-1}$$

$$+ \sum_{n=1}^{\infty} r^{n-1} \left\{ \left[A'_{2n} + (n+1) A_{2n} \right] \sin^2\theta \right.$$

$$\left. + n(n+1) A_{2n} \cos^2\theta - 2n A'_{2n} \sin\theta \cos\theta \right\} a_{2n}$$

$$+ \sum_{n=1}^{\infty} r^{n-1} \left\{ \left[B''_{2n} + (n+1) B_{2n} \right] \sin^2\theta \right.$$

$$\left. + n(n+1) B_{2n} \cos^2\theta - 2n B'_{2n} \sin\theta \cos\theta \right\} b_{2n} \qquad (9b)$$

$$\tau_{xy} = \sum_{n=1}^{\infty} r^{n-3/2} \left\{ \left[A''_{2n-1} - \left(n + \frac{1}{2}\right)\left(n - \frac{3}{2}\right) A_{2n-1} \right] \sin\theta \cos\theta \right.$$
$$\left. - \left(n - \frac{1}{2}\right) A'_{2n-1} \left(\cos^2\theta - \sin^2\theta\right) \right\} a_{2n-1}$$
$$+ \sum_{n=1}^{\infty} r^{n-3/2} \left\{ \left[B''_{2n-1} - \left(n + \frac{1}{2}\right)\left(n - \frac{3}{2}\right) B_{2n-1} \right] \sin\theta \cos\theta \right.$$
$$\left. - \left(n - \frac{1}{2}\right) B'_{2n-1} \left(\cos^2\theta - \sin^2\theta\right) \right\} b_{2n-1}$$
$$+ \sum_{n=1}^{\infty} r^{n-1} \left\{ \left[A''_{2n} - (n + 1)(n - 1) A_{2n} \right] \sin\theta \cos\theta \right.$$
$$\left. - n A'_{2n} \left(\cos^2\theta - \sin^2\theta\right) \right\} a_{2n}$$
$$+ \sum_{n=1}^{\infty} r^{n-1} \left\{ \left[B''_{2n} - (n + 1)(n - 1) B_{2n} \right] \sin\theta \cos\theta \right.$$
$$\left. - n B'_{2n} \left(\cos^2\theta - \sin^2\theta\right) \right\} b_{2n} \qquad (9c)$$

where (') indicates differentiation with respect to θ and

$$A_{2n-1} = \cos\left(n - \frac{3}{2}\right)\theta - \frac{2n - 3}{2n + 1} \cos(n + 1)\theta \qquad (10a)$$

$$B_{2n-1} = \sin\left(n - \frac{3}{2}\right)\theta - \sin\left(n + \frac{1}{2}\right)\theta \qquad (10b)$$

$$A_{2n} = \cos(n - 1)\theta - \cos(n + 1)\theta \qquad (10c)$$

$$B_{2n} = \sin(n - 1)\theta - \frac{n - 1}{n + 1} \sin(n + 1)\theta \qquad (10d)$$

In Eq. (9) for n = 1, if only the singular terms are considered, the cartesian components of stress become

$$\sigma_{xx} = r^{-1/2}\left[a_1 \cos\frac{\theta}{2}\left(1 - \sin\frac{\theta}{2}\sin\frac{3\theta}{2}\right) - b_1 \sin\frac{\theta}{2}\left(2 + \cos\frac{\theta}{2}\cos\frac{3\theta}{2}\right)\right] \tag{11a}$$

$$\sigma_{yy} = r^{-1/2}\left[a_1 \cos\frac{\theta}{2}\left(1 + \sin\frac{\theta}{2}\sin\frac{3\theta}{2}\right) + b_1 \sin\frac{\theta}{2}\cos\frac{\theta}{2}\cos\frac{3\theta}{2}\right] \tag{11b}$$

$$\tau_{xy} = r^{-1/2}\left[a_1 \sin\frac{\theta}{2}\cos\frac{\theta}{2}\cos\frac{3\theta}{2} + b_1 \cos\frac{\theta}{2}\left(1 - \sin\frac{\theta}{2}\sin\frac{3\theta}{2}\right)\right] \tag{11c}$$

Note that for n = 1, letting $a_1 = K_I(2\pi)^{-1/2}$ and $b_1 = K_{II}(2\pi)^{-1/2}$ in Eq. (5) yields the well-known Westergaard's equation [13] for the stress field at the crack tip.

Considering the nonsingular terms in addition to the singular terms when n = 1 in Eq. (9), it is found that the nonsingular terms in σ_{yy} and τ_{xy} vanish, and in σ_{xx} they reduce to $4a_2 = -\sigma_{ox}$. This is the "far field stress" in the x-direction, and the modified Westergaard equations [7] are obtained.

In Eq. (5) χ contains two functions of θ multiplied by an integer or a noninteger power of r. In this study, any given power of r together with the function of θ with which it is multiplied will be referred to as one term. The number of terms, k, considered in χ, is related to n through the equations

$$k = 2n - 1, \qquad k = 1, 3, 5, \ldots. \tag{11d}$$

$$k = 2n, \qquad k = 2, 4, 6, \ldots. \tag{11e}$$

Also, the k terms considered yield 2k - 1 unknown coefficients (a, b). This is because b_{2n} (Eq. (10d)) is identically zero when k = 2 (i.e., when n = 1).

K_I and K_{II} were extracted from the photoelastic data (r, θ, N) using the stress optic law that relates the in-plane principal stresses to the isochromatic fringe order N in the following form:

$$\sigma_1 - \sigma_2 = \frac{Nf_\sigma}{h} \tag{12}$$

where f_σ is the material fringe value and h is the specimen thickness. The maximum in-plane shear stress τ_m is related to the Cartesian component of the stress by

$$2\,\tau_m = \sigma_1 - \sigma_2 = \left[(\sigma_x - \sigma_y)^2 + 4\tau_{xy}^2\right]^{1/2} \tag{13}$$

Thus Eqs. (12) and (13) may be combined to yield

$$\left(\frac{Nf_\sigma}{h}\right)^2 = (\sigma_x - \sigma_y)^2 + 4\tau_{xy}^2 \tag{14}$$

The cartesian components of stress from Eq. (9) are now substituted into Eq. (14) and are obtained by an overdeterministic least squares technique proposed by Sanford and Dally [7]. This method does not have a preferred way of data acquisition. Therefore, the whole field in the vicinity of the crack tip may be used for data collection in order to imporove the overall accuracy of the results. To implement

this technique, Eq. (14) is rewritten as a function $g(a_1, b_1, a_2, \ldots)$ such that:

$$g(a_1, b_1, a_2, \ldots.) = (\sigma_x - \sigma_y)^2 + 4\tau_{xy}^2 - \left(\frac{Nf_\sigma}{h}\right)^2 = 0 \tag{15}$$

An iterative scheme was then set up on function $g(a_1, b_1, a_2, \ldots)$ using a linearized Taylor series expansion of g to determine the coefficients a_1, b_1, a_2... [14]. The previous study [15], indicated that the optimal number of terms in Eq. (15) should be four. This required the determination of seven coefficients: a_1, b_1, a_2, a_3, b_3, a_4, and b_4.

Results

Half fringe photoelasticity requires the fringe orders to be less than 0.5, hence isochromatic photographs do not contain any distinctly clear visual information. For this reason no isochromatic photograph is presented. However, fringes corresponding to partial fringe orders ($0 \leq N \leq 0.5$) can be displayed by using the light intensity in Eq. (4) and contour plotting [2]. Figure 4 shows examples of partial fringe orders in the vicinity of the crack for Models 1, 2, and 3. The far-field stress in each of them was σ_o = 265 kPa (38.46 psi).

Numerical SIFs were obtained by a boundary elements algorithm [15] that computes the stress intensity factors from limiting forms of interior stress identity, that is, in terms of an integral over the

equation method. The implementation employed here uses the specialized Green's Function approach [16]. In this approach, the presence of a straight and enclosed crack is explicitly incorporated into the governing boundary integral equations through Green's functions that satisfy the stress free conditions on the crack surface. Since these specialized functions represent exact solutions to the equations of elasticity, the analytically exact character of the stress singularity near the crack tip is incorporated into the analysis technique. Near and far field effects are then coupled through the boundary integral equation with approximations required only for the exterior boundary conditions. Field stresses, as well as stress intensity factors, are directly determined by integrals over the exterior boundary in this method. The discretized boundary model is shown in Fig. 6 where 37 quadratic boundary segments provide a 74 degree-of-freedom representation of the boundary tractions.

A non-zero uniform stress σ was imposed on upper and lower boundaries of the rectangular region. Figure 6 depicts the boundary conditions imposed at the boundaries. For any interior point, the appropriate derivatives of the displacement components are used in conjunction with Hooke's law to obtain an expression for the stress components in plane stress. For a point at the crack tip, this expression contains the singularity of stresses in the direction normal to the crack line.

Stress intensity factors (SIFs) are computed from the usual definition of the in-plane stress intensity factors K_I and K_{II} as follows:

$$\begin{Bmatrix} K_I \\ K_{II} \end{Bmatrix}_{\pm a} = \lim_{x \to \pm a} \left[\sqrt{2\pi(x - a)} \begin{Bmatrix} \sigma_{yy} \\ \tau_{xy} \end{Bmatrix} \right]$$

where the approach to the crack tip in the limit is taken along the line of the crack (see Fig. 3). In this definition, σ_{yy} and τ_{xy} are normal and shear stresses at the crack tip and a is the half-crack length. The SIFs are then written in terms of the boundary integral by using the stress expressions for a point at the crack tip in the above definition. Note that the $1/\sqrt{r}$ singularity is removed from the expressions for stresses when multiplied by $\sqrt{2\pi(x - a)}$ and then the limit is taken to yield integrable expressions for SIFs. In this fashion the SIFs are evaluated from exact analytical expressions pertaining to the precise crack tip and not from extrapolation of stresses around the crack tip. Also note that in the definition for SIFs used in this technique, the origin of the coordinate system is located midway between the two crack tips (which are located at $x = +a$ and $x = -a$); therefore, this technique is valid only for internal cracks and can not be applied to edge crack problems.

Experimental SIFs from HFP and Trace are compared to each other and to the numerical results from the boundary element method (BEM) given in Table 2 and in Figs. 7 and 8. For HFP, a few individual values differ from the numerical results by more than 10%. In these cases the experimental values are erratic. Trace results show satisfactory consistency; the difference between the Trace and numerical values range from 2.6% in Model 4 to 10.9% in Model 5.

Conclusions

Half fringe photoelasticity applied to the evaluation of stress intensity factor results in a method that is relatively fast and accurate. On-line computer capabilities allow fast and accurate data collection and repeatability of the experiments. However, since the fringe orders are low (less than 0.5), the method, in its present state of development, requires optically clean, stress-free specimens. This is also a requirement in traditional photoelasticity, but its effect will not be as severe as in HFP because the fringe orders are higher so that the "signal to noise ratio" is larger.

In application of the Trace method, the EyeCom II system increased the accuracy of photoelastic data by sharpening the fringes and magnifying the image of data extraction zone.

Acknowledgment

This research was supported by grant MEA 8300376 from the National Science Foundation, the Engineering Research Institute, and the Department of Engineering Science and Mechanics at Iowa State University.

Table 1. Summary of specimen geometries and material properties

Model	α	c	d	d/a
1	30°	7.6 mm (0.30 in.)	2.5 mm (0.1 in.)	0.250
2	30°	8.9 mm (0.35 in.)	3.8 mm (0.15 in.)	0.375
3	30°	11.4 mm (0.45 in.)	5.1 mm (0.2 in.)	0.500
4	30°	12.7 mm (0.50 in.)	7.6 mm (0.3 in.)	0.750
5	30°	15.2 mm (0.60 in.)	10.2 mm (0.4 in.)	1.000
6	60°	11.3 mm (0.446 in.)	2.5 mm (0.1 in.)	0.250
7	90°	12.7 mm (0.50 in.)	2.5 mm (0.1 in.)	0.250

For all models: $2a = 20.3$ mm (0.8 in.)
$\nu = 0.38$
$E = 2.39$ GN/m^2 (3.47×10^5 psi)
$f_\sigma = 7$ KN/fringe-m (40 lb/fringe-in)

Table 2. Summary of the SIF results obtained by HFP and Trace (experimental) and BEM (numerical)

		Tip A			Tip A		
		HFP	BEM	% diff	Trace	BEM	% diff
Model 1.	K_I/K_o	0.296	0.284	4.2	0.302	0.284	6.3
	K_{II}/K_o	0.593	0.619	4.2	0.669	0.619	8.1
Model 2.	K_I/K_o	0.287	0.289	0.7	0.270	0.289	6.6
	K_{II}/K_o	0.611	0.579	5.5	0.645	0.579	11.4
Model 3.	K_I/K_o	0.287	0.289	0.7	0.294	0.289	1.7
	K_{II}/K_o	0.667	0.553	17.1	0.623	0.553	12.6
Model 4.	K_I/K_o	0.298	0.287	3.8	0.274	0.287	4.5
	K_{II}/K_o	0.558	0.518	7.7	0.551	0.518	6.4
Model 5.	K_I/K_o	0.289	0.287	0.7	0.297	0.287	6.4
	K_{II}/K_o	0.481	0.497	3.2	0.529	0.497	6.4
Model 6.	K_I/K_o	1.223	1.225	0.2	1.228	1.225	0.2
	K_{II}/K_o	0.514	0.688	25.3	0.641	0.688	6.8
Model 7.	K_I/K_o	n.a.	1.711	--	1.614	1.711	5.7
	K_{II}/K_o	--	--	--	--	--	--

Table 2. Continued

		Tip B			Tip B		
		HFP	BEM	% diff	Trace	BEM	% diff
Model 1.	K_I/K_o	0.380	0.428	11.2	0.396	0.428	7.5
	K_{II}/K_o	0.417	0.452	7.7	0.478	0.452	5.7
Model 2.	K_I/K_o	0.325	0.396	17.9	0.412	0.396	4.0
	K_{II}/K_o	0.435	0.455	4.4	0.498	0.455	9.4
Model 3.	K_I/K_o	0.380	0.373	1.9	0.401	0.373	7.5
	K_{II}/K_o	0.491	0.457	7.4	0.489	0.457	7.0
Model 4.	K_I/K_o	0.303	0.341	11.1	0.350	0.341	2.6
	K_{II}/K_o	0.482	0.460	4.8	0.478	0.460	3.9
Model 5.	K_I/K_o	0.307	0.321	4.4	0.356	0.321	10.9
	K_{II}/K_o	0.428	0.460	7.0	0.480	0.460	4.3
Model 6.	K_I/K_o	0.937	1.033	9.3	1.003	1.033	2.9
	K_{II}/K_o	0.396	0.454	12.8	0.477	0.454	5.1
Model 7.	K_I/K_o	1.263	1.308	3.4	1.366	1.308	4.4
	K_{II}/K_o	--	--	--	--	--	--

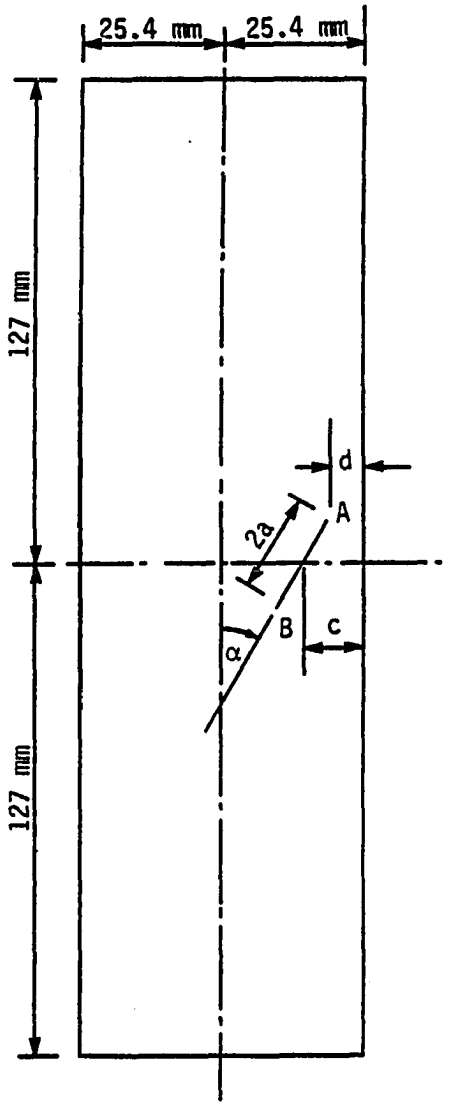

Fig. 1. Test specimen.

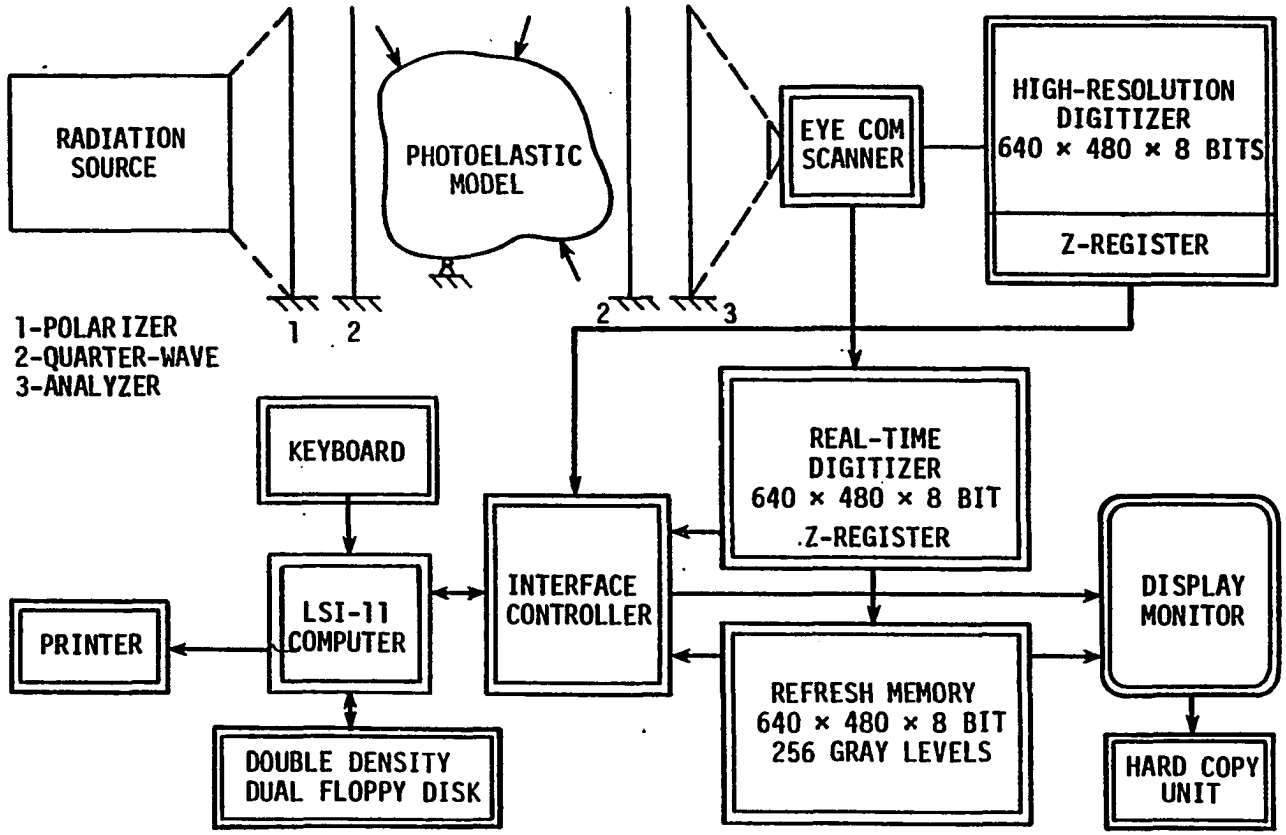

Fig. 2. Diagram of the EyeCom II system.

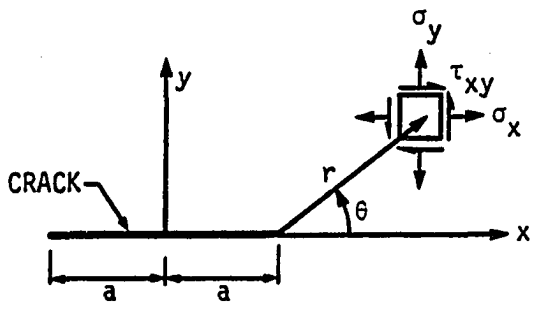

Fig. 3. Coordinate systems with respect to a crack. The cartesian system has its origin at a distance (a) from each crack tip as used in the boundary integral equation method. The cylindrical system has its origin at the crack tip and is used in data collection.

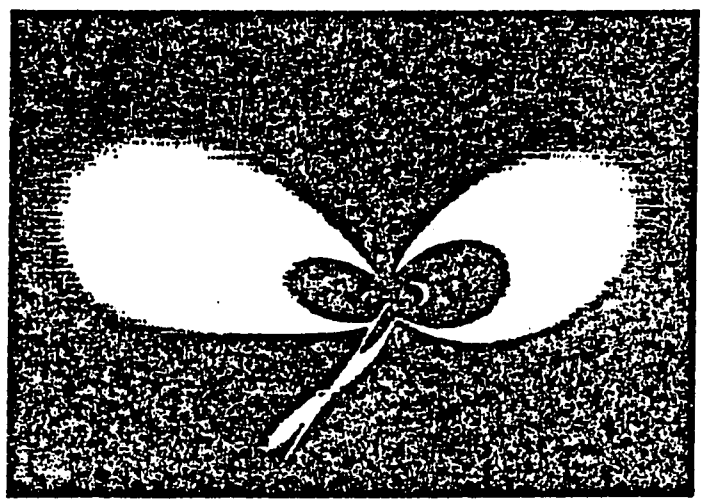

4(a)

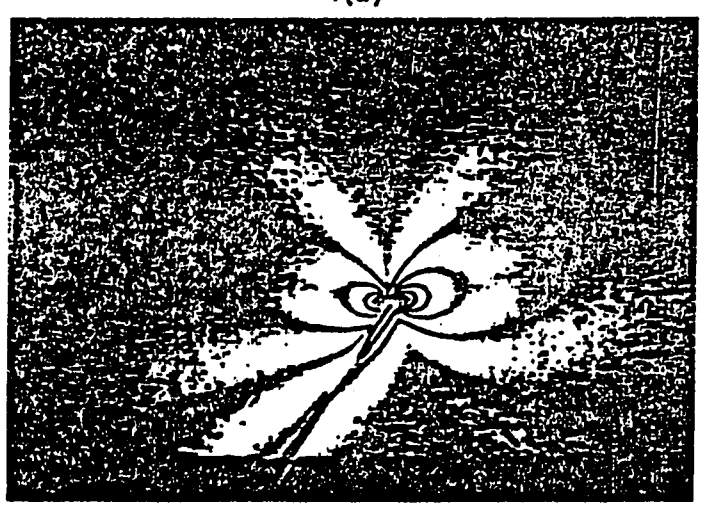

4(b)

Fig. 4. An example of digital sharpening of the isochromatic fringe pattern.

(a) Original fringe pattern for Model 3.

(b) Sharpened fringe pattern for Model 3.

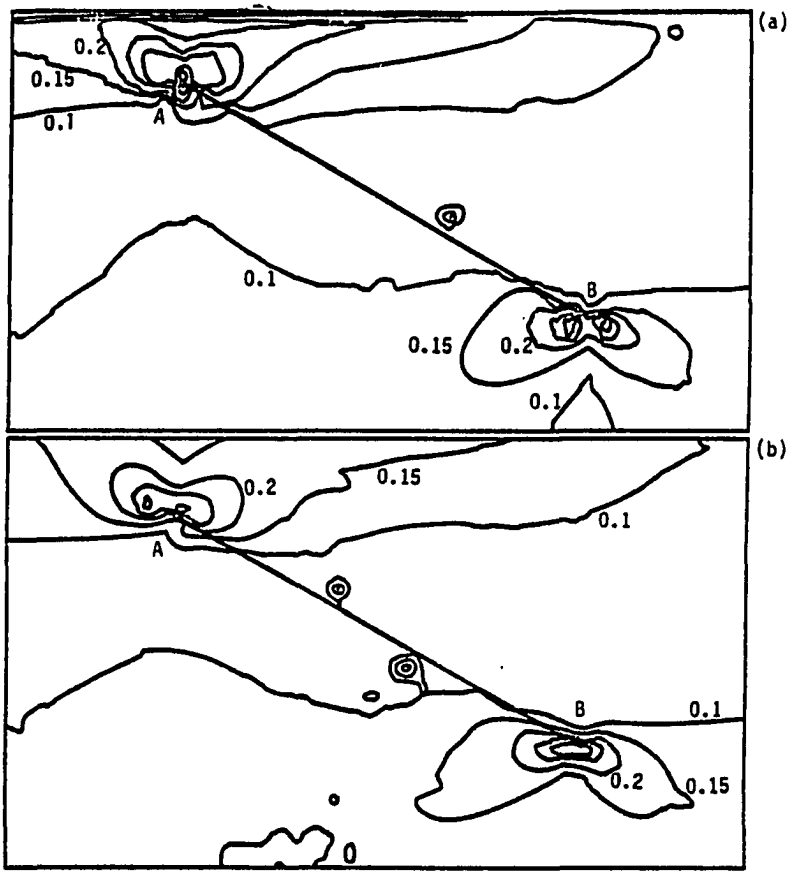

Fig. 5. Plot of the isochromatic fringes in the vicinity of the crack tips from the light intensity data for $\alpha = 30°$, for $\sigma_o = 265$ kPa (38.44 psi)

(a) Model 1, d = 2.5 mm

(b) Model 2, d = 3.8 mm

(c) Model 3, d = 5.1 mm

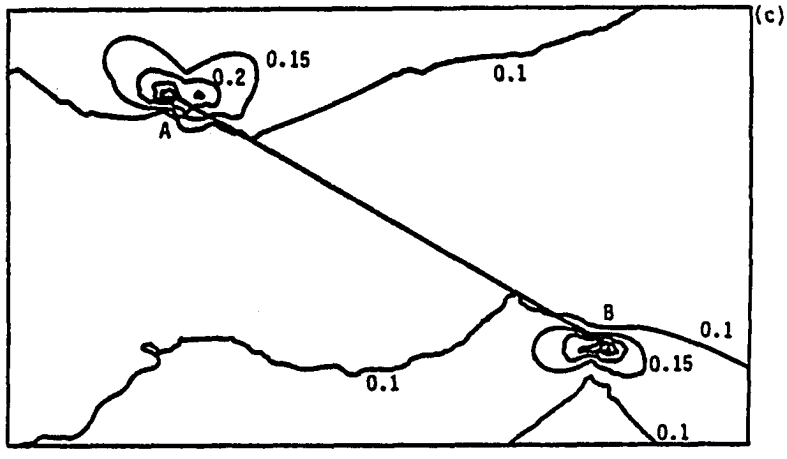

Fig. 5. Continued

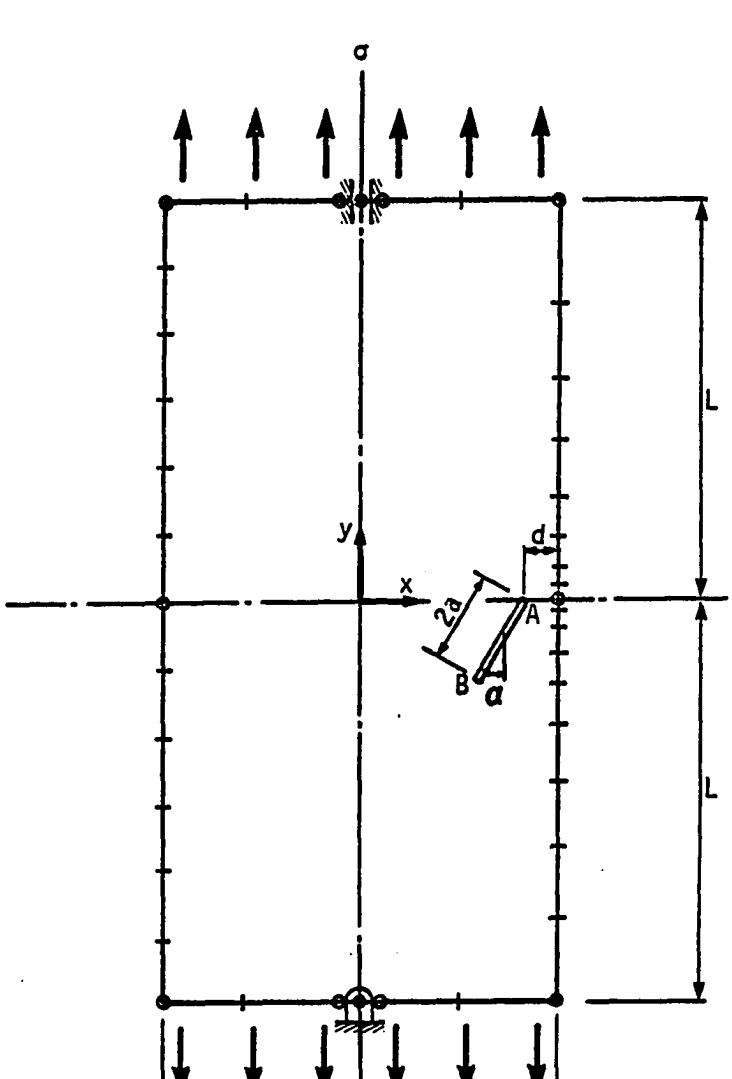

Fig. 6. Numerical model used to obtain BEM results.

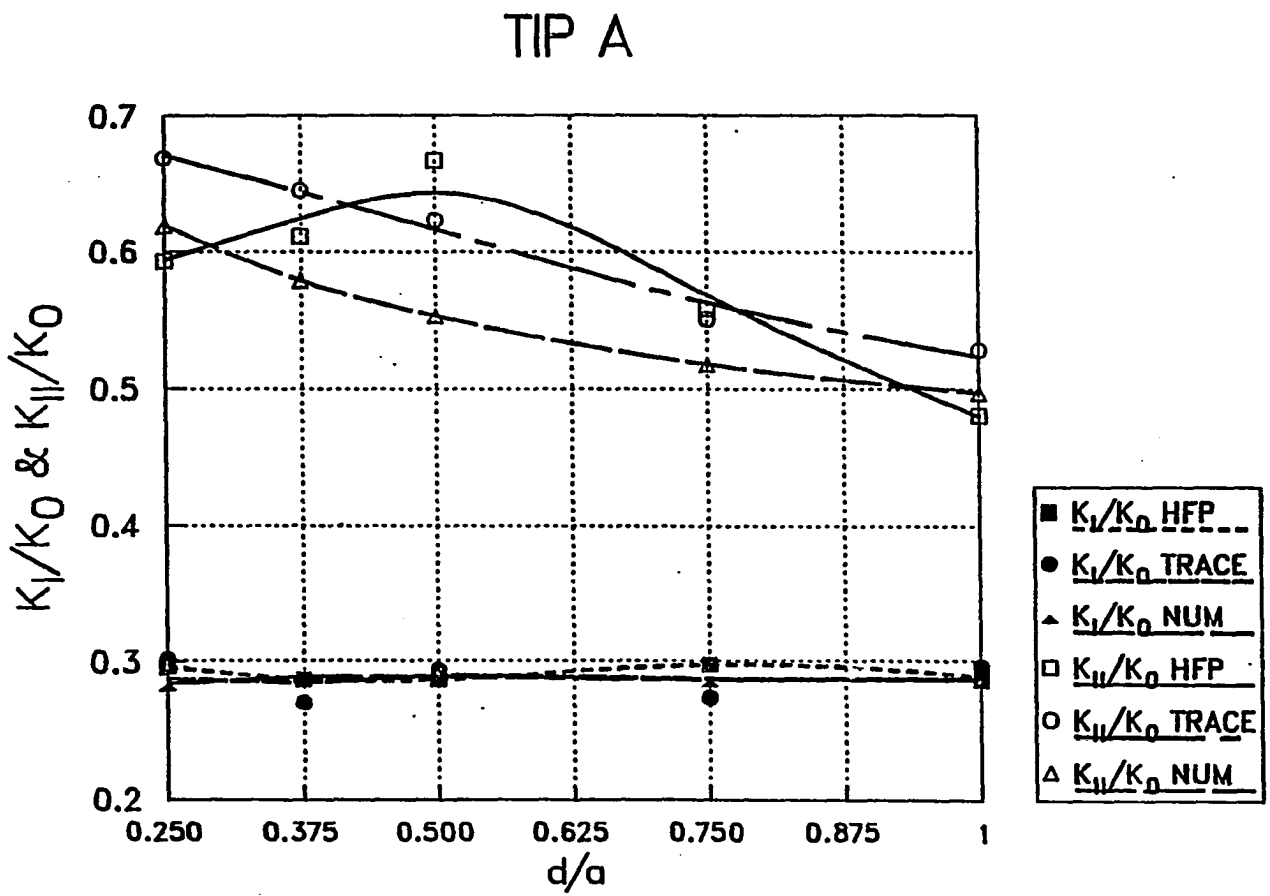

Fig. 7. Variation of experimental and numerical SIFs with d/a for $\alpha = 30°$.

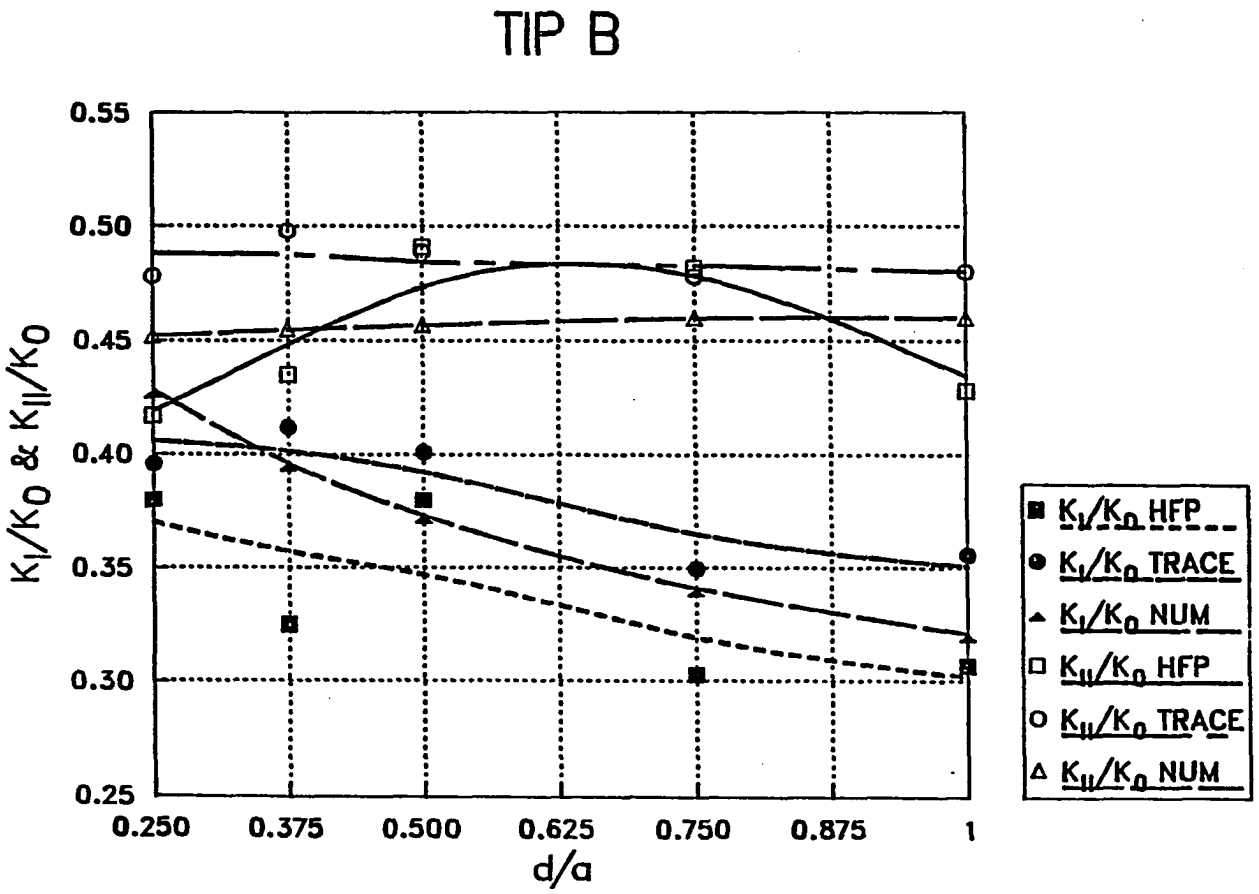

Fig. 7. Continued

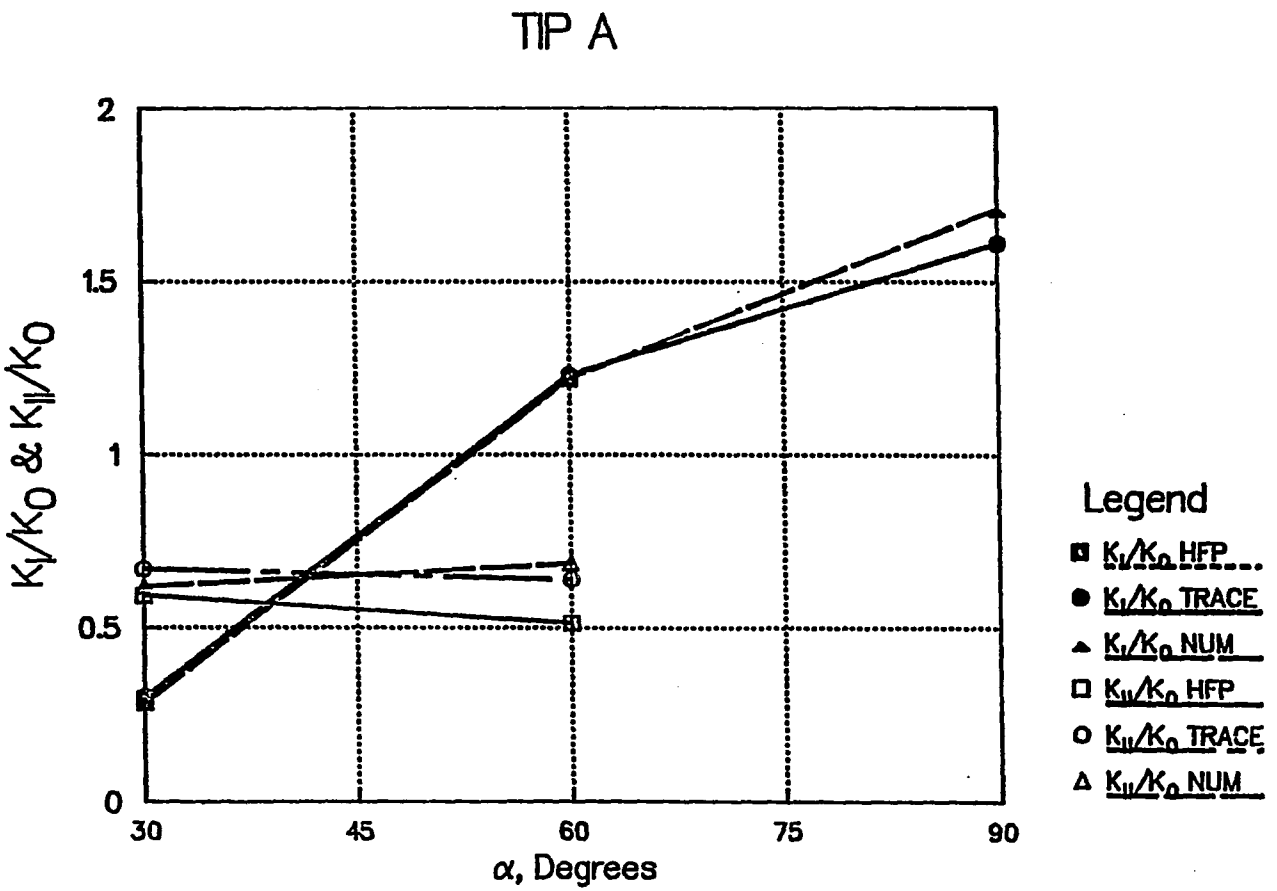

Fig. 8. Variation of experimental and numerical SIFs with α for d/a = 0.25.

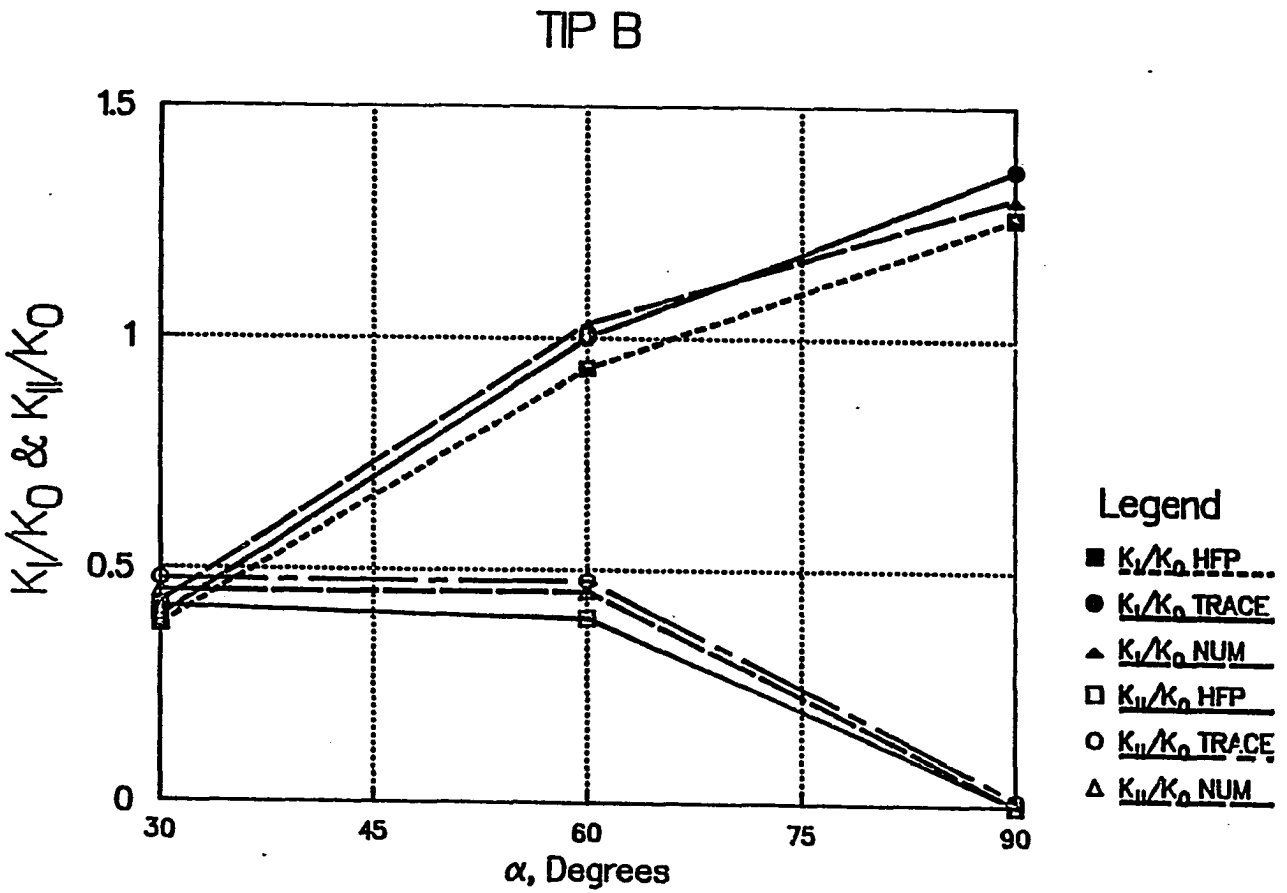

Fig. 8. Continued

References

1. A. S. Voloshin and C. P. Burger. "Half Fringe Photoelasticity: A New Approach to Whole Field Stress Analysis." Expt. Mech., 23 (1983), 304.

2. I. Miskioglu and C. P. Burger. "Half Fringe Photoelasticity Applied to the Evaluation of Stress Intensity Factors." Submitted for publication to the Society of Engineering Science.

3. W. K. Wilson. "The Combined Mode Fracture Mechanics." Report 69-1E7-F Mech-R1. Westinghouse Research Laboratories, 1969.

4. L. W. Zachary and B. J. Skillings. "Displacement Discontinuity Method Applied to NDE related Stress Problems." Int. J. Numer. Methods in Eng., 18 (1982), 1231.

5. M. L. Williams. "On the Stress Distributionat the Base of a Stationary Crack." J. Appl. Mech., 224 (1957), 109.

6. B. Kroner. Program TRACE. Photomechanics Program Bank, Dept. of Engineering Science and Mechanics, Iowa State University, Ames, Iowa, 1984.

7. R. J. Sanford and J. W. Dally. "Stress Intensity Factors in the Third Stage Fan Disk of the TF-30 Turbine Engine." Eng. Fract. Mech., 11 (1979), 621.

8. M. K. Oladimeji. "Photoelastic Analysis of Practical Mode I Fracture Test Specimens." Engin. Fract. Mech., 19 (1984), 717.

9. Photomechanics Program Bank, Dept. of Engineering Science and Mechanics, Iowa State University, Ames, Iowa, 1982.

10. I. Miskioglu. Program CLMN. Photomechanics Program Bank, Dept. of Engineering Science and Mechanics, Iowa State University, Ames, Iowa, 1985.

11. K. Hellan. Introduction to Fracture Mechanics. New York: McGraw Hill, 1984.

12. S. P. Timoshenko and J. N. Goodies. Theory of Elasticity. New York: McGraw Hill, 1970.

13. H. M. Westergaard. "Bearing Pressures And Cracks." J. Appl. Mech., 61 (1939), 49.

14. I. Miskioglu. Program SFW. Photomechanics Program Bank, Dept. of Engineering Science and Mechanics, Iowa State University, Ames, Iowa, 1985.

15. I. Miskioglu, A. Mehdi-Soozani, C. P. Burger, and A. S. Voloshin. "K-Determination of Multiple Cracks Through Half Fringe Photoelasticity." 1985 SEM Spring Conference on Experimental Mechanics, Las Vegas, June 9-14, 1985.

16. T. J. Rudolphi and L. S. Koo. "Boundary Element Solutions of Multiple, Interacting Crack Problems in Plane Elastic Media." Eng. Anal., 2(4) (1985), 211.

PAPER II. STRESS INTENSITY FACTORS FOR INTERACTING CRACKS

Abstract

Experimental stress intensity factors (SIFs) for two interacting straight cracks in plane-homogeneous regions were determined. Photoelastic data were collected from digitally sharpened isochromatic fringe patterns by using a digital image analysis system. SIFs were extracted by using the field equations derived from Williams' stress function. Numerical SIFs were obtained by modeling the problem with a boundary elements program. Good agreement was observed between experimental and numerical results.

Notation

A,B,C,D, = crack tips as shown in Fig. 4

a = one-half crack length

b = one-half horizontal distance between crack tips A and D

h = one-half vertical distance between crack tips B and C

L = one-half length of specimens

W = one-half width of specimens

α = orientation of crack AB with respect to the long direction of the specimens

r,θ = polar coordinates as shown in Fig. 9

σ = applied far-field tensile stress

SIF = stress intensity factor

K_I = mode I SIF

K_{II} = mode II SIF

K_0 = term used to normalize SIFs (= $\sigma\sqrt{\pi a}$ in this study)

E = Young's Modulus

ν = Poisson's Ratio

f_σ = material fringe value

Introduction

The mechanism of fracture of a material in the microscale is closely associated with the interaction, coalescence, growth, and propagation of minute defects such as cracks, voids, and inclusions. The study of the interaction of the above defects existing in a body subjected to a given form of loading is therefore of particular importance. In this paper, attention is focused mainly on the determination of the opening-mode and sliding-mode SIFs at the tips of two interacting cracks.

With the emergence of computers and image-processing techniques as optical stress-analysis tools, the full potential of whole-field fringe-pattern-analysis methods can be more readily utilized. Photoelasticity has recently emerged as a viable technique for the determination of the SIFs. Both two- and three-dimensional problems have been studied [1,2].

In this paper, the isochromatic fringe loops are digitally sharpened by a computer program called TRACE [3]. A digital image analysis system, EyeCom II,[1] was used in collecting random data points on the sharpened fringe loops.

---

[1] Product of Spatial Data Systems, Inc.

Use of photoelastic data in the vicinity of the crack tip for determination of K_I was first suggested by Irwin [4] in a discussion of the paper by Wells and Post [5]. Irwin also advocated the inclusion of an adjustable, nonsingular stress term in the maximum shear expression. Evans and Luxmoore [6] discussed the inadequacy of ignoring the nonsingular stress term in the maximum shear expression. They observed that ignoring this term could introduce a systematic error of approximately 10%. Specific expressions have been developed [7,8] that show the relationship of this nonsingular stress to boundary loading and to the geometry of the specimen.

The problems inherent in the application of photoelasticity to fracture mechanics analysis were extensively examined by Schroedl et al. [9] and also Gdoutus and Theocaris [10]. In all these discussions, it appeared that some of the existing techniques would work well if data collection was restricted to certain regions. Etheridge and Dally [11] showed that a certain maximum tilt range (i.e., $69° < \theta m < 145°$) was more conducive to accurate analysis than any data outside of this range. M. K. Oladimeji [12] has reviewed most of the techniques proposed for extraction of SIFs from photoelastic data.

In this study, EyeCom II was used to collect photoelastic data, N, r, and θ, at 40 points distributed randomly close to the crack tip. The whole-field isochromatic fringe patterns from live models were stored and digitized by EyeCom II and then sharpened digitally through the use of a program called TRACE. Data were collected from these sharpened fringe patterns by using EyeCom II and an interactive computer

program [13]. A multiple-points overdeterministic technique proposed by Sanford and Dally [14] was used to extract mixed-mode SIFs. This technique involves both the Newton-Raphson finite-difference method and the minimization process associated with a least squares method. The stress field equation used was obtained from Williams' stress function [15].

Numerical Approach

A boundary elements computer program [16] was used to obtain numerical values for normalized SIFs for each specimen. This algorithm computes the SIFs from limiting forms of interior stress identity, that is, in terms of an integral over the outer boundary of the region. The numerical model used for this analysis is shown in Fig. 1.

This numerical model was also used to obtain information on the geometry of photoelastic models to ensure interaction between the cracks before model fabrication. The variation of K_I versus the two parameters h/a and b/a was determined and is shown in Figs. 2 and 3 respectively. On the basis of these results, photoelastic models were fabricated such that $h/a < 1$ and $b/a > 3$ in all models.

Experimental Procedure

The photoelastic material used was a polycarbonate PSM1, which is completely free of time-edge effects and exhibits very little creep at room temperature. PSM1 is sensitive to localized heating from the cutting operation. However, PSM1 is insensitive to moisture and therefore all machining was done with the specimens submerged in a coolant.

Models were manufactured from 3.17 mm (1/8 in.) thick strips with dimensions of 114.30 mm × 381.00 mm (4.5 in. × 15.0 in.). Each specimen contained two straight cracks, each of length 20.30 mm (0.8 in.). Machined slits 0.52 mm (0.006 in.) wide were used to simulate real cracks. The interacting crack tips were kept on the long center line of the specimens. One crack remained stationary and was perpendicular to the long direction of the specimen while the other crack's orientation varied with respect to the long direction as shown in Fig. 4. The overall geometry and material properties of the specimens are shown in Table 1.

Dead weights were used to produce a uniform tension in the long direction of specimens. The magnitude of the far-field stress for each model is given in Table 1. Figure 5 shows the loading equipment and experimental setup. Loads were applied for a long enough time to store the image of the scanning area by EyeCom II but a short enough time to avoid introducing any residual stresses at the crack tips.

Loaded models were placed in a circular polariscope. EyeCom II was used to analyze the live image of the isochromatic fringe pattern. The EyeCom II unit consists of an image scanner, a real-time digitizer, a display system, and an LSI-11 minicomputer (Fig. 6). The image scanner consists of a special Vidicon television camera. The image area is divided into 480 lines, and each line is divided into 640 picture elements, called pixels. The brightness or light intensity of each of the 307,200 pixels is converted into digital values (Z-values). The x-values range from 0 to 639, and y-values range from 0 to 479. The

Z-values range from 0 to 255. In other words, the total light intensity scale in this viewing area, from dark to light, has an eight-bit resolution. The real-time digitizer can digitize the entire video image in only 1/30 second, and it stores the resultant values in a "Refresh Memory" where they can be accessed later by the computer and displayed on the monitor. Figure 7 shows one such image.

A high-resolution digital fringe-sharpening procedure was performed by a computer program called TRACE [3] to increase the accuracy of data collection. The TRACE program is an image enhancement routine designed specifically for locating photoelastic fringes of the order of n/2 (n representing all positive integers from zero to infinity). The sharpened fringe pattern was then displayed on the image monitor. Figures 8(a) and 8(b) show an example of an original and a sharpened magnified image of isochromatic fringes at a crack tip. Data were collected by manually positioning a cursor on different points along the sharpened fringe. The polar coordinates (r,θ) of each data point were recorded by EyeCom with the origin at the crack tip as shown in Fig. 9. The corresponding fringe orders were entered at the same time. Forty such data points were used for each crack tip [13].

The common fringe loops (fringe loops connecting the two tips B and C) were used for both these tips. An example of this is shown in Fig. 10. Figure 10a shows the digitally sharpened fringe loops for model 3. Figures 10b and 10c show data points used in the extraction of SIFs for tips B and C respectively. The data extraction zone was confined to $0.1 < r/a < 0.4$ and $69° < \theta_m < 145°$.

Interpretation of Experimental Data

For a crack subjected to both tensile and shearing stresses, as is the case presented in this paper, the two-dimensional stress field in the neighborhood of the crack tip may be approximated by the following stress function in polar coordinates given by Hellan [17] who uses Williams' approach [14]:

$$\chi = \sum_{n=1} r^{n+1/2} \left\{ a_{2n-1} \left[\cos(n - 3/2)\theta - \frac{2n - 3}{2n + 1} \cos (n - 1/2)\theta \right] + b_{2n-1} [\sin (n - 3/2)\theta - \sin (n + 1/2)\theta] \right\} + \sum_{n=1} r^{n+1} \left\{ a_{2n} [\cos (n - 1)\theta - \cos (n + 1)\theta] + b_{2n} \left[\sin (n - 1)\theta - \frac{n - 1}{n + 1} \sin (n + 1)\theta\right] \right\} \quad (1a)$$

where the terms multiplied by a_{2n-1} and a_{2n} are symmetric (mode I) and the terms multiplied by b_{2n-1} and b_{2n} are antisymmetric (mode II) with respect to $\theta = 0$. Note that the polar coordinates are measured from the crack tip in the above equation. The stress intensity factors K_I and K_{II} are related to a_1 and b_1 through

$$a_1 = K_I (2\pi)^{-1/2}$$

$$b_1 = K_{II} (2\pi)^{-1/2} \quad (1b)$$

The polar components of stress are

$$\sigma_r = \frac{1}{r} \frac{\partial \chi}{\partial r} + \frac{1}{r^2} \frac{\partial^2 \chi}{\partial \theta^2} \quad (2a)$$

$$\sigma_\theta = \frac{\partial^2 \chi}{\partial r^2} \tag{2b}$$

$$\tau_{r\theta} = \frac{1}{r^2}\frac{\partial \chi}{\partial \theta} - \frac{1}{r}\frac{\partial^2 \chi}{\partial r \partial \theta} = -\frac{\partial}{\partial r}\left(\frac{1}{r}\frac{\partial \chi}{\partial \theta}\right) \tag{2c}$$

The cartesian components of stress can be expressed in terms of the polar components in the following form:

$$\sigma_x = \sigma_r \cos^2\theta + \sigma_\theta \sin^2\theta - 2\tau_{r\theta} \sin\theta \cos\theta \tag{3a}$$

$$\sigma_y = \sigma_r \sin^2\theta + \sigma_\theta \cos^2\theta + 2\tau_{r\theta} \sin\theta \cos\theta \tag{3b}$$

$$\tau_{xy} = (\sigma_r - \sigma_\theta) \sin\theta \cos\theta + \tau_{r\theta}(\cos^2\theta - \sin^2\theta) \tag{3c}$$

Thus, cartesian components of the stress may be obtained from Eq. (1a) as

$$\begin{aligned}
\sigma_{xx} = \sum_{n=1}^{\infty} r^{n-3/2} \Bigg\{ & \left[A''_{2n-1} + \left(n + \tfrac{1}{2}\right) A_{2n-1} \right] \cos^2\theta \\
& + \left(n + \tfrac{1}{2}\right)\left(n - \tfrac{1}{2}\right) A_{2n-1} \sin^2\theta \\
& + 2\left(n - \tfrac{1}{2}\right) A'_{2n-1} \sin\theta \cos\theta \Bigg\} a_{2n-1} \\
& + \sum_{n=1}^{\infty} r^{n-3/2} \Bigg\{ \left[B''_{2n-1} + \left(n + \tfrac{1}{2}\right) B_{2n-1} \right] \cos^2\theta \\
& + \left(n + \tfrac{1}{2}\right)\left(n - \tfrac{1}{2}\right) B_{2n-1} \sin^2\theta \\
& + 2\left(n - \tfrac{1}{2}\right) B'_{2n-1} \sin\theta \cos\theta \Bigg\} b_{2n-1}
\end{aligned}$$

$$+ \sum_{n=1}^{\infty} r^{n-1} \left\{ \left[A''_{2n} + (n+1) A_{2n} \right] \cos^2\theta \right.$$

$$\left. + n(n+1) A_{2n} \sin^2\theta + 2n A'_{2n} \sin\theta \cos\theta \right\} a_{2n}$$

$$+ \sum_{n=1}^{\infty} r^{n-1} \left\{ \left[B''_{2n} + (n+1) B_{2n} \right] \cos^2\theta \right.$$

$$\left. + n(n+1) B_{2n} \sin^2\theta + 2n B'_{2n} \sin\theta \cos\theta \right\} b_{2n} \qquad (4a)$$

$$\sigma_{yy} = \sum_{n=1}^{\infty} r^{n-3/2} \left\{ \left[A''_{2n-1} + \left(n + \tfrac{1}{2}\right) A_{2n-1} \right] \sin^2\theta \right.$$

$$+ \left(n + \tfrac{1}{2}\right)\left(n - \tfrac{1}{2}\right) A_{2n-1} \cos^2\theta$$

$$\left. - 2\left(n - \tfrac{1}{2}\right) A'_{2n-1} \sin\theta \cos\theta \right\} a_{2n-1}$$

$$+ \sum_{n=1}^{\infty} r^{n-3/2} \left\{ \left[B''_{2n-1} + \left(n + \tfrac{1}{2}\right) B_{2n-1} \right] \sin^2\theta \right.$$

$$+ \left(n + \tfrac{1}{2}\right)\left(n - \tfrac{1}{2}\right) B_{2n-1} \cos^2\theta$$

$$\left. - 2\left(n - \tfrac{1}{2}\right) B'_{2n-1} \sin\theta \cos\theta \right\} b_{2n-1}$$

$$+ \sum_{n=1}^{\infty} r^{n-1} \left\{ \left[A'_{2n} + (n+1) A_{2n} \right] \sin^2\theta \right.$$

$$\left. + n(n+1) A_{2n} \cos^2\theta - 2n A'_{2n} \sin\theta \cos\theta \right\} a_{2n}$$

$$+ \sum_{n=1}^{\infty} r^{n-1} \left\{ \left[B''_{2n} + (n+1) B_{2n} \right] \sin^2\theta \right.$$

$$\left. + n(n+1) B_{2n} \cos^2\theta - 2n B'_{2n} \sin\theta \cos\theta \right\} b_{2n} \qquad (4b)$$

$$\tau_{xy} = \sum_{n=1}^{\infty} r^{n-3/2} \left\{ \left[A''_{2n-1} - \left(n + \tfrac{1}{2}\right)\left(n - \tfrac{3}{2}\right) A_{2n-1} \right] \sin\theta \cos\theta \right.$$
$$\left. - \left(n - \tfrac{1}{2}\right) A'_{2n-1} \left(\cos^2\theta - \sin^2\theta\right) \right\} a_{2n-1}$$
$$+ \sum_{n=1}^{\infty} r^{n-3/2} \left\{ \left[B''_{2n-1} - \left(n + \tfrac{1}{2}\right)\left(n - \tfrac{3}{2}\right) B_{2n-1} \right] \sin\theta \cos\theta \right.$$
$$\left. - \left(n - \tfrac{1}{2}\right) B'_{2n-1} \left(\cos^2\theta - \sin^2\theta\right) \right\} b_{2n-1}$$
$$+ \sum_{n=1}^{\infty} r^{n-1} \left\{ \left[A''_{2n} - (n+1)(n-1) A_{2n} \right] \sin\theta \cos\theta \right.$$
$$\left. - n A'_{2n} \left(\cos^2\theta - \sin^2\theta\right) \right\} a_{2n}$$
$$+ \sum_{n=1}^{\infty} r^{n-1} \left\{ \left[B''_{2n} - (n+1)(n-1) B_{2n} \right] \sin\theta \cos\theta \right.$$
$$\left. - n B'_{2n} \left(\cos^2\theta - \sin^2\theta\right) \right\} b_{2n} \qquad (4c)$$

where (') indicates differentiation with respect to θ and

$$A_{2n-1} = \cos\left(n - \tfrac{3}{2}\right)\theta - \frac{2n-3}{2n+1} \cos(n+1)\theta \qquad (5a)$$

$$B_{2n-1} = \sin\left(n - \tfrac{3}{2}\right)\theta - \sin\left(n + \tfrac{1}{2}\right)\theta \qquad (5b)$$

$$A_{2n} = \cos(n-1)\theta - \cos(n+1)\theta \qquad (5c)$$

$$B_{2n} = \sin(n-1)\theta - \frac{n-1}{n+1} \sin(n+1)\theta \qquad (5d)$$

In Eq. (4) for n = 1, if only the singular terms are considered, the cartesian components of stress become

$$\sigma_{xx} = r^{-1/2}\left[a_1 \cos\frac{\theta}{2}\left(1 - \sin\frac{\theta}{2}\sin\frac{3\theta}{2}\right) - b_1 \sin\frac{\theta}{2}\left(2 + \cos\frac{\theta}{2}\cos\frac{3\theta}{2}\right)\right] \tag{6a}$$

$$\sigma_{yy} = r^{-1/2}\left[a_1 \cos\frac{\theta}{2}\left(1 + \sin\frac{\theta}{2}\sin\frac{3\theta}{2}\right) + b_1 \sin\frac{\theta}{2}\cos\frac{\theta}{2}\cos\frac{3\theta}{2}\right] \tag{6b}$$

$$\tau_{xy} = r^{-1/2}\left[a_1 \sin\frac{\theta}{2}\cos\frac{\theta}{2}\cos\frac{3\theta}{2} + b_1 \cos\frac{\theta}{2}\left(1 - \sin\frac{\theta}{2}\sin\frac{3\theta}{2}\right)\right] \tag{6c}$$

Note that for n = 1, letting $a_1 = K_I(2\pi)^{-1/2}$ and $b_1 = K_{II}(2\pi)^{-1/2}$ in Eq. (1) yields the well known Westergaard's equation [18] for the stress field at the crack tip.

If the nonsingular terms in addition to the singular terms are considered when n = 1 in Eq. (4), the nonsingular terms in σ_{yy} and τ_{xy} vanish, and in σ_{xx} they reduce to $4a_2 = -\sigma_{ox}$. This is the "far-field stress" in the x-direction, and the modified Westergaard equations [4, 13] are obtained.

In Eq. (1a) χ contains two functions of θ multiplied by an integer or a noninteger power of r. In this study, any given power of r together with the function of θ with which it is multiplied will be referred to as one term. The number of terms, k, considered in χ, is related to n through the equations

$$k = 2n - 1, \qquad k = 1, 3, 5, \ldots. \tag{7a}$$

$$k = 2n, \qquad k = 2, 4, 6, \ldots. \tag{7b}$$

Also, the k terms considered yield 2k - 1 unknown coefficients (a, b) because b_{2n} (Eq. [5d]) is identically zero when k = 2 (i.e., when n = 1).

K_I and K_{II} were extracted from the photoelastic data (r, θ, N) by using the stress optic law that relates the in-plane principal stresses to the isochromatic fringe order N in the following form:

$$\sigma_1 - \sigma_2 = \frac{Nf_\sigma}{h} \tag{8}$$

where f_σ is the material fringe constant and h is the specimen thickness. The maximum in-plane shear stress τ_m is related to the cartesian component of the stress by

$$2\,\tau_m = \sigma_1 - \sigma_2 = \left[(\sigma_x - \sigma_y)^2 + 4\tau_{xy}^2\right]^{1/2} \tag{9}$$

Thus Eqs. (8) and (9) may be combined to yield

$$\left(\frac{Nf_\sigma}{h}\right)^2 = (\sigma_x - \sigma_y)^2 + 4\tau_{xy}^2 \tag{10}$$

The cartesian components of stress from Eq. (4) are now substituted into Eq. (10) and are obtained by an overdeterministic least squares technique proposed by Sanford and Dally [14]. This method does not have a preferred way of data acquisition. Therefore, the whole field

in the vicinity of the crack tip may be used for data collection in order to improve the overall accuracy of the results. To implement this technique, we rewrite Eq. (10) as a function $g(a_1, b_1, a_2, \ldots)$ such that

$$g(a_1, b_1, a_2, \ldots.) = (\sigma_x - \sigma_y)^2 + 4\tau_{xy}^2 - \left(\frac{Nf_\sigma}{h}\right)^2 = 0 \tag{11}$$

An iterative scheme was then set up on function $g(a_1, b_1, a_2, \ldots.)$ by using a linearized Taylor series expansion of g to determine the coefficients $a_1, b_1, a_2 \ldots$ [19]. The previous study [20] indicated that the optimal number of terms in Eq. (11) should be four. This required the determination of seven coefficients: $a_1, b_1, a_2, a_3, b_3, a_4$, and b_4.

Results and Discussion

Good agreement was observed between experimental and numerical results obtained in this study. Tables 2 and 3 summarize these results and show the percentage difference between them.

Figure 11 shows the variation of normalized SIFs versus the angle α for tip A. K_I/K_0 decreased nearly linearly from 1.22 at $\alpha = 0°$ to 0.14 at $\alpha = 75°$. K_{II}/K_0 first increased as α increased, then reached its maximum value of 0.59 at $\alpha \simeq 45°$, and finally decreased with a further increase in α. No experimental data were obtained for tip A at $\alpha = 90°$ because there were no fringes at the tip.

Figure 12 shows the variation of normalized SIFs for tip B. This variation is similar to that of tip A and indicates that the interaction between tips B and C, while affecting the magnitude of SIFs, does not appear to influence the shape of the variation of SIFs versus angle α. For tip B, K_I/K_0 varied from 1.47 at $\alpha = 0°$ to 0.06 at $\alpha = 90°$, and K_{II}/K_0 increased from 0.16 at $\alpha = 0°$ to its maximum value of 0.68 at $\alpha = 60°$ and then decreased to 0.32 at $\alpha = 90°$.

Figures 13 and 14 show the variation of normalized SIFs versus angle α for tips C and D respectively. For both of these tips, K_I/K_0 decreased slightly and linearly as angle α increased. For tip C, K_I/K_0 varied from 1.42 at $\alpha = 0°$ to 1.05 at $\alpha = 90°$, and K_{II}/K_0 decreased linearly from 0.21 at $\alpha = 0°$ to 0.08 at $\alpha = 90°$. For tip D, K_I/K_0 varied from 1.28 at $\alpha = 0°$ to 1.10 at $\alpha = 90°$, and K_{II}/K_0 remained at nearly zero for all values of α.

Classical fracture mechanics expresses SIFs with reference to a uniform far-field stress. For interacting cracks, however, the tips are in disturbed fields. The analysis used in this paper for extracting SIFs from the photoelastic field data assumes that the classical William's equations apply in the regions close to the individual crack tips while data are taken. The results justify the assumption.

Acknowledgment

This research was supported in part by NSF grant MEA-8300376, the Engineering Research Institute, and the Department of Engineering

Science and Mechanics at Iowa State University. The assistance of Dr. T. J. Rudolphi with the numerical part of this study is greatly appreciated.

Table 1. Geometry, material properties, and magnitude of applied tensile far-field stress for photoelastic models

Model	α Degrees	σ, MPa (psi)
1	0	1.22 (177.78)
2	15	1.22 (177.78)
3	30	1.22 (177.78)
4	45	1.22 (177.78)
5	60	0.61 (88.89)
6	75	0.61 (88.89)
7	90	0.61 (177.78)

For all models: $2a = 20.32$ mm (0.80 in.)

$2h = 8.13$ mm (0.32 in.)

$2W = 114.30$ mm (4.50 in.)

$2L = 381.00$ mm (15.00 in.)

$E = 2.39\ GN/m^2$ (3.47×10^5 psi)

$\nu = 0.38$

$f_\sigma = 7$ KN/fringe-m (40 lb/fringe-in.)

Table 2. Experimental vs. numerical results for K_I/K_0

	Tip A		Tip B		Tip C		Tip D	
α Degrees	EXP	NUM	EXP	NUM	EXP	NUM	EXP	NUM
0	1.22	1.35	1.47	1.39	1.42	1.39	1.28	1.35
15	1.18	1.31	1.19	1.18	1.30	1.27	1.28	1.25
30	0.94	0.95	1.10	0.95	1.27	1.22	1.18	1.21
45	0.64	0.79	0.70	0.64	1.14	1.18	1.16	1.18
60	0.36	0.43	0.38	0.34	1.14	1.14	1.15	1.14
75	0.14	0.11	0.10	0.11	1.08	1.11	1.06	1.12
90	--	0.09	0.06	0.00	1.05	1.08	1.10	1.09

Table 3. Experimental vs. numerical results for K_{II}/K_0

	Tip A		Tip B		Tip C		Tip D	
α Degrees	EXP	NUM	EXP	NUM	EXP	NUM	EXP	NUM
0	0.04	0.02	0.16	0.22	0.21	0.22	0.00	0.02
15	0.31	0.15	0.17	0.30	0.20	0.22	0.00	0.00
30	0.49	0.52	0.44	0.52	0.19	0.19	0.01	0.01
45	0.59	0.65	0.58	0.61	0.14	0.14	0.04	0.01
60	0.56	0.68	0.68	0.56	0.08	0.10	0.06	0.00
75	0.45	0.54	0.58	0.39	0.05	0.05	0.02	0.01
90	--	0.28	0.33	0.13	0.08	0.02	0.02	0.01

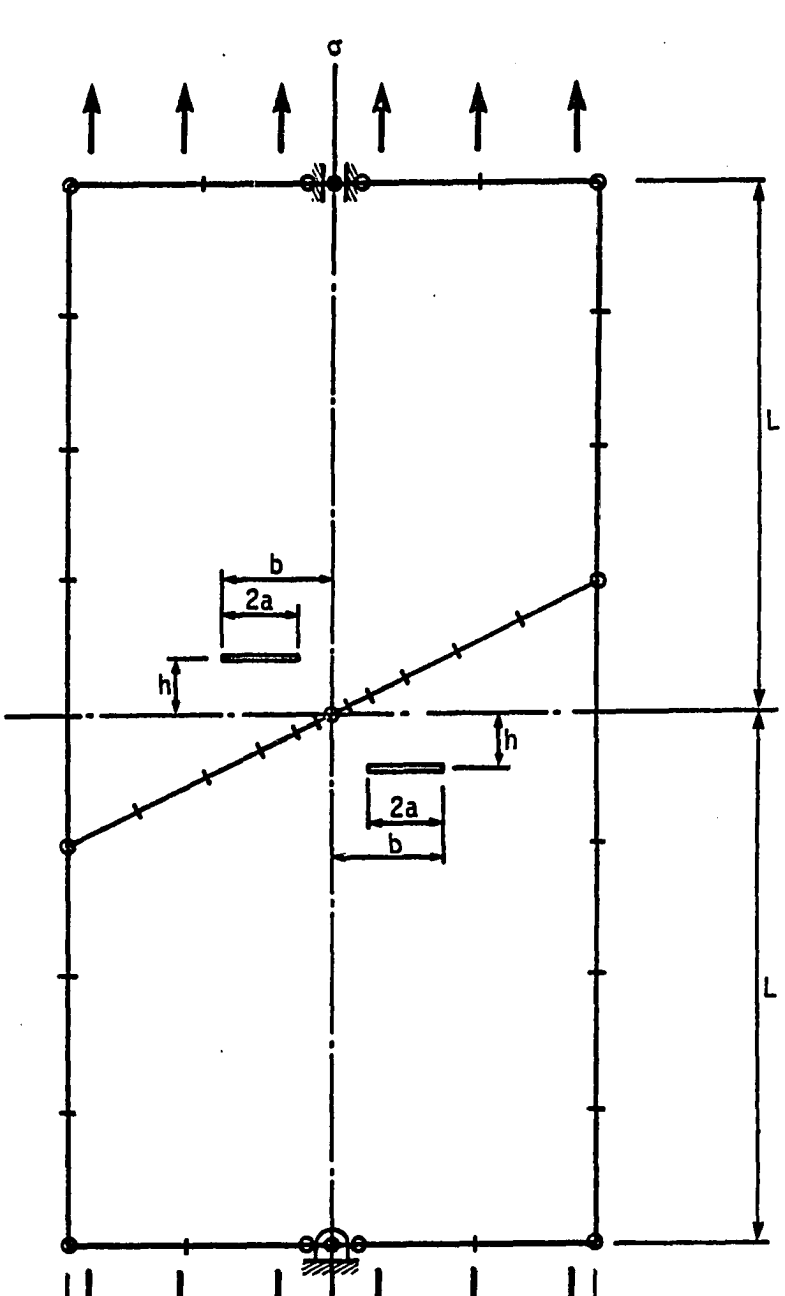

Fig. 1. The numerical model used in the boundary element program

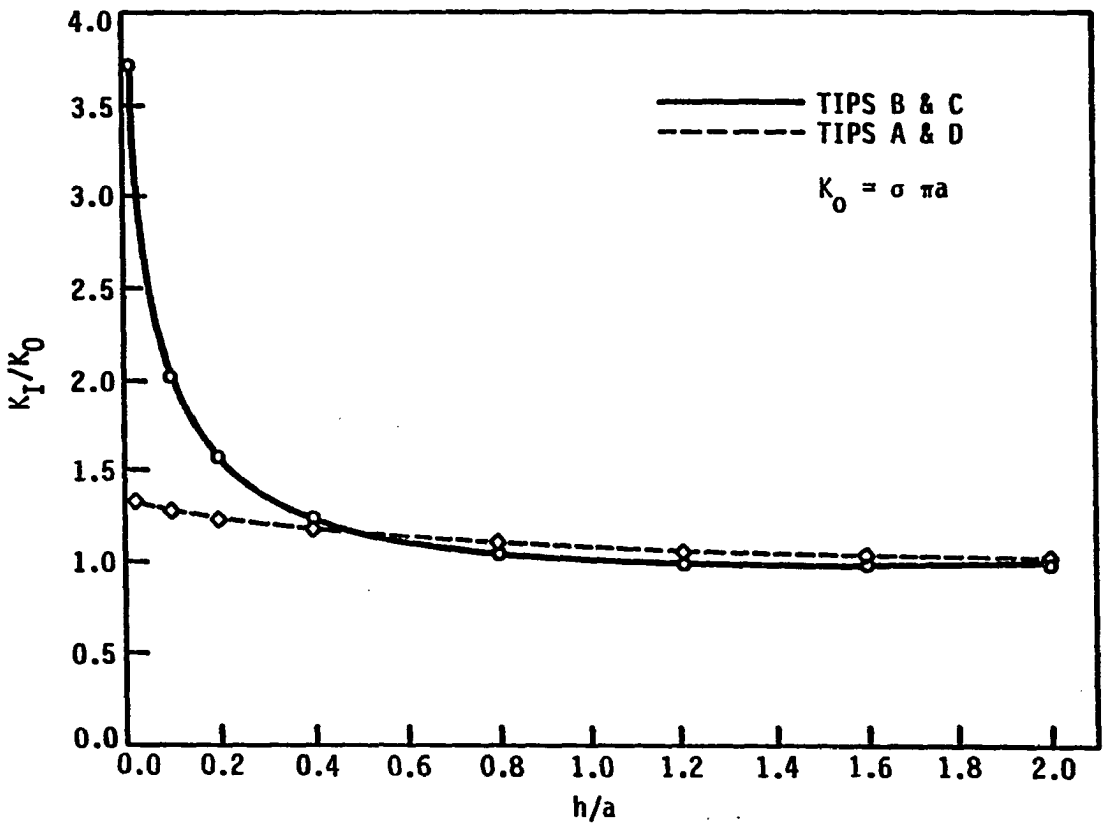

Fig. 2. Variation of K_I/K_0 vs. h/a obtained from the boundary element program

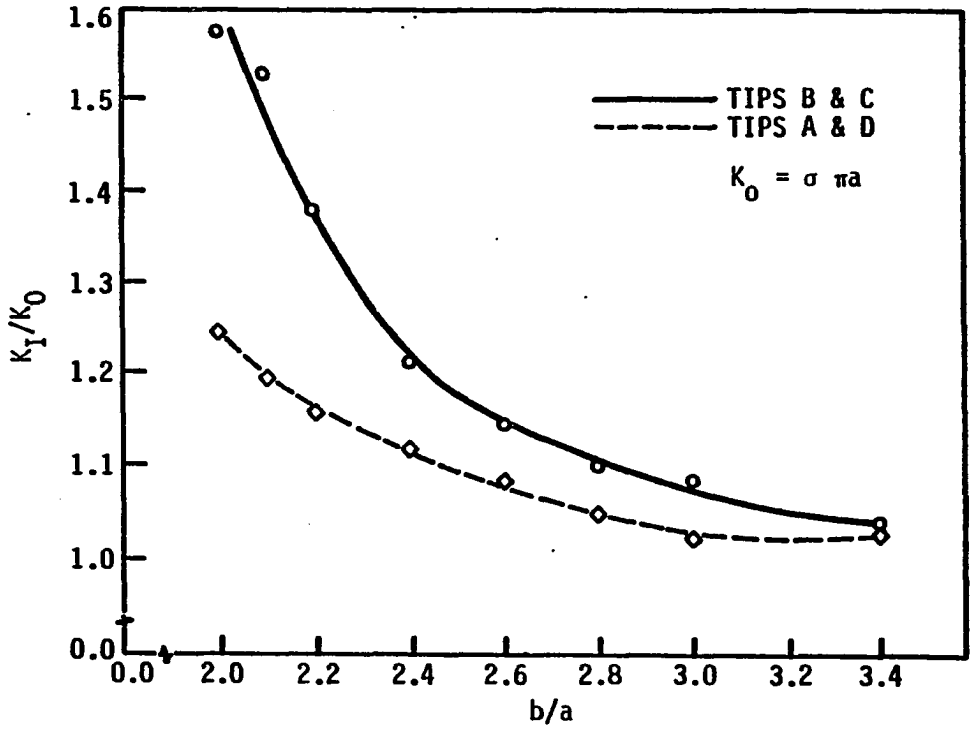

Fig. 3. Variation of K_I/K_0 vs. b/a obtained from the boundary element program

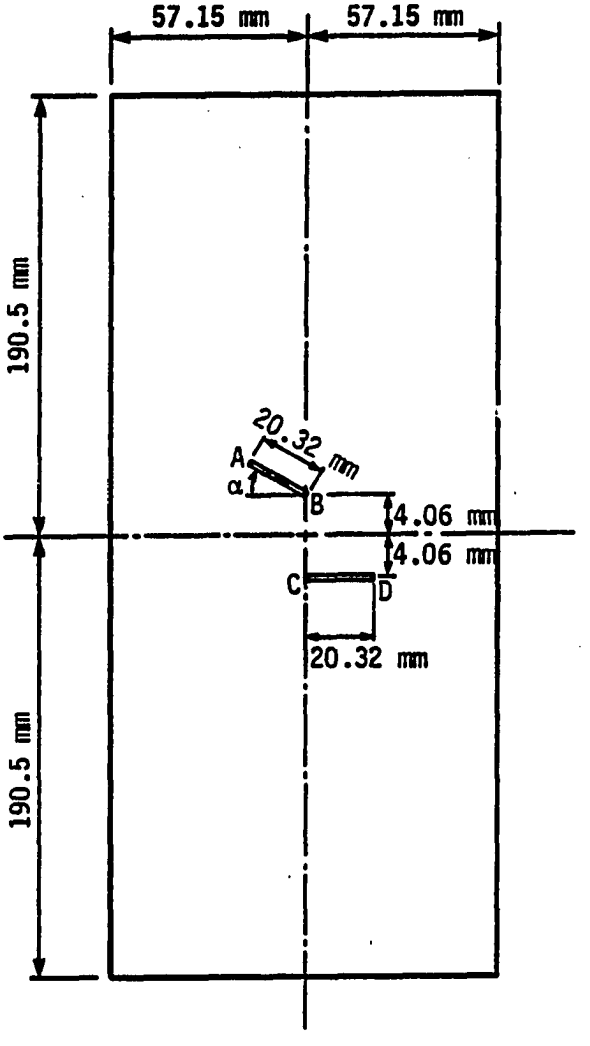

Fig. 4. Test specimens

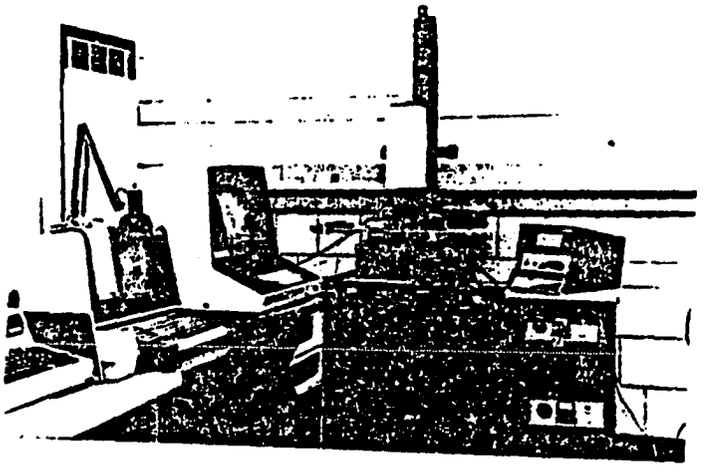

Fig. 5. Experimental setup

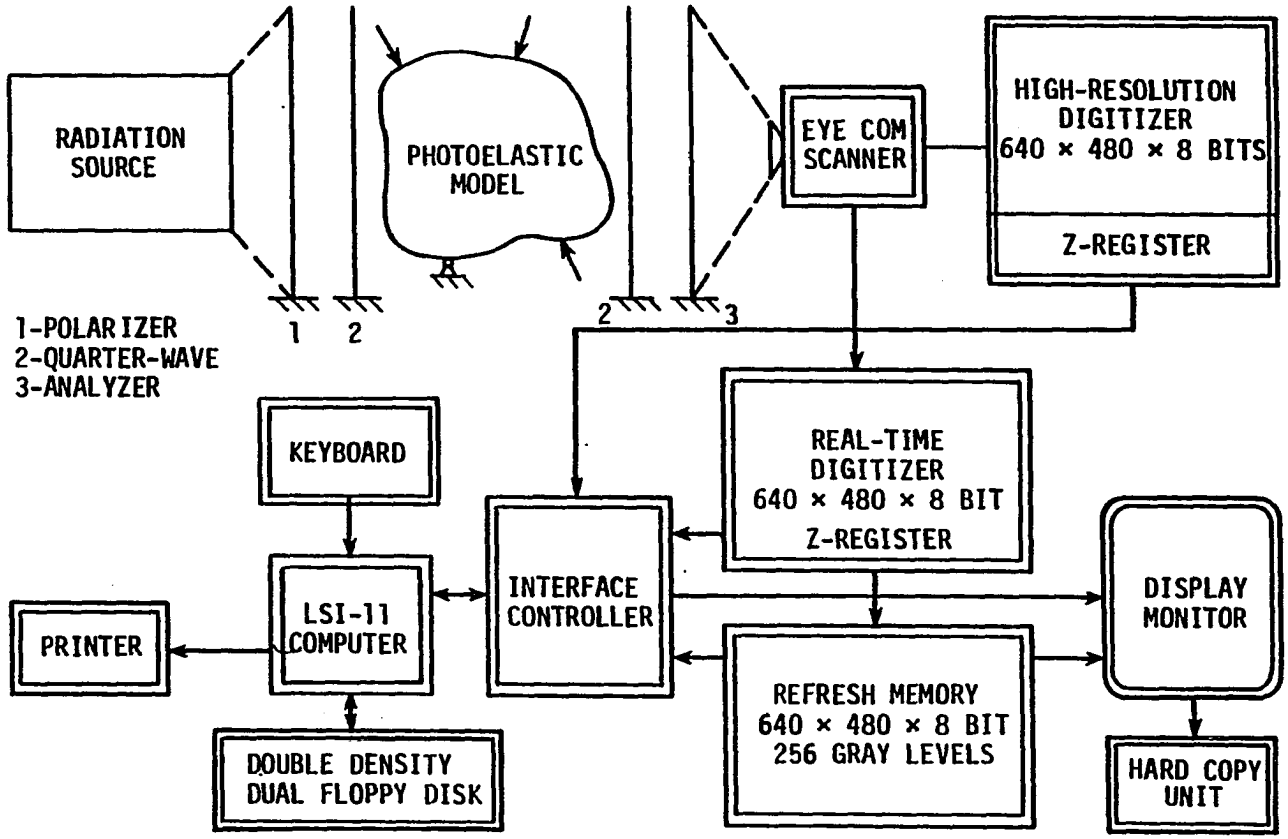

Fig. 6. Diagram of EyeCom II system

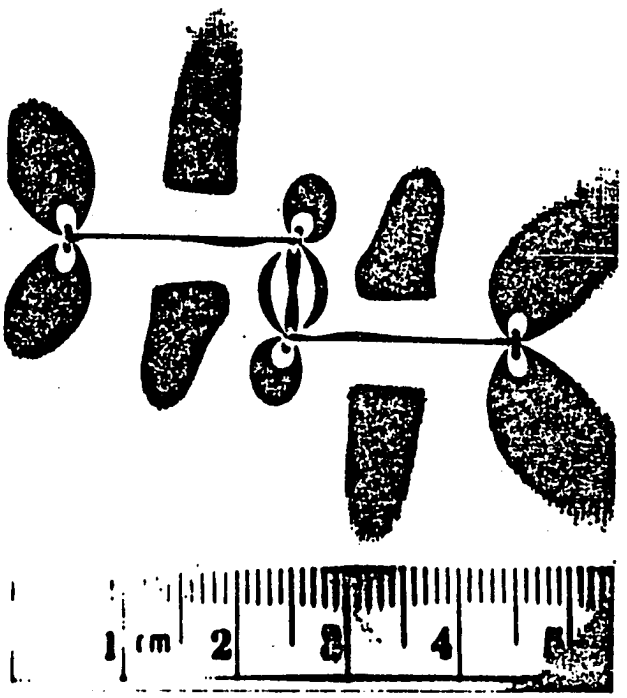

Fig. 7. Digitized image of isochromatic fringes for model 1

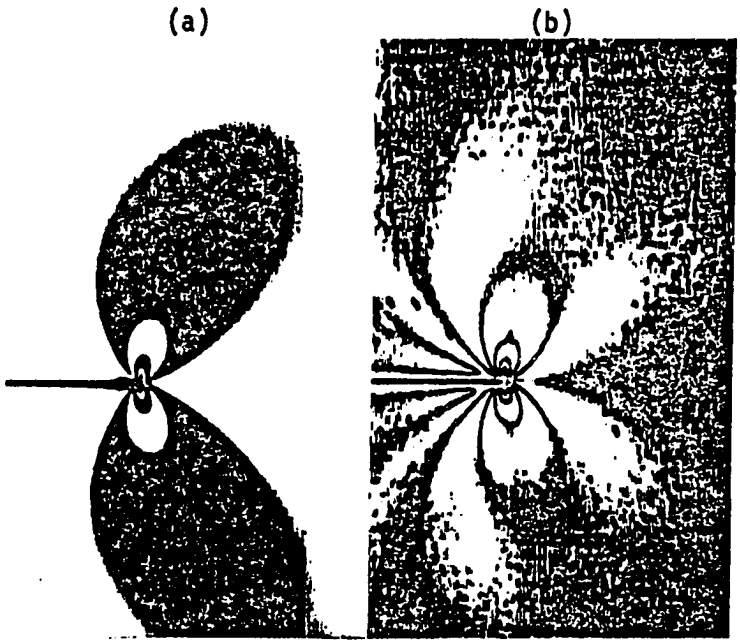

Fig. 8. a. An original magnified image of isochromatic fringes at a crack tip

b. Digitally sharpened fringes at the same crack tip

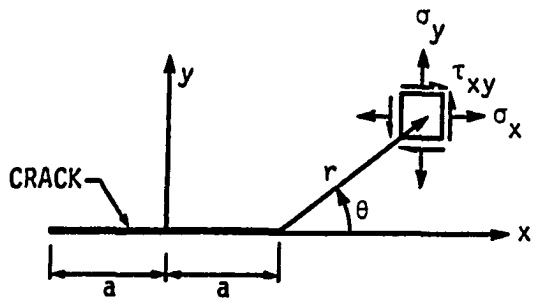

Fig. 9. Coordinate systems with respect to a crack. The cartesian system has origin at a distance "a" from each crack tip as used in the boundary integral equation method. The cylindrical system has its origin at the crack tip and is used in data collection.

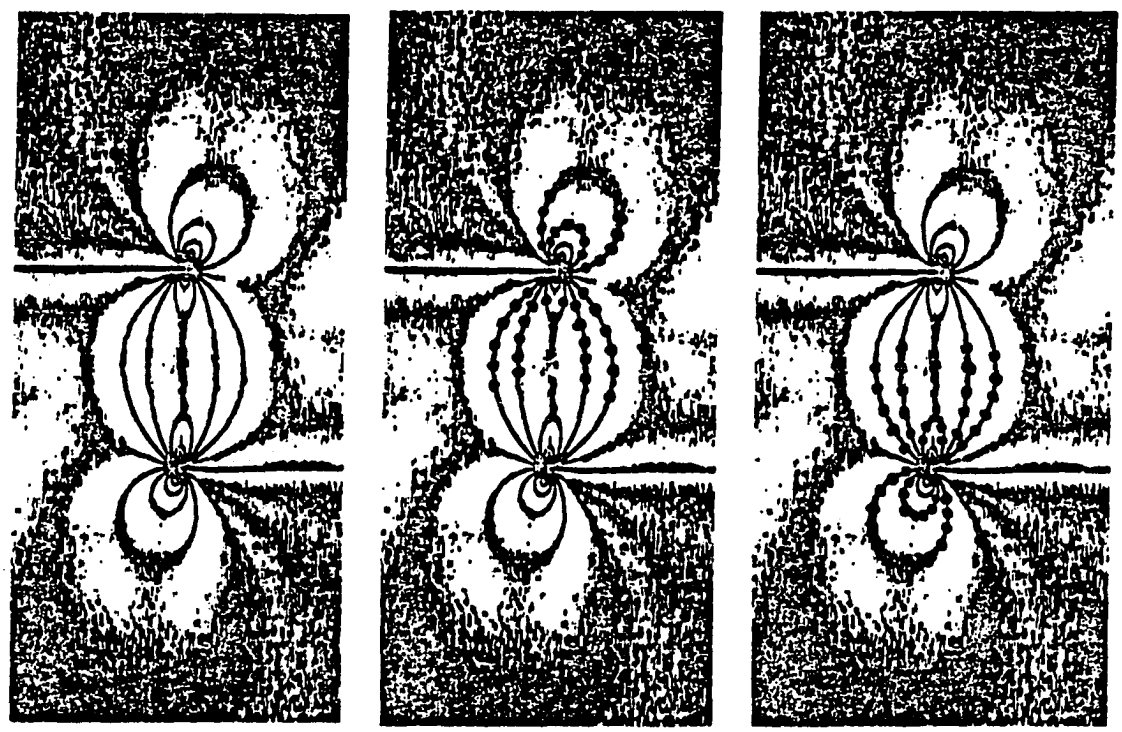

Fig. 10. a. Digitally sharpened and magnified image of isochromatic fringes at the interacting crack tips B and C for model 1

b. Data points collected for crack tip B

c. Data points collected for crack tip C

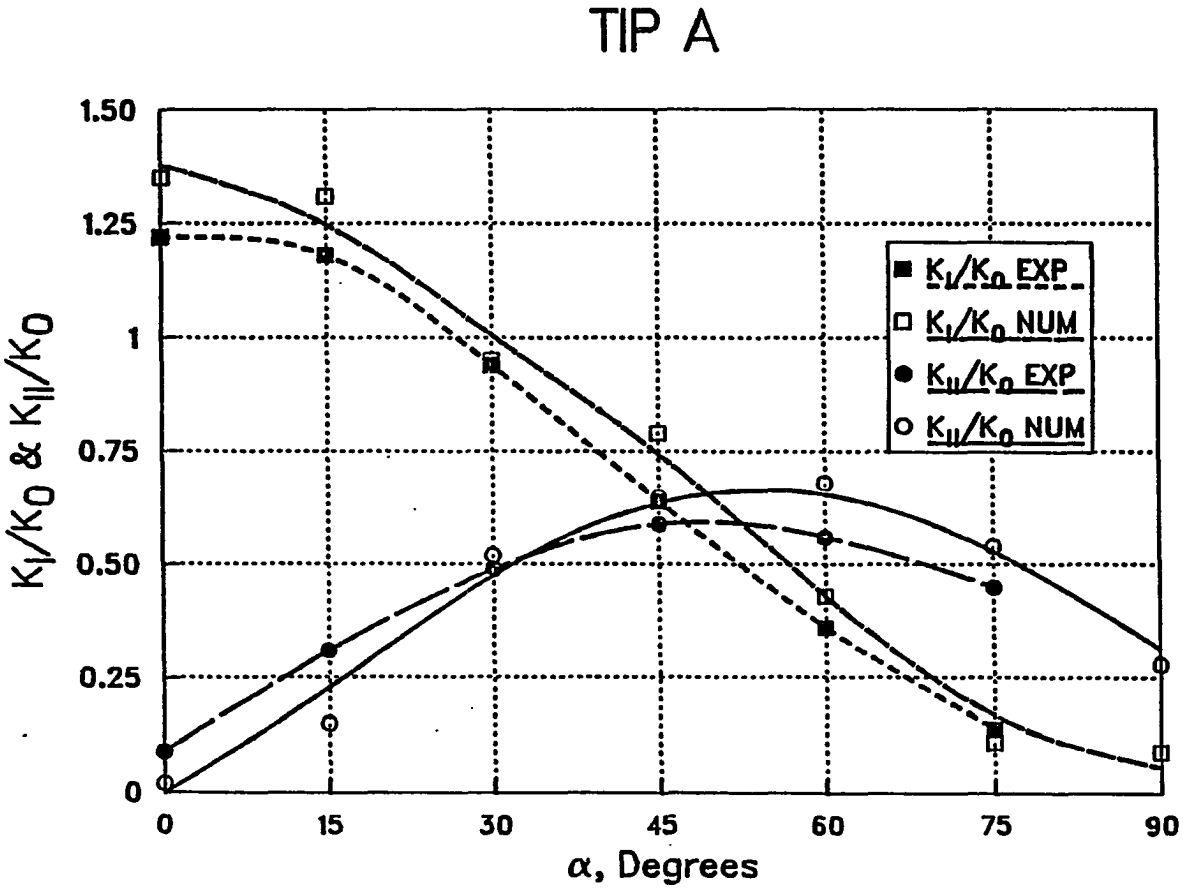

Fig. 11. Variation of normalized SIFs vs α for tip A

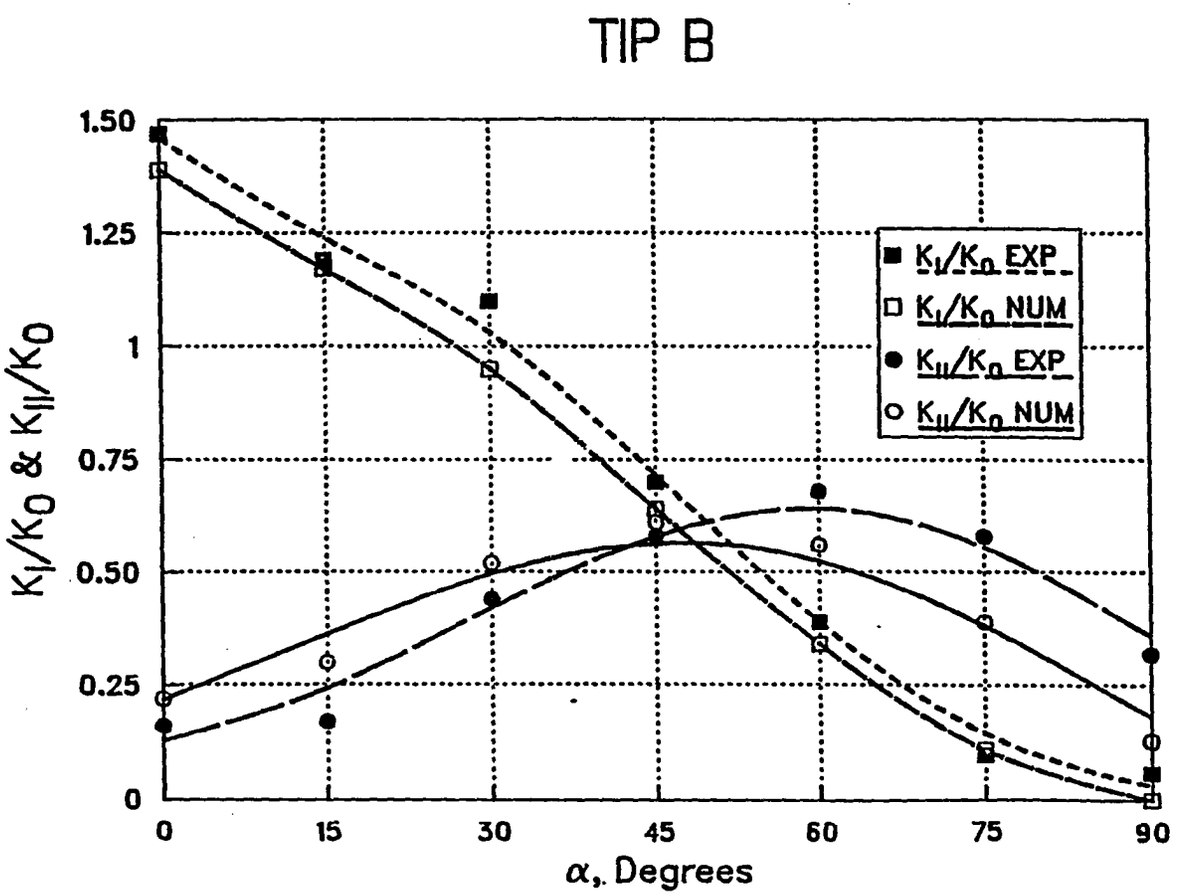

Fig. 12. Variation of normalized SIFs vs α for tip B

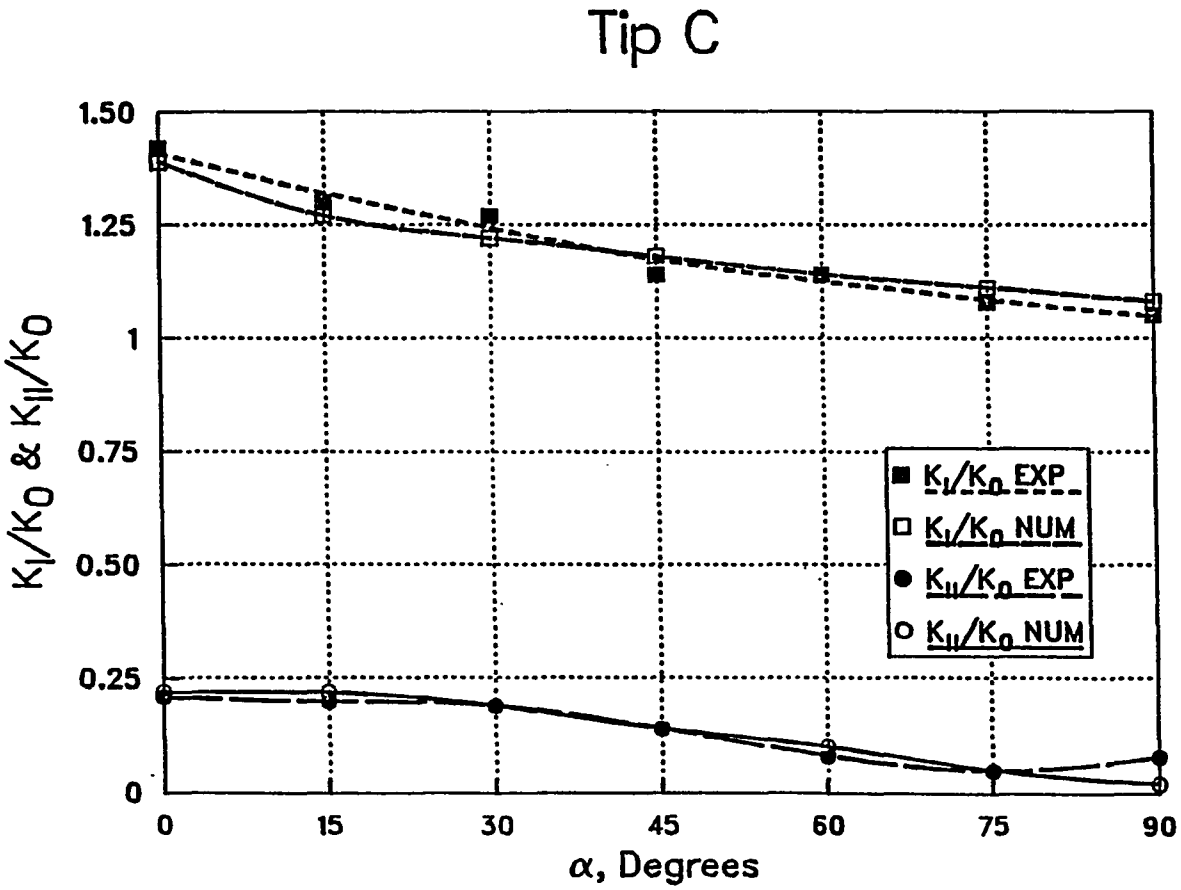

Fig. 13. Variation of normalized SIFs vs α for tip C

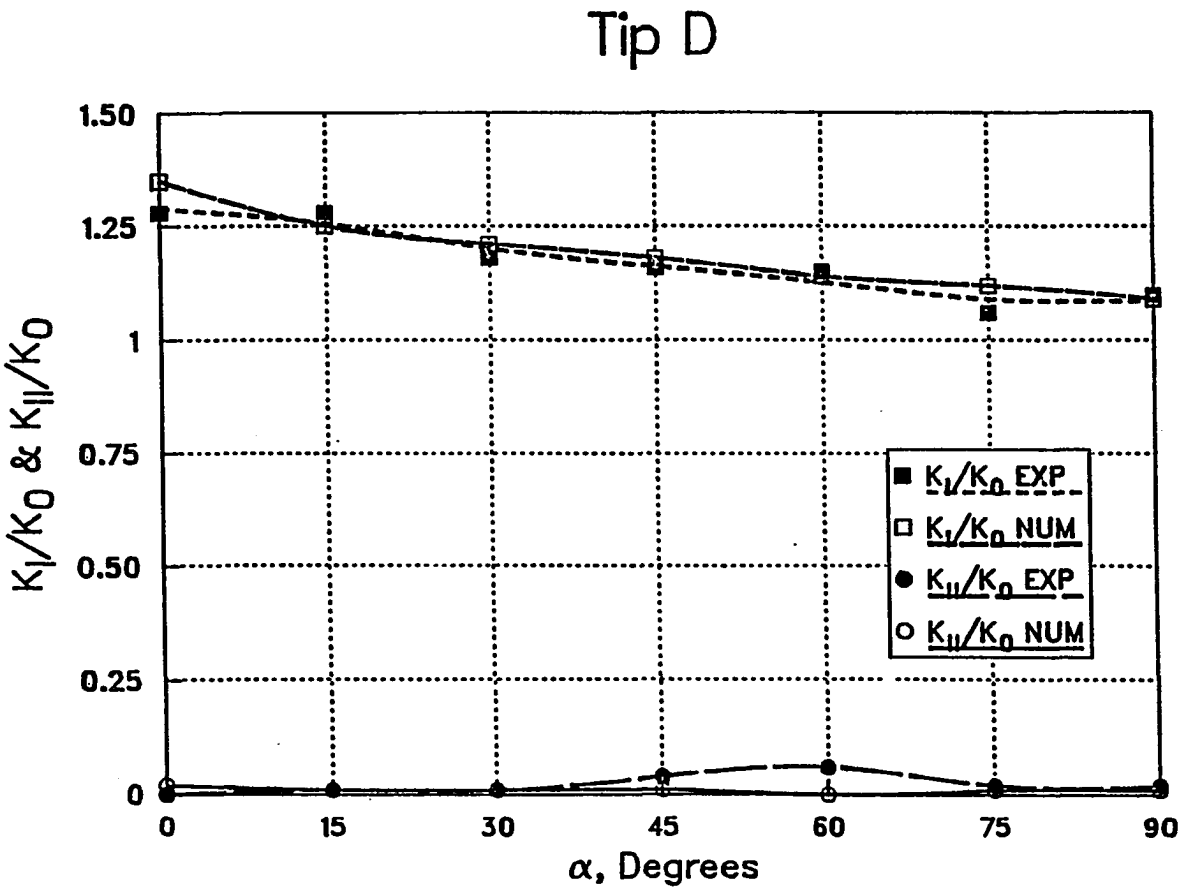

Fig. 14. Variation of normalized SIFs vs α for tip D

References

1. Y. Phang and C. Ruiz. "Photoelastic Determination of S.I.F. for Single and Interacting Cracks and Comparison with Calculated Result: Paret 1--Two-Dimensional Problems." J. Strain Anal., 19 (1984), 23.

2. F. W. Smith, A. F. Emery, and A. S. Kobayashi. "S.I.F. for Semi-Elliptical Crack: Part 2, Semi-Infinite Solid." J. Appl. Mech., 34 (1967), 953.

3. B. Kroner. Program TRACE. Photomechanics Program Bank, Dept. of Engineering Science and Mechanics, Iowa State University, Ames, Iowa, 1984.

4. G. R. Irwin. "Discussion of a Paper by A. A. Wells and D. Post." Proceedings, SESA, 16 (1958), 93.

5. A. A. Wells and D. Post. "The Dynamic Stress Distribution Surrounding a Running Crack--A Photoelastic Analysis." Proceedings, SESA, 16(1958), 69.

6. W. T. Evans and A. R. Luxmoore. "For Experimental Evaluation of Stress Intensity Factors." J. Strain Anal., 11 (1976), 177.

7. G. C. Sih. "On the Westergaard Method of Crack Analysis." Int. J. Fract. Mech., 2 (1966), 628.

8. M. K. Oladimeji. "Crack Emanating from a Circular Hole under Biaxial Load." Eng. Fract. Mech., 15(3-4) (1981), 391.

9. M. A. Schroedl, J. J. McGowan, and C. W. Smith. "An Assessment of Factors Influencing Data Obtained by the Photoelastic Stress Freezing Technique for Stress Fields Near Cracktip." Eng. Fract. Mech., 4 (1972), 801.

10. E. E. Gdoutos and P. S. Theocaris. "A Photoelastic Determination of Mixed Mode Stress Intensity Factors." Expt. Mech., 18(3) (1978), 87.

11. J. M. Etheridge and J. W. Dally. "A Three Parameter Method for Determining Stress Intensity Factors from Isochromatic Fringe Pattern." J. Strain Anal., 13(2) (1978), 91.

12. M. K. Oladimeji. "Photoelastic Analysis of Practical Mode I Fracture Test Specimens." Engin. Fract. Mech., 19 (1984), 717.

13. I. Miskioglu. Program CLMN. Photomechanics Program Bank, Dept. of Engineering Science and Mechanics, Iowa State University, Ames, Iowa, 1985.

14. R. J. Sanford and J. W. Dally. "Stress Intensity Factors in

the Third Stage Fan Disk of the TF-30 Turbine Engine." Eng. Fract. Mech., 11 (1979), 621.

15. M. L. Williams. "On the Stress Distribution at the Base of a Stationary Crack." J. Appl. Mech., 224 (1957), 109.

16. T. J. Rudolphi and L. S. Koo. "Boundary Element Solutions of Multiple, Interacting Crack Problems in Plane Elastic Media." Eng. Anal., 2(4) (1985), 211.

17. K. Hellan. Introduction to Fracture Mechanics. New York: McGraw Hill, 1984.

18. H. M. Westergaard. "Bearing Pressures And Cracks." J. Appl. Mech., 61 (1939), 49.

19. I. Miskioglu. Program SFW. Photomechanics Program Bank. Dept. of Engineering Science and Mechanics, Iowa State University, Ames, Iowa, 1985.

20. I. Miskioglu, A. Mehdi-Soozani, C. P. Burger, and A. S. Voloshin. "K-Determination of Multiple Cracks Through Half Fringe Photoelasticity." 1985 SEM Spring Conference on Experimental Mechanics, Las Vegas, June 9-14, 1985.

PAPER III. STRESS INTENSITY FACTORS FOR NEAR-EDGE CRACKS IN RECTANGULAR BARS UNDER PURE BENDING

Abstract

Mixed mode stress intensity factors (SIFs) for single, inclined cracks near an edge in a rectangular bar subjected to pure bending are evaluated using on line photoelastic procedures. Photoelastic data were collected from whole field images of sharpened isochromatic fringe patterns close to the crack tips using a digital image analysis system. The effect of change in the distance between the free edge and the closer crack tip on K_I and K_{II} is presented.

Notation

α = orientation of crack line with respect to the neutral axis

a = one-half crack length

A = crack tip further from the neutral axis

b = one-half of rectangular bar width

B = crack tip closer to the neutral axis

c = distance from the center of crack to the closer free edge

d = ligament size (i.e., distance between the free edge and the closer crack tip)

f_σ = material fringe value

K_I = mode one stress intensity factor

K_{II} = mode two stress intensity factor

l = one half of the support span

M = bending moment

r,θ = polar coordinates (as defined in Fig. 8)

σ = stress

SIF = stress intensity factor

Introduction

Today, fracture mechanics is considered to be an effective tool in failure analysis. Experimentally determined values for mode I and II SIFs have been reported for many geometries, and there is good agreement on the parameters of the stress field around a crack tip that can be used to determine the SIFs for elastic behavior. No experimental work, however, has been reported on one important geometry, a rectangular bar having an internal slant crack near the edge and loaded in pure bending. One major interest for this geometry is the analysis of the effect of the ligament size, that is, the distance from the free edge to the nearest crack tip, on SIFs. This is an important problem because it concerns the interaction between the crack tip with a free edge.

Use of photoelastic data in the vicinity of the crack tip for determination of K_I was first suggested by Irwin [1] in a discussion of the paper by Wells and Post [2]. Irwin also introduced an additional

parameter, σ_{ox}, the far field stress, into Westergaard's equation [3] to take into account the effect of the far field stresses in the direction of the crack. Since then, several photoelastic methods have been proposed for extraction of stress intensity factors from photoelastic data. M. K. Oladimeji [4] has reviewed most of these methods.

In this study a digital image analysis system, "EyeCom II[1]," was used to collect photoelastic data, N, r, and θ, at 40 points distributed randomly close to the crack tip. The whole field isochromatic fringe patterns from live models were stored and digitized by EyeCom II and then sharpened digitally through the use of a program called TRACE. Data were collected from these sharpened fringe patterns using EyeCom II and an interactive computer program. An overdeterministic, least squares technique proposed by Sanford and Dally [5] was used to extract mixed-mode SIFs. The stress field equation used was obtained from Williams' stress function [6].

Experimental Procedure

Models were manufactured from 3.2 mm (1/8 in.) thick strips of PSM1[2], a polycarbonate that is free of time-edge effect, with dimensions of 254 mm X 50.8 mm (2" X 10"). A 0.15 mm (0.006") wide, 20.3 mm (0.8") long slit was machined close to one of the long edges of the strips as shown in Fig. 1. PSM1 is sensitive to localized heating but completely insensitive to moisture, and therefore all machining was

[1] Product of Spatial Data Systems, Inc.

[2] Product of Measurements Group, Inc.

done with specimens submerged in coolant. A total of five such specimens was used in this study. The specimen geometries and material properties are summarized in Table 1.

Test Cases Since we were not aware of any solution to this problem that could produce the fracture parameters K_I and K_{II}, additional experiments were performed to verify the validity of the experimental technique used in this study. Three more models were fabricated, with the same geometry as the original five, from the same strip of PSM1. These models were loaded in pure bending using the same loading apparatus. Slits were machined in them to produce models for three known cases. These cases were a slant edge crack, a normal edge crack, and an internal crack normal to the long direction of the bar and closer to one edge. Test cases and their results are shown in Fig. 2.

All specimens were loaded in four point bending as shown in Fig. 3. To verify that the experimental setup actually produced pure bending, a bar identical to the models but with no cracks was manufactured and loaded. Figure 4 shows the isochromatic fringe pattern produced.

Loaded models were placed in a circular polariscope. EyeCom II was used to analyze the live image of the isochromatic fringe pattern. The EyeCom II unit consists of an image scanner, a real time digitizer, a display system, and an LSI-11 minicomputer (Fig. 5). The image scanner consists of a special Vidicon television camera. This image area is divided into 480 lines, and each line is divided into 640 picture elements, called pixels. The brightness or light intensity of each of the 307,200 pixels is converted into digital values (Z values).

The x values range from 0 to 639, and y values range from 0 to 479. The Z values range from 0 to 255. In other words, the total light intensity scale in this viewing area, from dark to light, is digitized to eight-bit resolution. The real-time digitizer can digitize the entire video image in only 1/30 second, and it stores the resultant values in a "Refresh Memory" where they can be accessed later by the computer and displayed on the monitor. Figure 6 shows one such image. A high-resolution digital fringe-sharpening procedure was performed by a computer program called TRACE [7] to increase the accuracy of data collection. The TRACE program is an image enhancement routine designed specifically for locating photoelastic fringes of the order of n/2 (n representing all positive integers from zero to infinity). The sharpened fringe pattern was then displayed on the image monitor. Figures 7(a) and 7(b) show an example of an original and a sharpened image. Data were collected by manually positioning a cursor on different points along the sharpened fringe. The polar coordinates (r,θ) of each data point were recorded by EyeCom with the origin at the crack tip as shown in Fig. 8. The corresponding fringe orders were entered at the same time. Forty such data points were used for each crack tip [8]. The region of data extraction was kept in the range $0.1 < r/a < 0.4$. Figure 9 shows an example of a typical set of data points.

Interpretation of Experimental Data

For a crack subjected to both tensile and shearing stresses, as is the case in this paper, the two-dimensional stress field in the

neighborhood of the crack tip may be approximated by the following stress function in polar coordinates given by Hellan [9] who used Williams' approach [6]:

$$\chi = \sum_{n=1} r^{n+1/2} \left\{ a_{2n-1} \left[\cos (n - 3/2)\theta - \frac{2n - 3}{2n + 1} \cos(n - 1/2)\theta \right] + b_{2n-1} [\sin (n - 3/2)\theta - \sin (n + 1/2)\theta] \right\} + \sum_{n=1} r^{n+1} \left\{ a_{2n} [\cos (n - 1)\theta - \cos (n + 1)\theta] + b_{2n} \left[\sin (n - 1)\theta - \frac{n - 1}{n + 1} \sin (n + 1)\theta\right] \right\} \quad (1a)$$

where the terms multiplied by a_{2n-1} and a_{2n} are symmetric (mode I), and the terms multiplied by b_{2n-1} and b_{2n} are antisymmetric (mode II) with respect to $\theta = 0$. Note that the polar coordinates are measured from the crack tip in the above equation. The stress intensity factors K_I and K_{II} are related to a_1 and b_1 through

$$a_1 = K_I (2\pi)^{-1/2}$$

$$b_1 = K_{II} (2\pi)^{-1/2} \quad (1b)$$

The polar components of stress are

$$\sigma_r = \frac{1}{r} \frac{\partial \chi}{\partial r} + \frac{1}{r^2} \frac{\partial^2 \chi}{\partial \theta^2} \quad (2a)$$

$$\sigma_\theta = \frac{\partial^2 \chi}{\partial r^2} \quad (2b)$$

$$\tau_{r\theta} = \frac{1}{r^2}\frac{\partial \chi}{\partial \theta} - \frac{1}{r}\frac{\partial^2 \chi}{\partial r \partial \theta} = -\frac{\partial}{\partial r}\left(\frac{1}{r}\frac{\partial \chi}{\partial \theta}\right) \tag{2c}$$

The cartesian components of stress can be expressed in terms of the polar components in the following form:

$$\sigma_x = \sigma_r \cos^2\theta + \sigma_\theta \sin^2\theta - 2\tau_{r\theta} \sin\theta \cos\theta \tag{3a}$$

$$\sigma_y = \sigma_r \sin^2\theta + \sigma_\theta \cos^2\theta + 2\tau_{r\theta} \sin\theta \cos\theta \tag{3b}$$

$$\tau_{xy} = (\sigma_r - \sigma_\theta) \sin\theta \cos\theta + \tau_{r\theta}(\cos^2\theta - \sin^2\theta) \tag{3c}$$

Thus, cartesian components of the stress may be obtained from Eq. (1) as

$$\begin{aligned}
\sigma_{xx} = \sum_{n=1}^{\infty} r^{n-3/2} \Bigg\{ & \left[A''_{2n-1} + \left(n + \tfrac{1}{2}\right) A_{2n-1}\right] \cos^2\theta + \\
& + \left(n + \tfrac{1}{2}\right)\left(n - \tfrac{1}{2}\right) A_{2n-1} \sin^2\theta \\
& + 2\left(n - \tfrac{1}{2}\right) A'_{2n-1} \sin\theta \cos\theta \Bigg\} a_{2n-1} \\
& + \sum_{n=1}^{\infty} r^{n-3/2} \Bigg\{ \left[B''_{2n-1} + \left(n + \tfrac{1}{2}\right) B_{2n-1}\right] \cos^2\theta \\
& + \left(n + \tfrac{1}{2}\right)\left(n - \tfrac{1}{2}\right) B_{2n-1} \sin^2\theta \\
& + 2\left(n - \tfrac{1}{2}\right) B'_{2n-1} \sin\theta \cos\theta \Bigg\} b_{2n-1} \\
& + \sum_{n=1}^{\infty} r^{n-1} \Bigg\{ \left[A''_{2n} + (n+1) A_{2n}\right] \cos^2\theta \\
& + n(n+1) A_{2n} \sin^2\theta + 2n A'_{2n} \sin\theta \cos\theta \Bigg\} a_{2n}
\end{aligned}$$

$$+ \sum_{n=1}^{\infty} r^{n-1} \left\{ \left[B''_{2n} + (n+1)\, B_{2n} \right] \cos^2\theta \right.$$

$$\left. + n(n+1)\, B_{2n} \sin^2\theta + 2n\, B'_{2n} \sin\theta \cos\theta \;\; b_{2n} \right\} \quad (4a)$$

$$\sigma_{yy} = \sum_{n=1}^{\infty} r^{n-3/2} \left\{ \left[A''_{2n-1} + \left(n + \tfrac{1}{2}\right) A_{2n-1} \right] \sin^2\theta \right.$$

$$+ \left(n + \tfrac{1}{2}\right)\left(n - \tfrac{1}{2}\right) A_{2n-1} \cos^2\theta$$

$$\left. - 2\left(n - \tfrac{1}{2}\right) A'_{2n-1} \sin\theta \cos\theta \right\} \;\; a_{2n-1}$$

$$+ \sum_{n=1}^{\infty} r^{n-3/2} \left\{ \left[B''_{2n-1} + \left(n + \tfrac{1}{2}\right) B_{2n-1} \right] \sin^2\theta \right.$$

$$+ \left(n + \tfrac{1}{2}\right)\left(n - \tfrac{1}{2}\right) B_{2n-1} \cos^2$$

$$\left. - 2\left(n - \tfrac{1}{2}\right) B'_{2n-1} \sin\theta \cos\theta \right\} \;\; b_{2n-1}$$

$$+ \sum_{n=1}^{\infty} r^{n-1} \left\{ \left[A'_{2n} + (n+1)\, A_{2n} \right] \sin^2\theta \right.$$

$$\left. + n(n+1)\, A_{2n} \cos^2\theta - 2n\, A'_{2n} \sin\theta \cos\theta \right\} a_{2n}$$

$$+ \sum_{n=1}^{\infty} r^{n-1} \left\{ \left[B''_{2n} + (n+1)\, B_{2n} \right] \sin^2\theta \right.$$

$$\left. + n(n+1)\, B_{2n} \cos^2\theta - 2n\, B'_{2n} \sin\theta \cos\theta \right\} b_{2n} \quad (4b)$$

$$\tau_{xy} = \sum_{n=1}^{\infty} r^{n-3/2} \left\{ \left[A''_{2n-1} - \left(n + \tfrac{1}{2}\right)\left(n - \tfrac{3}{2}\right) A_{2n-1} \right] \sin\theta \cos\theta \right.$$

$$\left. - \left(n - \tfrac{1}{2}\right) A'_{2n-1} \left(\cos^2\theta - \sin^2\theta\right) \right\} a_{2n-1}$$

$$+ \sum_{n=1}^{\infty} r^{n-3/2} \left\{ \left[B''_{2n-1} - \left(n + \frac{1}{2}\right)\left(n - \frac{3}{2}\right) B_{2n-1} \right] \sin\theta \cos\theta \right.$$

$$\left. - \left(n - \frac{1}{2}\right) B'_{2n-1} \left(\cos^2\theta - \sin^2\theta\right) \right\} b_{2n-1}$$

$$+ \sum_{n=1}^{\infty} r^{n-1} \left\{ \left[A''_{2n} - (n + 1)(n - 1) A_{2n} \right] \sin\theta \cos\theta \right.$$

$$\left. - n A'_{2n} \left(\cos^2\theta - \sin^2\theta\right) \right\} a_{2n}$$

$$+ \sum_{n=1}^{\infty} r^{n-1} \left\{ \left[B''_{2n} - (n + 1)(n - 1) B_{2n} \right] \sin\theta \cos\theta \right.$$

$$\left. - n B'_{2n} \left(\cos^2\theta - \sin^2\theta\right) \right\} b_{2n} \qquad (4c)$$

where (') indicates differentiation with respect to θ and

$$A_{2n-1} = \cos\left(n - \frac{3}{2}\right)\theta - \frac{2n - 3}{2n + 1} \cos(n + 1)\theta \qquad (5a)$$

$$B_{2n-1} = \sin\left(n - \frac{3}{2}\right)\theta - \sin\left(n + \frac{1}{2}\right)\theta \qquad (5b)$$

$$A_{2n} = \cos(n - 1)\theta - \cos(n + 1)\theta \qquad (5c)$$

$$B_{2n} = \sin(n - 1)\theta - \frac{n - 1}{n + 1} \sin(n + 1)\theta \qquad (5d)$$

In Eq. (4) for n = 1, if only the singular terms are considered, the cartesian components of stress become

$$\sigma_{xx} = r^{-1/2}\left[a_1 \cos\frac{\theta}{2}\left(1 - \sin\frac{\theta}{2}\sin\frac{3\theta}{2}\right)\right.$$

$$\left. - b_1 \sin\frac{\theta}{2}\left(2 + \cos\frac{\theta}{2}\cos\frac{3\theta}{2}\right)\right] \qquad (6a)$$

$$\sigma_{yy} = r^{-1/2}\left[a_1 \cos\frac{\theta}{2}\left(1 + \sin\frac{\theta}{2}\sin\frac{3\theta}{2}\right) + b_1 \sin\frac{\theta}{2}\cos\frac{\theta}{2}\cos\frac{3\theta}{2}\right] \tag{6b}$$

$$\tau_{xy} = r^{-1/2}\left[a_1 \sin\frac{\theta}{2}\cos\frac{\theta}{2}\cos\frac{3\theta}{2} + b_1 \cos\frac{\theta}{2}\left(1 - \sin\frac{\theta}{2}\sin\frac{3\theta}{2}\right)\right] \tag{6c}$$

Note that for n = 1, letting $a_1 = K_I(2\pi)^{-1/2}$ and $b_1 = K_{II}(2\pi)^{-1/2}$ in Eq. (1) yields the well known Westergaard's equation [3] for the stress field at the crack tip.

Considering the nonsingular terms in addition to the singular terms when n = 1 in Eq. (4), it is found that the nonsingular terms in σ_{yy} and τ_{xy} vanish, and in σ_{xx} they reduce to $4a_2 = -\sigma_{ox}$. This is the "far field stress" in the x-direction and the modified Westergaard equations [1,5] are obtained.

In Eq. (1a) χ contains two functions of θ multiplied by an integer or a noninteger power of r. In this study, any given power of r together with the function of θ with which it is multiplied will be referred to as one term. The number of terms, k, considered in χ, is related to n through the equations

$$k = 2n - 1, \qquad k = 1, 3, 5, \ldots. \tag{6d}$$

$$k = 2n, \qquad k = 2, 4, 6, \ldots. \tag{6e}$$

Also, the k terms considered yield 2k - 1 unknown coefficients (a, b) because b_{2n} (Eq. (5d)) is identically zero when k = 2 (i.e., n = 1).

K_I and K_{II} were extracted from the photoelastic data (r, θ, N) using the stress optic law that relates the in-plane principal stresses to the isochromatic fringe order N in the following form:

$$\sigma_1 - \sigma_2 = \frac{Nf_\sigma}{h} \tag{7}$$

where f_σ is the material fringe constant and h is the specimen thickness. The maximum in-plane shear stress τ_m is related to the Cartesian components of stress by

$$2\,\tau_m = \sigma_1 - \sigma_2 = \left[(\sigma_x - \sigma_y)^2 + 4\tau_{xy}^2\right]^{1/2} \tag{8}$$

Thus Eqs. (7) and (8) may be combined to yield

$$\left(\frac{Nf_\sigma}{h}\right)^2 = (\sigma_x - \sigma_y)^2 + 4\tau_{xy}^2 \tag{9}$$

The cartesian components of stress from Eq. (4) are now substituted into Eq. (9) and are obtained by an overdeterministic least squares technique proposed by Sanford and Dally [5]. This method does not have a preferred way of data acquisition. Therefore, the whole field in the vicinity of the crack tip may be used for data collection in order to improve the overall accuracy of the results. To implement this technique, Eq. (9) is rewritten as a function $g(a_1, b_1, a_2, \ldots)$ such that:

$$g(a_1, b_1, a_2, \ldots.) = (\sigma_x - \sigma_y)^2 + 4\tau_{xy}^2 - \left(\frac{Nf_\sigma}{h}\right)^2 = 0 \tag{10}$$

An iterative scheme was then set up on function $g(a_1, b_1, a_2, \ldots.)$ using a linearized Taylor series expansion of g to determine the coefficients a_1, b_1, a_2... [10]. The previous study [11], indicated that the optimal number of terms in Eq. (10) should be four. This required the determination of seven coefficients: a_1, b_1, a_2, a_3, b_3, a_4, and b_4.

Results and Conclusions

The experimental results obtained for test cases are compared to numerical ones [12] in Fig. 2. In all three cases there is good agreement between experimental and numerical results. The percentage error ranged from zero to four percent. On the basis of these results, the experimental technique used in this paper is reliable in determination of mode I and mixed mode SIFs for plane problems.

In order to obtain dimensionless SIFs, K_I and K_{II} were divided by $K_0 = Ma^{1/2}/b^2$. Figure 10 shows the variation of K_I/K_0 and K_{II}/K_0 vs the ligament size for tip A, the tip closer to the edge. The stress field is dominated by K_{II}, the shear mode. Both K_I/K_0 and K_{II}/K_0 dropped as the ligament size increased. The drop in K_{II}/K_0 however, is more significant in comparison with the drop in K_I/K_0. Figure 11 shows the variation of K_I/K_0 and K_{II}/K_0 vs the ligament size for tip B, the tip closer to the centroidal axis of the bar. The stress field tends to be dominated more by the shear mode, K_{II}, as the ligament size increases.

The EyeCom II system proved to be an effective tool in increasing the accuracy of photoelastic data by (a) sharpening the isochromatic fringe loops and (b) magnifying the image of the data extraction zone.

Table 1. Summary of specimen geometries

Model	α	c	d	d/a
1	30°	7.6 mm (0.30 in.)	2.5 mm (0.1 in.)	0.250
2	30°	8.9 mm (0.35 in.)	3.8 mm (0.15 in.)	0.375
3	30°	11.4 mm (0.45 in.)	5.1 mm (0.2 in.)	0.500
4	30°	12.7 mm (0.50 in.)	7.6 mm (0.3 in.)	0.750
5	30°	15.2 mm (0.60 in.)	10.2 mm (0.4 in.)	1.000

For all models $2a = 20.3$ mm (0.8 in.)

$E = 2.39\ GN/m^2$ (3.47×10^5 psi)

$\nu = 0.38$

$f_\sigma = 7$ KN/fringe-m (40 lb/fringe-in.)

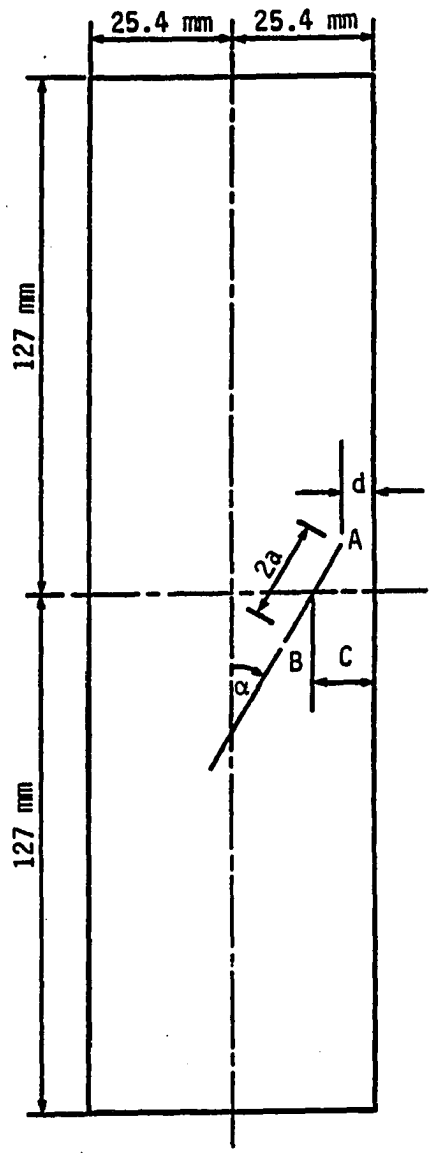

Fig. 1. Test specimen.

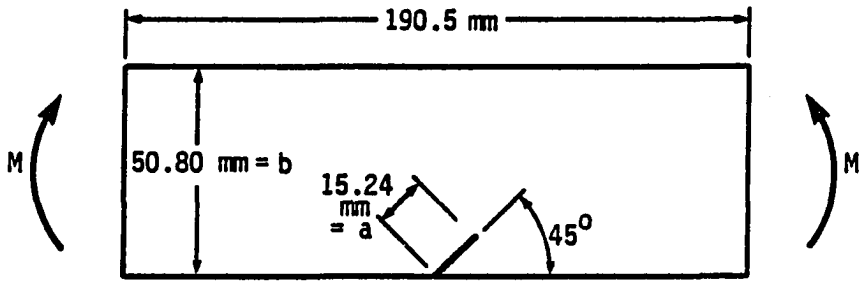

CASE 1

M = 908.10 N.m/m

$K_0 = 6M\sqrt{\pi a}/b^2$

	EXP	NUM	%DIFF
K_I/K_0	0.68	0.70	2.8
K_{II}/K_0	0.31	0.31	0.0

(a)

Fig. 2. Geometry of and test results for three test cases.

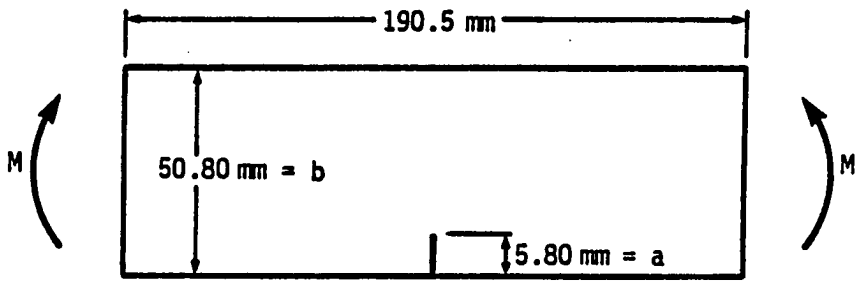

CASE 2

M = 908.10 N.m/m

$K_o = 6M\sqrt{\pi a}/b^2$

	EXP	NUM	%DIFF
K_I/K_0	1.00	1.04	4.0

Fig. 2. Continued (b)

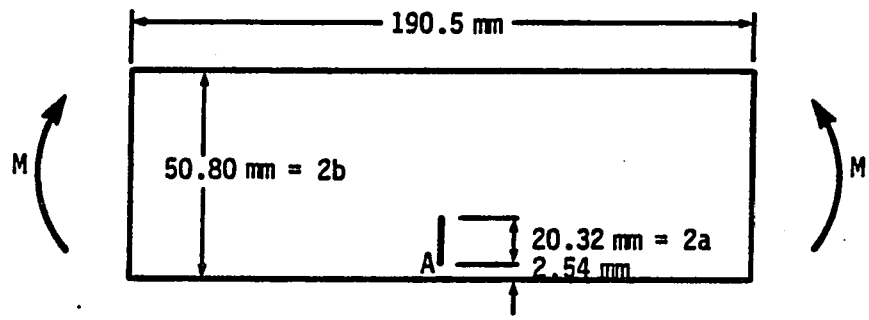

CASE 3

M = 1336.45 N.m/m

$K_o = 3\sqrt{\pi}\ M\ a^{3/2}/4b^3$

	EXP	NUM	%DIFF
$(K_I/K_o)_A$	3.53	3.50	0.8

Fig. 2. Continued (c)

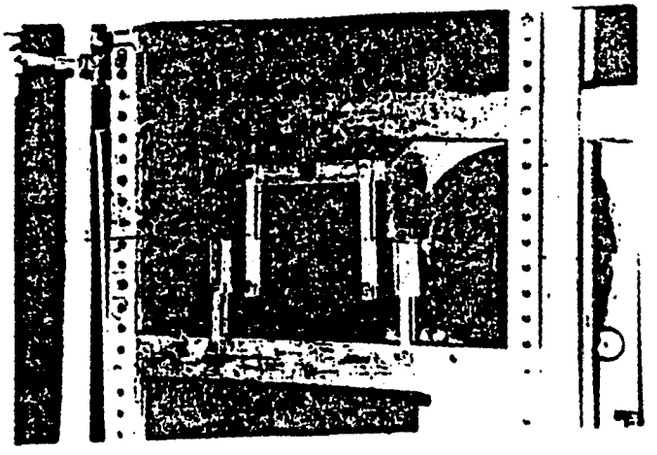

Fig. 3. Four point bending setup.

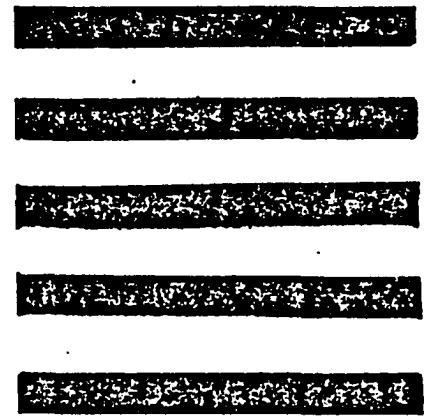

Fig. 4. Dark-field isochromatic fringe pattern for a rectangular bar in pure bending.

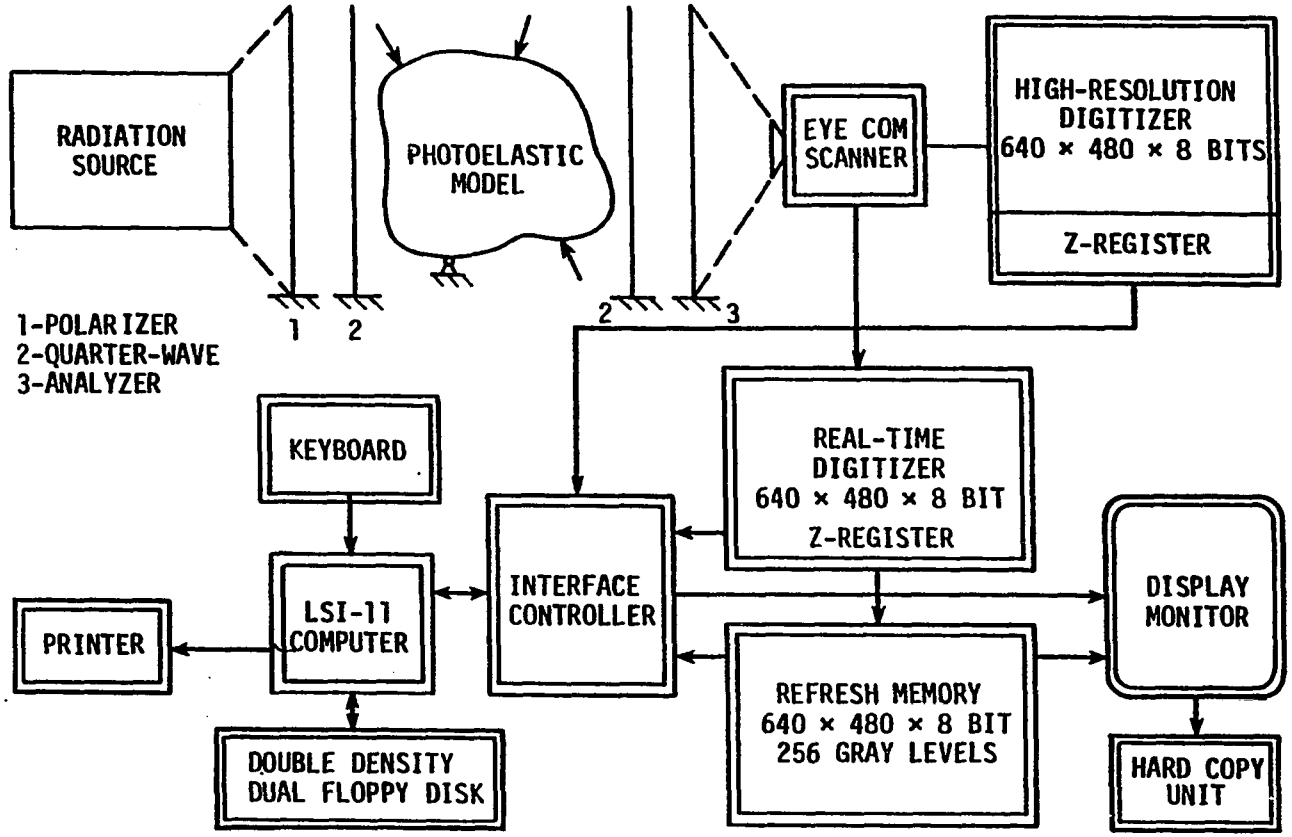

Fig. 5. Diagrammatic of the EyeCom II system.

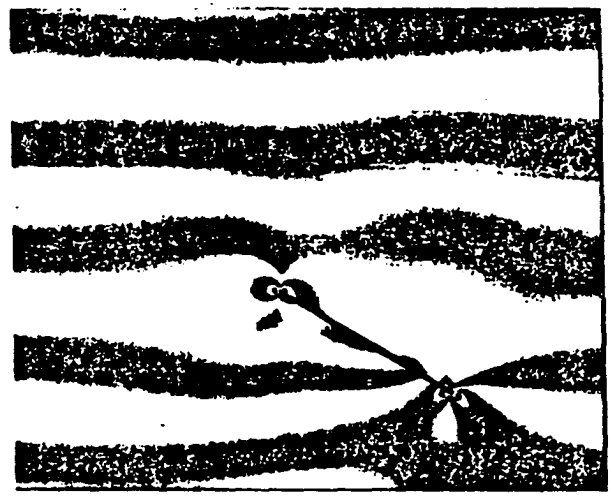

Fig. 6. Dark-field isochromatic fringe pattern of a specimen in pure bending.

(a)

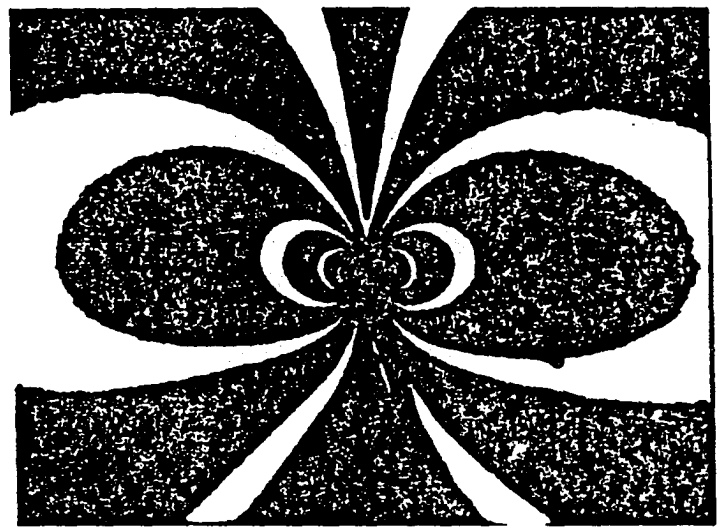

Fig. 7a. Light-field isochromatic fringe pattern.

b. "Trace" pattern from Fig. 7a, after digital fringe sharpening.

(b)

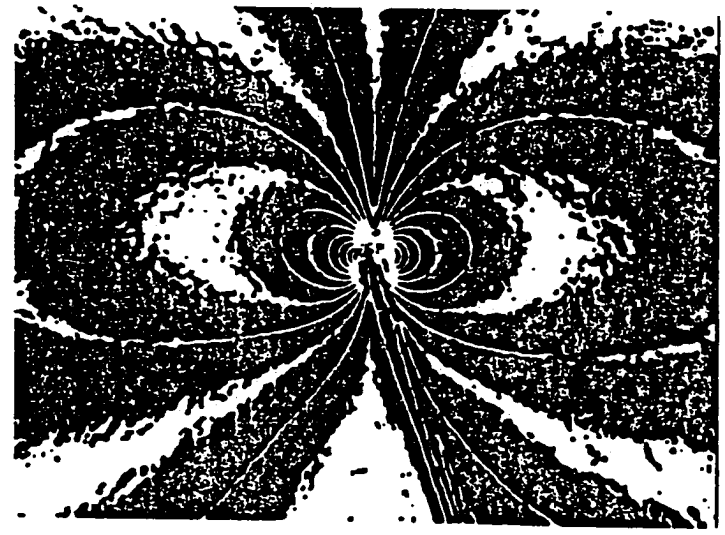

Fig. 7. Continued

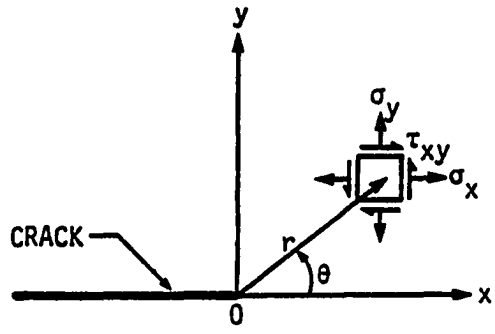

Fig. 8. Coordinate system with respect to the crack tip.

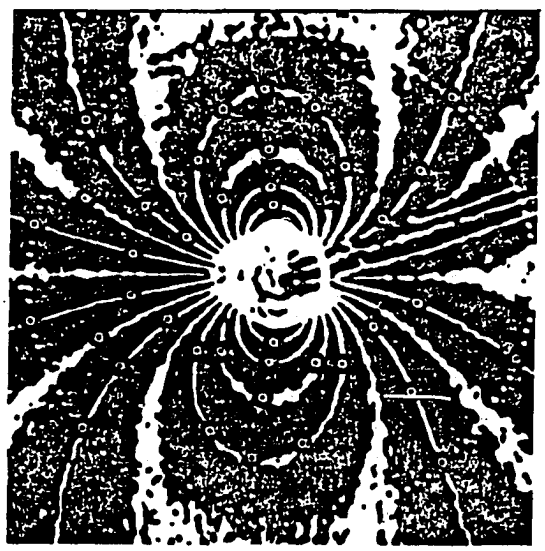

Fig. 9. Typical locations of 40 randomly chosen data points on the sharpened fringe loops.

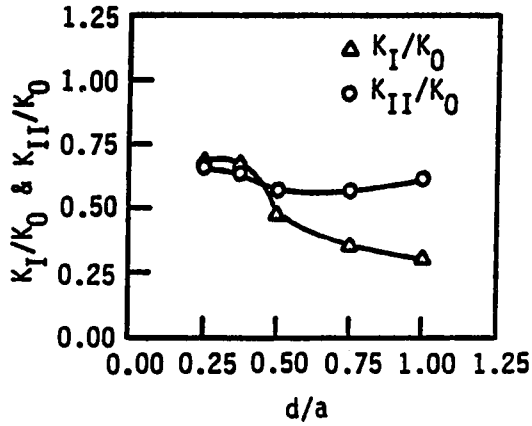

Fig. 10. Variation of normalized SIFs with d/a for tip A.

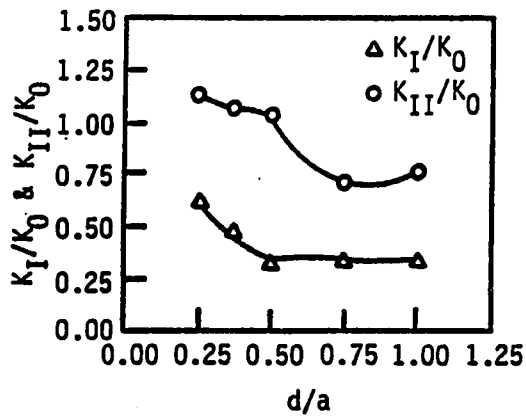

Fig. 11. Variation of normalized SIFs with d/a for tip B.

References

1. G. R. Irwin. "Discussion of a Paper by A. A. Wells and D. Post." Proceeding, SESA, 16 (1958), 93.

2. A. A. Wells and D. Post. "The Dynamic Stress Distribution Surrounding a Running Crack--A Photoelastic Analysis." Proceedings, SESA, 16(1958), 69.

3. H. M. Westergaard. "Bearing Pressures And Cracks." J. Appl. Mech., 61 (1939), 49.

4. M. K. Oladimeji. "Photoelastic Analysis of Practical Mode I Fracture Test Specimens." Engin. Fract. Mech., 19 (1984), 717.

5. R. J. Sanford and J. W. Dally. "Stress Intensity Factors in the Third Stage Fan Disk of the TF-30 Turbine Engine." Eng. Fract. Mech., 11 (1979), 621.

6. M. L. Williams. "On the Stress Distribution at the Base of a Stationary Crack." J. Appl. Mech., 224 (1957), 109.

7. B. Kroner. Program TRACE. Photomechanics Program Bank, Dept. of Engineering Science and Mechanics, Iowa State University, Ames, Iowa, 1984.

8. I. Miskioglu. Program CLMN. Photomechanics Program Bank, Dept. of Engineering Science and Mechanics, Iowa State University, Ames, Iowa, 1985.

9. K. Hellan. Introduction to Fracture Mechanics. New York: McGraw Hill, 1984.

10. I. Miskioglu. Program SFW. Photomechanics Program Bank. Dept. of Engineering Science and Mechanics, Iowa State University, Ames, Iowa, 1985.

11. I. Miskioglu, A. Mehdi-Soozani, C. P. Burger, and A. S. Voloshin. "K-Determination of Multiple Cracks Through Half Fringe Photoelasticity." 1985 SEM Spring Conference on Experimental Mechanics, Las Vegas, June 9-14, 1985.

12. D. P. Rooke and D. J. Cartwright. Compendium of Stress Intensity Factors. Uxbridge, Middlesex: The Hillingdon Press, 1976.

CHAPTER 4. SUMMARY

In this study two-dimensional mixed mode stress intensity factors for a crack tip in the neighborhood of a free edge or another crack tip were determined both experimentally and numerically.

In the experimental approach on-line digital image analysis procedures are used to extract photoelastic data from the whole field isochromatic fringe patterns. Two different techniques were used to obtain information on the near crack tip stress field: (1) Half Fringe Photoelasticity (HFP), which requires adjusting the load to keep the maximum fringe order less than 0.5 in the data extraction zone, and (2) Trace, a digital fringe sharpening procedure, which accurately produces trace of all half- and full-order fringes. The load is adjusted to yield multiple fringes in the field of data extraction.

Numerical SIFs were determined by the boundary integral equation method and compared to experimental results.